P-14-19

Miniature Canister (MiniCan) Corrosion experiment Progress report 5 for 2008–2013

Nick Smart, Bharti Reddy, David Nixon, Andy Rance

Amec Foster Wheeler

Adam Johannes Johansson, Svensk Kärnbränslehantering AB

October 2015

Svensk Kärnbränslehantering AB
Swedish Nuclear Fuel
and Waste Management Co

Box 250, SE-101 24 Stockholm
Phone +46 8 459 84 00

ISSN 1651-4416
SKB P-14-19
ID 1433155
October 2015

Miniature Canister (MiniCan) Corrosion experiment Progress report 5 for 2008–2013

Nick Smart, Bharti Reddy, David Nixon, Andy Rance

Amec Foster Wheeler

Adam Johannes Johansson, Svensk Kärnbränslehantering AB

Executive Summary

To ensure the safe encapsulation of spent nuclear fuel assemblies for geological disposal, SKB of Sweden has proposed using the copper-iron canister, which consists of an outer copper canister and a cast iron insert. Over the years a programme of laboratory work has been carried out to investigate a range of corrosion issues associated with the canister, including the possibility of expansion of the outer copper canister as a result of the anaerobic corrosion of the cast iron insert. Previous experimental work using stacks of test specimens has not shown any evidence of corrosion-induced expansion. However, as a further step in developing an understanding of the likely performance of the canister in a repository environment, Amec Foster Wheeler has set up a series of experiments in SKB's Äspö Hard Rock Laboratory (HRL) using inactive model canisters, in which leaks were deliberately introduced into the outer copper canister while surrounded by bentonite, with the aim of obtaining information about the corrosion evolution of the internal environment. The experiments use five small-scale model canisters (300 mm long × 150 mm diameter) that simulate the main features of the SKB canister design (hence the project name, 'MiniCan'). The main aim of the work is to examine how corrosion of the cast iron insert will evolve if a leak is present in the outer copper canister.

This report describes the progress on the five experiments running at the Äspö Hard Rock Laboratory and the data obtained from the start of the experiments in late 2006 up to February 2013. The full details of the design and installation of the experiments are given in a previous report and this report concentrates on summarising and interpreting the data obtained to date. This report follows the earlier progress reports presenting results up to December 2011. The current document (progress report 5) describes work up to February 2013.

The current report presents the results of the water analyses obtained in 2007, 2008 and 2010 including gas composition and microbial activity. These data show an increase in the dissolved iron concentration inside the support cage, together with a decrease in the pH. Both these observations appear to be mainly due to microbial activity, but it is also possible that abiotic processes could have contributed to changes in the local chemistry. Microbial analysis has shown the presence of sulphate reducing bacteria (SRB) and autotrophic acetogens. The presence of low density bentonite did not suppress the growth of SRB, but recent studies reported in the literature indicate that high density fully compacted bentonite inhibits SRB activity. Further water analysis and microbial analysis for Experiment 3 was carried out before it was removed for analysis in 2011, but the results from this analysis are presented in a separate report.

The electrochemical measurements provide an in situ E_h value which is comparable with published data. The E_h value inside the boreholes decreased with time as oxygen was consumed by microbial activity, reaction with minerals in the surrounding rock and/or corrosion of the MiniCan experiment and its support cage.

Corrosion rates have been obtained using a range of electrochemical methods. The copper corrosion rate was initially measured electrochemically as being < 3.5 μm yr^{-1}, but the measured corrosion rates of iron and copper appear to have accelerated to unexpectedly high values. The electrochemically measured corrosion rate of iron was considerably higher (> 1 mm yr^{-1} in some cases) than expected on the basis of laboratory experiments in the absence of microbial activity. The increase in corrosion rates appeared to coincide with a minimum value for the E_h being reached and this may correspond to the onset of enhanced anaerobic microbial activity (e.g. SRB) and hence increased production of sulphide. Reports in the literature suggest that there is reason to believe that the corrosion rate of iron measured using the Linear Polarisation Resistance (LPR) and AC Impedance (ACI) techniques may overestimate the corrosion rate when sulphide films are present on the surface. However, recent analysis of the iron weight loss coupon from Experiment 3 indicates that the corrosion rate was actually at least 500 μm yr^{-1}.

The corrosion potentials of the copper and iron electrodes are compared with published Pourbaix diagrams for iron and copper in the presence of chloride and sulphur species and they are found to be consistent with corrosion by dissolved sulphide to produce metal sulphide films.

The corrosion rates measured using the electrochemical noise technique yielded values that were significantly lower than the values measured using the LPR and ACI techniques. The lowest corrosion rates for copper were measured using the electrical resistance technique using copper wires. This technique gave corrosion rates of less than 1 μm yr^{-1} in Experiment 2 (low density bentonite) and Experiment 5 (no bentonite). Experiment 3 was dismantled during 2011 and a weight loss measurement was carried out on the copper weight loss coupon from this experiment. The corrosion rate derived from the weight loss measurement for Experiment 3 was compared with the corrosion rate measured electrochemically and found to be considerably lower (0.15 μm yr^{-1}). Detailed analysis of the dismantling and analysis of the data from Experiment 3 is presented in a separate report.

It should be noted that only one experiment (Experiment 4) is a close representation of the proposed SKB disposal concept as it uses compacted bentonite, whereas the other experiments use low density bentonite or no bentonite at all. The results from the experiments with low density bentonite or no bentonite (i.e. high levels of microbial activity and high corrosion rates) are therefore only applicable to a fault situation where the density of the bentonite is compromised.

The main conclusions from the project to date are as follows:

1. Water analysis has shown that there are compositional differences between the water inside the support cages compared to the external borehole water. These can be explained on the basis of corrosion of the iron and microbial activity inside the support cages. There has been a large increase in the concentration of dissolved iron, which is mainly present in the form of Fe^{2+}, and a parallel decrease in the pH from the groundwater pH value of ~7.6 to a value inside the support cage of ~6.6.
2. Microbial analysis has demonstrated that SRB are active in the experimental boreholes.
3. E_h measurements have shown that the test conditions within the support cages around the MiniCan experiments became reducing over a period of a few thousand hours at the start of the experiments.
4. The corrosion potentials of the copper and iron electrodes in the experiments with low density bentonite (Experiments 1 to 3) are consistent with the formation of copper sulphide and iron sulphide corrosion products.
5. The electrochemically measured corrosion rates have increased for both copper and iron. Analysis of the weight loss sample in Experiment 3 has confirmed that the corrosion rate for iron is at least 500 μm yr^{-1}. The corrosion rates measured for iron by LPR and ACI are overestimated due to the electrochemical properties of the sulphide films formed on the surface by SRB activity, by a factor of approximately × 5.
6. High corrosion rates have been measured electrochemically for copper in low density bentonite and unconditioned groundwater, but these values are believed to be an overestimate caused by the surface precipitation of iron sulphide produced by corrosion of cast iron in the vicinity (as observed when Experiment 3 was dismantled). The measured values are considerably higher than that measured by weight loss in Experiment 3, where a value of 0.15 μm yr^{-1} was obtained.
7. Strain gauge measurements showed that no expansion of the copper canister had occurred as a result of corrosion of the cast iron insert.
8. It should be recognised that these test conditions are not directly comparable with the proposed repository conditions. It appears that the low density bentonite is conducive to microbial activity, particularly that of sulphate reducing bacteria (SRB), and this has led to an increase in the corrosion rate of the cast iron. However, the copper corrosion rates measured by the electrical resistance method in low density bentonite and raw groundwater are considerably lower (< 1 μm yr^{-1}).

Contents

1 Introduction

To ensure the safe encapsulation of spent nuclear fuel assemblies for geological disposal, SKB of Sweden is considering using the Copper-Iron Canister, which consists of an outer copper canister and a cast iron insert. A programme of work has been carried out over a number of years to investigate a range of corrosion issues associated with the canister, including the possibility of expansion of the outer copper canister as a result of the anaerobic corrosion of the cast iron insert. Experimental work using stacks of copper and iron test specimens has not shown any evidence of corrosion-induced expansion (Smart et al. 2006). However, as a further step in developing an understanding of the likely performance of the canister in a repository environment, Amec Foster Wheeler has set up a series of experiments in SKB's Äspö Hard Rock Laboratory (HRL) using inactive model canisters, in which leaks were deliberately introduced into the outer copper canister while surrounded by bentonite, with the aim of obtaining information about the corrosion evolution of the internal environment (Smart et al. 2007).

The experiments use small-scale (300 mm long × 150 mm diameter) model canisters that simulate the main features of the SKB canister design (hence the project name, 'MiniCan'). The main aim of the work is to examine how corrosion of the cast iron insert will develop if a leak is introduced into the outer copper canister, but a number of other issues are also being addressed, such as:

- Does water penetrate into the annulus through a small defect?
- How does corrosion product spread around the annulus from the leak point?
- Does the formation of corrosion product in a constricted annulus cause any expansive damage to the copper canister?
- What is the effect of water penetration on the insert lid seal?
- Is there any detectable corrosion at the copper welds?
- Are there any deleterious galvanic interactions between copper and cast iron?
- Does corrosion lead to failure of the lid on the iron insert?

The experiments were set up between September 2006 and February 2007 and the detailed design, experimental set up and initial results up to May 2008 are reported in Smart and Rance (2009). The five experiments are automatically monitored and the experimental data were obtained and analysed. This progress report includes the data obtained up to February 2013 and follows four previous progress reports that present data up to December 2011 (Smart et al. 2010a, b, 2011a, 2012b). The present report is the final progress report in this sequence, although monitoring will continue. This report contains a summary of the all the processed data obtained up to February 2013. The results of the test programme were presented at the 4th International Workshop on Long-Term Prediction of Corrosion Damage in Nuclear Waste Systems, Bruges, June 2010 (Smart et al. 2011b). One of the MiniCan experiments, Experiment 3, was removed for analysis during 2011 and details of this analysis are presented in a separate report (Smart et al. 2012a).

2 Experimental

The four remaining experiments set up in the boreholes at Äspö HRL are being logged automatically by computer-controlled data logging equipment. The detailed experimental layout and test conditions are given in reference Smart and Rance (2009) and summarised below.

2.1 Test layout and test conditions

Figure 2-1 shows the layout of the experiments in the boreholes in the Äspö HRL, Figure 2-2 shows the layout of the canisters and the other test pieces inside the support cages and Figure 2-3 shows the insertion of the copper model canisters into the support cages. A summary of the test environments inside the five experiments is given in Table 2-1. In three out of the five experiments a layer of bentonite was mounted inside an annulus between two concentric cylinders around the model canister. The purpose of the bentonite is to condition the chemistry of the incoming groundwater so that it is representative of the repository situation. However, it should be noted that these experiments use a lower bentonite density than is proposed for the SKB repository. The cage prevents direct contact between the bentonite and the surface of the canister in order to avoid blockage of the defect introduced into the copper container. The bentonite holder was filled with compacted bentonite pellets mixed with bentonite powder at a density designed to give a high permeability and low swelling pressure, with the aim of allowing bentonite-conditioned groundwater to reach the model canister rapidly.

In the fourth experiment the model canister was surrounded by compacted bentonite, to simulate as exactly as possible the real exposure conditions in the repository, although in this situation it is expected that the extent of corrosion will be limited by the supply of water and diffusion of sulphide through the compacted, low permeability bentonite (Bond et al. 1997). In this experiment, where the model canister was in direct contact with the compacted bentonite, there was no inner cylinder and hence no annulus of bentonite, but rings of saturated compacted bentonite were machined to slide over the model canister, inside the outer cylinder. Clay Technology (Lund, Sweden) machined the rings to size. The use of fully saturated bentonite should minimise the time required to achieve full saturation and hence to achieve the full swelling pressure of the bentonite. The thicknesses of the outer cylinder of the support cage and the outer filter cylinder were selected to withstand the swelling pressure exerted by the compacted bentonite (7 MPa). Small holes or slots were machined in the compact bentonite rings to accommodate electrodes and corrosion coupons in the compacted bentonite, and strain gauges on the surface of the model canister.

The fifth experiment was set up without any bentonite around the model canister so that the model canister is exposed directly to raw groundwater without any conditioning by bentonite; this experiment was included to provide a comparison with the experiments with bentonite present to examine whether any biofilm develops on the surface of the canister and to examine its effect on corrosion behaviour. For this experiment, where the canister is directly exposed to groundwater, the perforated steel cage was used to hold the model canister, but no bentonite was placed inside it. Consequently the groundwater enters directly into the vicinity of the model canister.

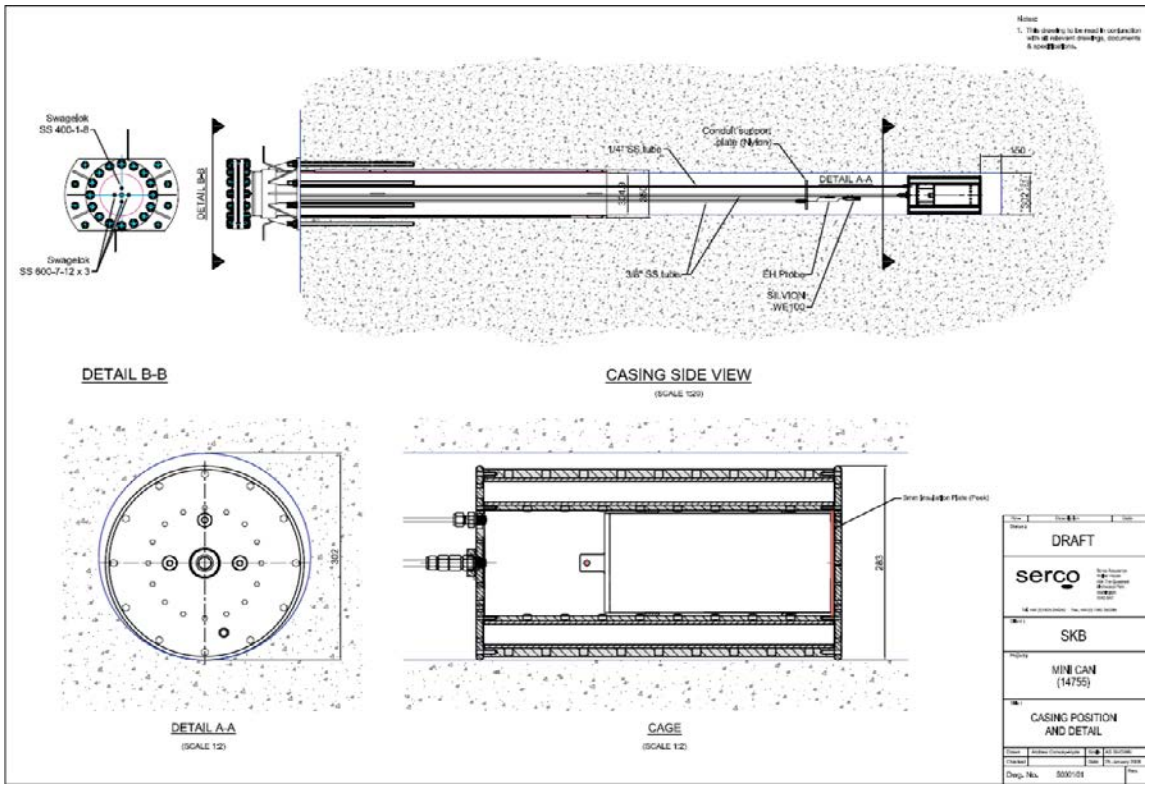

Figure 2-1. *Layout of model canister experiments in borehole.*

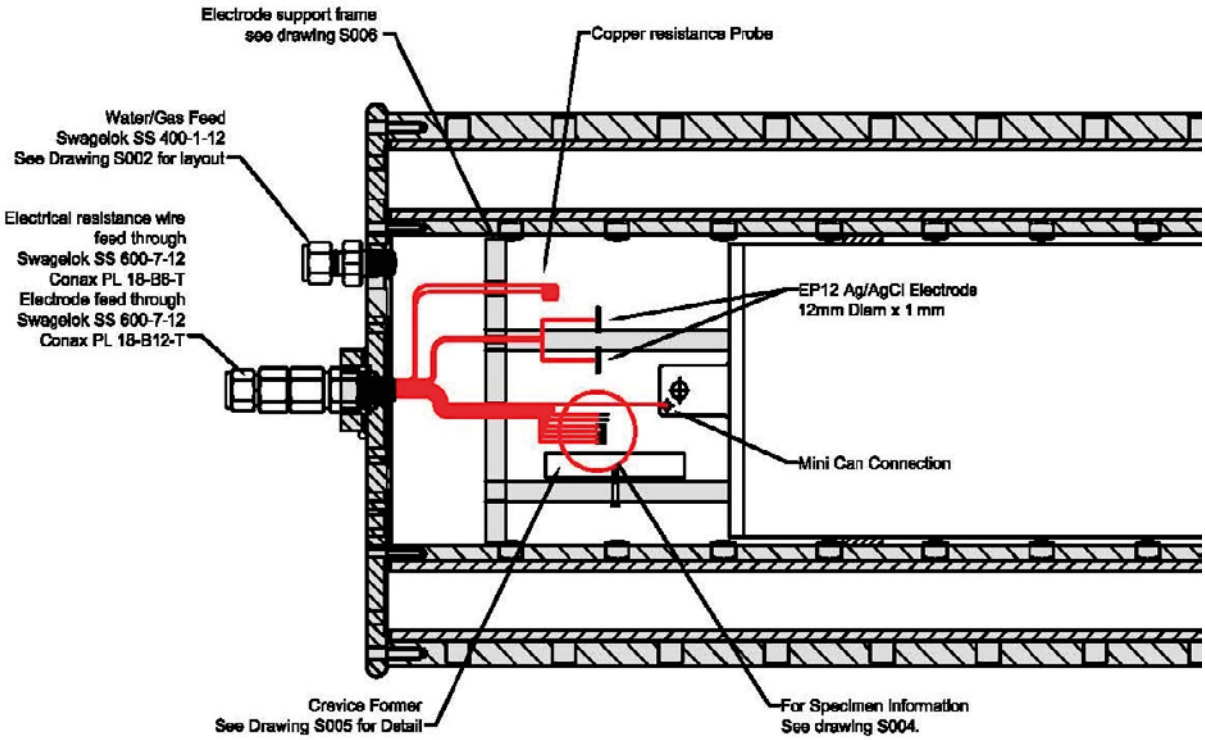

Figure 2-2. *Layout of model canister and sensors inside support cage.*

Figure 2-3. Left: Strain gauges mounted on model canister; Centre: Positioning of bentonite pellets inside annulus of support cage; Right: insertion of model canister assembly into support cage.

Table 2-1. Summary of test conditions for model canister experiments.

Experiment number (Borehole number)	Environment and defect details
1 (KA3386A02)	Low density, high permeability bentonite in annulus around model canister. Single defect near top weld, pointing vertically upwards. Strain gauges fitted.
2 (KA3386A03)	Low density, high permeability bentonite in annulus around model canister. Single defect near top weld, pointing vertically downwards. Electrical resistance corrosion rate probes fitted.
3 (KA3386A04)	Low density, high permeability bentonite in annulus around model canister. Two defects, one near top weld, pointing vertically upwards, near bottom weld, pointing vertically downwards.
4 (KA3386A05)	Compacted bentonite. Single defect near top weld, pointing vertically downwards. Strain gauges fitted.
5 (KA3386A06)	No bentonite, direct contact of groundwater on model canister. Two defects, both near top weld, one pointing vertically upwards, the other vertically downwards. Electrical resistance corrosion rate probes fitted.

3 Monitoring performance of model canisters

A number of parameters have been measured and monitored over the period since the experiments were set up in late 2006 to February 2013, as follows:

- Electrochemical potential of gold and platinum, and the redox potential, E_h.
- Corrosion potential of cast iron, copper and the miniature canister itself.
- Response of strain gauges on two experiments.
- In situ corrosion rate measurements for copper and cast iron.
- Water composition (including gas analysis and microbial measurements).

The reference electrodes used were:

- Two small silver-silver chloride reference disc electrodes inside each support cage (World precision instruments EP series).
- Long-life reference electrodes for cathodic protection (CP) purposes (Silvion silver-silver chloride reference electrodes), which were mounted outside the support cage but immersed in the borehole water.

The redox potential of the environment was measured by means of a gold wire and a platinum flag located near to the model canister inside the support cage and an E_h sensor located outside the support cage (Cumberland Electrochemical Ltd Pt/Ir mixed metal oxide, MOx, probe, which has been successfully used embedded in cementitious grout to monitor fluctuations in redox conditions).

The sensors were supported from a nylon support rack inside the void above the model canister (see Figure 2-2). All reference electrodes were calibrated before installation.

3.1 Water analysis

After installation, water samples were taken for analysis at periodic intervals. Äspö staff carried out the required water analysis. Water samples were extracted through stainless steel tubes that passed out through the borehole flange. For each borehole it was possible to extract samples from both within the support cage itself and from the borehole surrounding the model canister experiment. There was a continuous bleed of gas from each borehole flange to prevent the development of a gas-filled space within the borehole. This gas is assumed to be nitrogen (see Section 4.1.5). The concentration of dissolved gases was determined by Microbial Analytics Sweden AB. The concentrations of the following gases were analysed: H_2, He, O_2, N_2, Ar, CH_4, CO_2, CO, C_2H_6, C_2H_4, C_2H_2, C_3H_8, C_3H_6. The microbial analysis was also carried out by Microbial Analytics and was used to measure a number of parameters including the following:

1. The total number of microorganisms.
2. The number of aerobic cultivable bacteria.
3. Biomass measured as adenosine triphosphate.
4. The most probable numbers of the following types of bacteria were determined: sulphate reducing bacteria (SRB) and autotrophic acetogens.

A programme of water analysis was carried out regularly in the period February to August 2007 and then no more water samples were taken until October 2008, in order to allow the water chemistry to stabilise without any perturbations. Additional water samples were taken at the end of 2010. To avoid disturbing the experiments, no further water analyses were carried out in 2011 and 2012, except for Experiment 3, prior to its removal for analysis. The water analysis results from 2007, 2008, 2009, 2010 and 2011 (Experiment 3 only) are included in the current report.

3.2 Pressure

The water pressure in the boreholes was initially measured by means of an analogue pressure gauge that was attached to the flanges on each borehole. Later, an electrical pressure gauge was attached to the outlet pipe on the flange and the output was recorded on the datalogging equipment.

3.3 Strain

Strain gauges were applied to measure changes in the strain on the outer surface of two of the copper canisters (Tests 1 and 4). The aim of these measurements was to provide an indication of whether expansion caused by internal corrosion has caused any dimensional changes. Standard strain gauge monitoring technology using bi-axial strain gauges was applied (e.g. Techni-Measure Ltd) using cyanoacrylate adhesives, and protected with waterproof coatings.

Experiments 1 and 4 both had two strain gauges mounted on the outer surface of the canister, one near the top (1a,b and 4a,b) and one near the middle (1c,d and 4c,d), with each strain gauge comprised of two perpendicular elements (see Figure 2-3). The elements were oriented at 45° to the vertical axis of the canister. The (a) and (c) elements, and the (b) and (d) elements for each of the sensors were oriented in the same direction with respect to the vertical axis of the canister.

3.4 Corrosion coupons

A number of types of corrosion coupons were mounted within the cage used for the model canister experiments, as follows:

- *Plain corrosion coupons of copper and cast iron.* The corrosion rate of the materials will be determined from weight loss measurements at the end of experiments. One weight loss sample for each material was installed in each experiment. These coupons were suspended from the nylon mounting rack using polypropylene thread.
- *Coupons of copper and cast iron that are electrically connected to the exterior of the borehole.* These were designed to allow the corrosion potential of the electrodes to be measured. It was also possible to carry out electrochemical measurements of the corrosion rate of these coupons using linear polarisation resistance, LPR, AC impedance, ACI, and electrochemical noise, ECN. Platinised titanium gauze was used as the counter electrode in a conventional 3-electrode electrochemical cell. Electrical connections were made to the coupons using copper wire for the copper coupons and carbon steel wire for the cast iron coupons.
- *Copper electrical resistance wire probes*. These were set up to measure the corrosion rate of copper using the technique proposed previously by VTT (e.g. Saario et al. 2004). Each coil consisted of a total length of 112.5 cm of 1 mm diameter copper wire (99.9% purity, Advent Cu513918). The wire was divided into three regions each of 37.5 cm length by applying heat shrinkable, adhesive-lined polymer tubing to the end sections, leaving the middle section exposed to the test environment. The complete wire was formed into a spiral with a diameter of ~1 cm. The two screened lengths were used as reference resistances and the change in the resistance of the exposed length was used to calculate the corrosion rate. This information was processed by the ACM Field Machine electrochemical unit (see Section 3.7).
- *Stress corrosion test specimens.* Four Wedge Opening-loaded (WOL) specimens were mounted in the boreholes. They were machined from a scrap copper lid provided by SKB and they were pre-cracked to give a range of stress intensity factors. In addition, four U-bend specimens were manufactured from the same lid material, with dimensions of 2.5×80×20 mm. Two U-bend specimens and two WOL specimens were mounted in each of experiment boreholes 3 and 4, by loosely suspending them from the stainless steel push rod using plastic connectors. They were thus exposed directly to the groundwater. They will be examined for any indications of SCC at the end of the experiments.

- *Copper-cast iron sandwich specimens to investigate jacking effects.* These specimens were based on the multi-crevice assembly specimen used in previous galvanic corrosion experiments (Smart et al. 2004a), in which cast iron castellated nuts were tightened against sheets of copper. The aim of these specimens was to investigate a number of possible corrosion mechanisms, including crevice corrosion, galvanic corrosion and expansive corrosion. They consisted of a sheet of copper which was clamped against a block of cast iron using a ring of nylon bolts. To investigate the effect of separation distance between mating surfaces a series of steps was machined into the surface of the cast iron to give separation distances between the mating surfaces ranging from direct contact around the edges of the specimens, increasing in steps of 10 μm to 30 μm. The materials used for the sandwich specimens were prepared from copper sheet and the same type of cast iron used for the insert in the model canisters. The specimens will be removed and examined at the end of the exposure period.

The corrosion coupons and electrodes present in Experiment 3 have been examined and the results of this examination are given in two separate reports (Smart et al. 2013, Aggarwal et al. 2015).

3.5 Mounting system for sensors and corrosion test pieces

The corrosion coupons and environmental sensors were supported on a nylon rack which was placed inside the stainless steel support cage above the model canisters before the support cage was sealed (Figure 2-2). It was positioned on the top of the model canisters by means of support legs. Electrical connections were taken out through Conax compression fittings in the support cage lid. For Test 4, where the model canister was embedded in compacted bentonite, the corrosion coupons and sensors were placed in slots that were machined into the compacted bentonite before it was loaded into the supporting cage.

3.6 Electrical connections

A summary of the sensors in each of the experiments and the conduits required for the connecting cables and details of output from each experiment is reported in Smart and Rance (2009). Connecting wires from metal samples inside the canister cage (i.e. corrosion coupons and the model canister itself) were passed through compression glands (316L stainless steel Conax fittings) and connected to cables that were taken out to the external environment through stainless steel tubes that were attached to the supporting cages using Swagelok-type pressure fittings. All connections were made using soldered joints, which were then sheathed in polymeric heat shrink tubing. It should be noted that the electrochemical measurements rely on the integrity of the sheathing system being maintained throughout the experiments (when Experiment 3 was removed the sheathing appeared to have retained its integrity satisfactorily (Smart et al. 2012a)). The tubes were passed through the stainless steel flange at the entrance to the boreholes using bulkhead compression fittings.

3.7 Monitoring equipment

The electrochemical monitoring is being performed using an ACM Ltd Field Machine and an Agilent datalogger. The ACM equipment is being used to carry out the electrochemical measurements of corrosion rate (10 channels) and measurements of electrical resistance of the copper wire electrodes (2 channels), and the Agilent datalogger is used to monitor the potentials of the various electrodes, together with monitoring the strain gauges. The datalogging equipment is located in a control room near the boreholes and data is then transmitted via the Internet to Amec Foster Wheeler for analysis.

Corrosion rate measurements were carried out using the following electrochemical techniques: linear polarisation resistance, AC impedance and electrochemical noise. The LPR measurements were carried out over a potential range of ± 10 mV with respect to the corrosion potential at a scan rate of 10 mV min^{-1} (starting with the electrode polarised to –10 mV). The corrosion rate is obtained by measuring the slopes of the plots and applying the Stern-Geary approximation (ASTM 2003),

with an assumed Stern-Geary constant of 26 mV[1]. The AC impedance measurements were carried out using a perturbation of ± 10 mV, starting at an initial frequency of 10 kHz and a final frequency of 10 mHz, with 100 readings taken per test. The electrochemical noise measurements were carried out at a sampling rate of ten readings per second for a period of one hour.

[1] This value is commonly assumed for measuring the corrosion rate of steel in concrete (e.g. J.A. Gonzalez and C. Andrade, *Effect of Carbonation and Relative Ambient Humidity on the Corrosion of Galvanized Rebars Embedded in Concrete*, British Corrosion Journal 17(1), 21, 1982.).

4 Results

It should be noted that the raw data for the electrochemical measurements are presented in Appendix 1 (Experiments 1–3 and 5, Figures A1-1 to A1-23) and Appendix 2 (Experiment 4, Figures A2-1 to A2-5), and the data from the microbial and gas analyses are presented in the reports Lydmark and Hallbeck (2011) and Hallbeck et al. (2011).

4.1 Water analysis

The results from the water analyses (SO_4^{2-}, HCO_3^-, sulphide, Fe^{2+} and pH) taken from both within the support cage and external to the support cage in the borehole for the five experiments for samples taken in May 2007, October 2008, December 2010 and August 2011 (Experiment 3, inside support cage only) are given in Table 4-1.[2] In December 2010 data were obtained from both outside and inside the support cages in Experiments 1 to 5 (except for Experiment 4, where it was not possible to extract a water sample from within the support cage containing compacted bentonite), whereas in 2007 and 2008 data from outside the support cages were only obtained for Experiment 2, in order to minimise any changes in experimental conditions inside the support cages of the other experiments. The previous data obtained up to October 2007 (Smart and Rance 2009) (Figure 4-1 to Figure 4-8) showed small differences between the internal and external compositions. The data given in Table 4-1 are shown graphically in Figure 4-9, Figure 4-10 and Figure 4-11 for sulphide, iron and pH respectively, to show the effect of time on the variation in the values. The results for each of these parameters are reviewed below.

4.1.1 Sulphide

The sulphide concentrations over the complete monitoring period were in the range 0 to 0.22 mg L^{-1}, with the greatest range observed in the 2007 data. The values measured in 2008 were lower than the values measured in 2007, in some experiments by a factor of two. The overall sulphide concentrations were generally low (at least three orders of magnitude less than the sulphate concentration). The data obtained in 2010 show that the sulphide concentrations had generally increased since 2008 (Figure 4-9), reaching a maximum value of 0.084 mg L^{-1} inside the experiment with no bentonite at all (Experiment 5). In some experiments the sulphide concentration was higher in the borehole compared to the concentration inside the support cage in the 2010 measurement (e.g. in Experiments 1 and 2), whereas in Experiments 3 and 5 the concentration was higher inside the support cage than in the borehole water. For comparison, the most recent sulphide concentration value for the interior of Experiment 3 taken in August 2011 (~1,600 days after sampling in May 2007), prior to removal of the canister for analysis, was 0.045 mg L^{-1} (Smart et al. 2012a).

4.1.2 Iron concentrations

The greatest variation between the internal and external ion concentrations (Figure 4-10) was found in the dissolved iron analyses, with values ranging in the 2010 analysis from a minimum value of 0.11 mg L^{-1} external to the support cage (e.g. in boreholes 1 and 2) compared to a maximum value of 55.69 mg L^{-1} inside the support cage in experiments with low density bentonite (Experiments 1 to 3) or no bentonite at all (Experiment 5). Similar variation was noted previously in 2007 and 2008. For example in 2008 there was a minimum Fe^{2+} concentration of 0.15 mg L^{-1} external to the support cage compared to values up to 19.2 mg L^{-1} inside the support cage. For comparison, the most recent iron concentration value for Experiment 3 taken in August 2011 (~1,600 days after sampling in May 2007), prior to removal of the canister for analysis, was 39.17 mg L^{-1} (Smart et al. 2012a, Hallbeck et al. 2011), which represents a further increase since the 2010 analysis. Overall the Fe^{2+} concentrations inside the support cages have increased significantly since 2008, as shown in Figure 4-10, and the rate of release appears to be increasing with increasing time.

[2] The ± figures in the tables containing water analyses refer to the uncertainty for the analyses. So for example, for a measured chloride value (± 5%) of 1,000 mg L^{-1}, the true value could be between 950 mg L^{-1} and 1050 mg L^{-1}. The reported uncertainty is the combined uncertainty covering all steps of the measurement process and has a confidence level of 95%.

Table 4-1. Chemical composition of the water from inside and the outside (the letter G after the experiment number indicates that the samples were taken from within the borehole but outside the model canister support cage) of the Model Canister experiments sampled in May 2007, October 2008, December 2010 and August 2011.

Experiment number	SO_4^{2-} (mg L^{-1}) (± 12%)				HCO_3^- (mg L^{-1}) (± 4%)				sulphide (mg L^{-1}) (± 32%)			
Sampling date	05-2007	10-2008	12-2010	08-2011	05-2007	10-2008	12–2010	08-2011	05-2007	10-2008	12-2010	08-2011
1	486	417	376		28	19	14		0.036	0.021	0.037	
1G			462				17				0.080	
2	506	413	430		27	20	14		0.057	0.020	0.044	
2G	354	481	444		28	23	17		0.062	0.023	0.055	
3	439	410	400	271	51	38	32	34	0.037	0.022	0.059	0.045
3G			411				34				0.049	
4G			385				43				0.049	
5	605	567	525		14	8	6		0.051	0.030	0.084	
5G			432				21				0.059	

Experiment number	Fe^{2+} (mg L^{-1}) (0.05–1 mg L^{-1} ± 13% 1–3 mg L^{-1} ± 8%)				pH (± 0.1 pH units)			
Sampling date	05-2007	10-2008	12-2010	08-2011	05-2007	10-2008	12-2010	08-2011
1	11.1	19.2	55.69		7.4	7.3	6.5	
1G			0.11				7.5	
2	2.33	4.15	22.56		7.6	7.4	6.7	
2G	0.16	0.15	0.11		7.6	7.6	7.6	
3	0.82	15.7	9.91	39.2	7.6	7.2	7.3	6.6
3G			0.23				7.5	
4G			0.29				7.4	
5	6.30	11.1	29.20		7.6	6.8	6.7	
5G			0.19				7.6	

Note: It is not possible to extract any water for analysis from inside the support cage of Experiment 4, because of the presence of compacted bentonite.

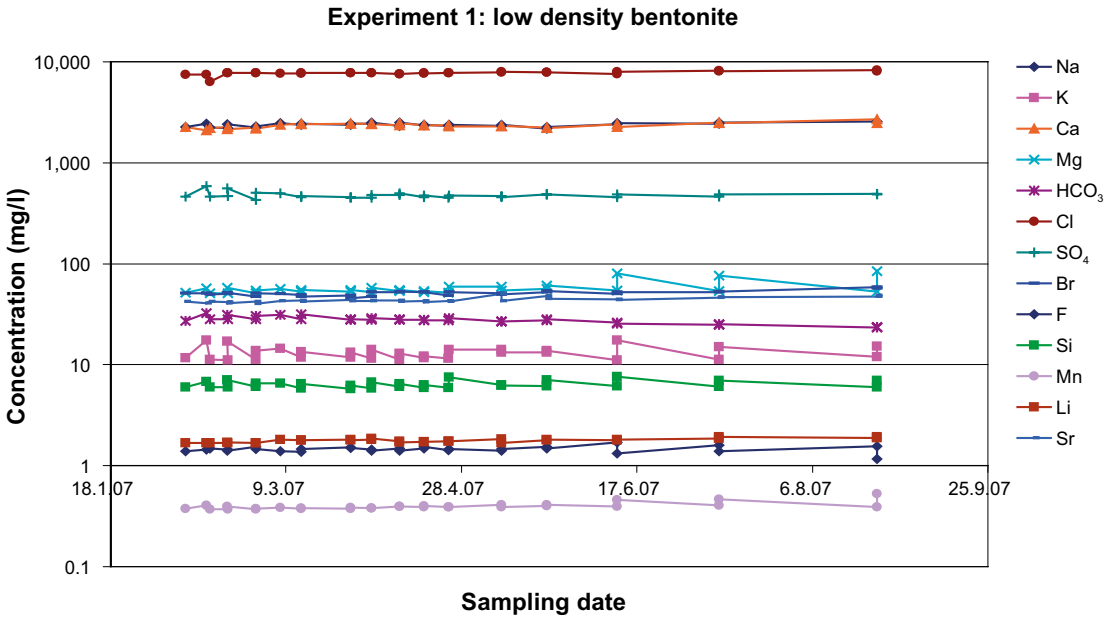

Figure 4-1. *Summary of water analyses: Experiment 1. For any given sampling date the first concentration shown when approaching along the line from the left hand side of the diagram refers to the analysis in the borehole, but outside the support cage, and the point on the right hand side, but on the same date, refers to the concentration on the inside of the support cage. The results of the iron analyses are shown in Figure 4-7.*

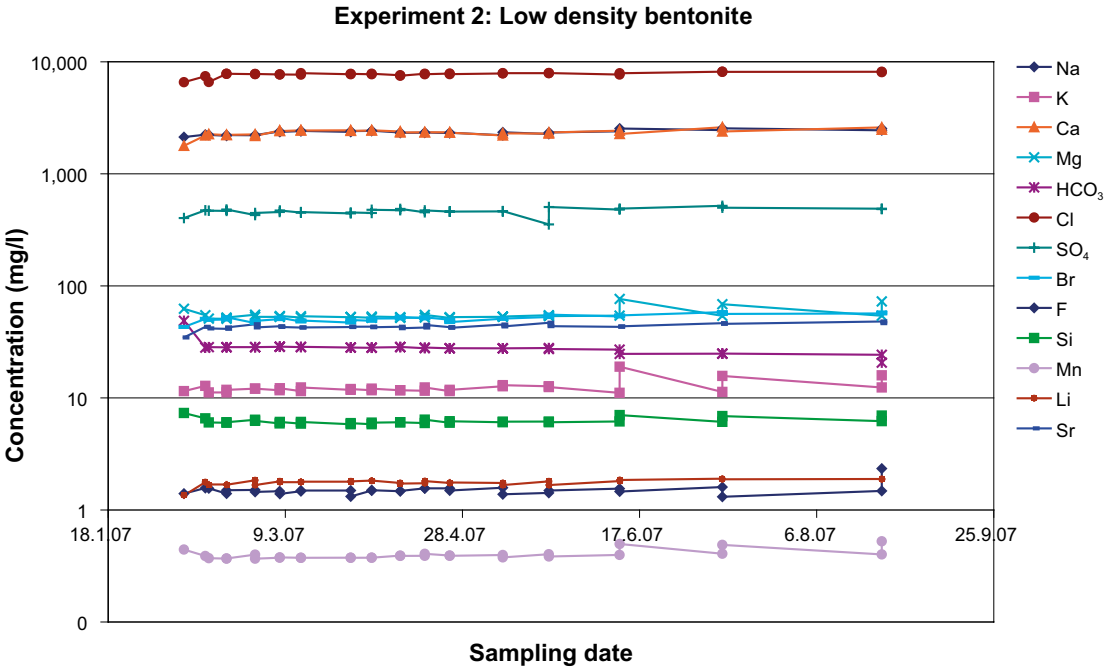

Figure 4-2. *Summary of water analyses: Experiment 2. For any given sampling date the first concentration shown when approaching along the line from the left hand side of the diagram refers to the analysis in the borehole, but outside the support cage, and the point on the right hand side, but on the same date, refers to the concentration on the inside of the support cage. The results of the iron analyses are shown in Figure 4-7.*

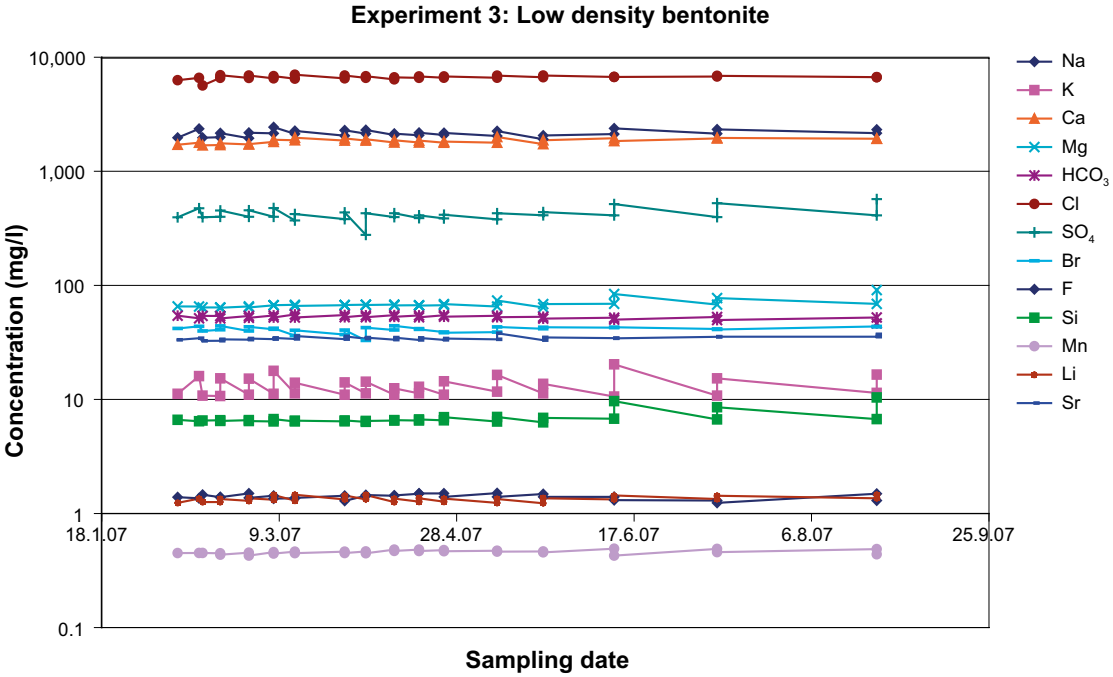

Figure 4-3. *Summary of water analyses: Experiment 3. For any given sampling date the first concentration shown when approaching along the line from the left hand side of the diagram refers to the analysis in the borehole, but outside the support cage, and the point on the right hand side, but on the same date, refers to the concentration on the inside of the support cage. The results of the iron analyses are shown in Figure 4-7.*

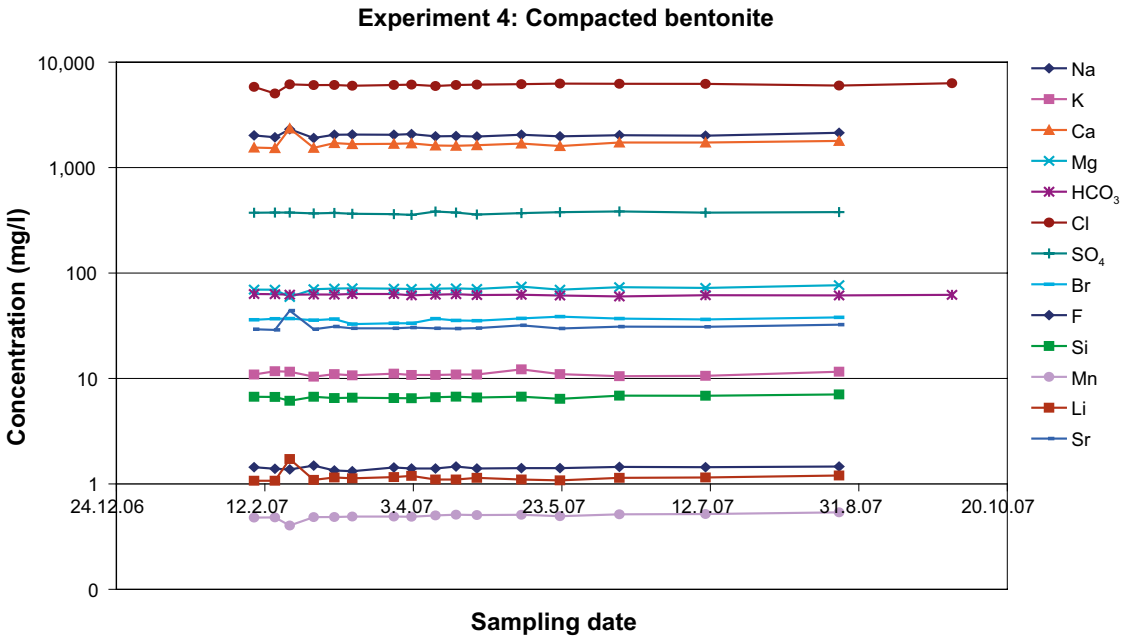

Figure 4-4. *Summary of water analyses: Experiment 4. It was not possible to remove any water from inside the support cage for analysis, so all data refer to a water sample taken from the borehole outside the support cage. The results of the iron analyses are shown in Figure 4-7.*

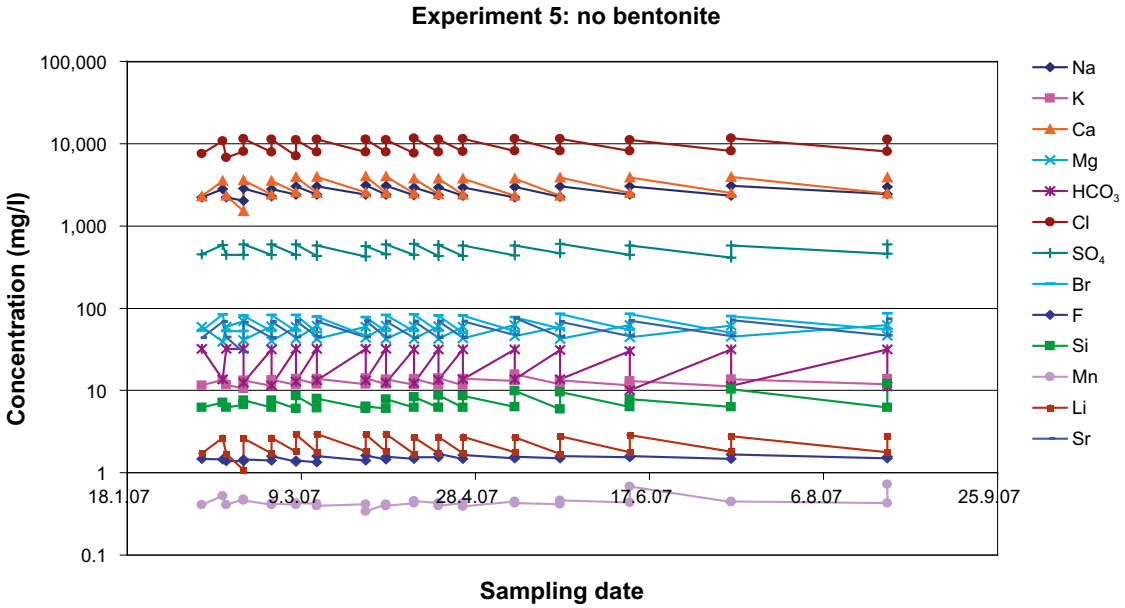

Figure 4-5. *Summary of water analyses: Experiment 5. For any given sampling date the first concentration shown when approaching along the line from the left hand side of the diagram refers to the analysis in the borehole, but outside the support cage, and the point on the right hand side, but on the same date, refers to the concentration on the inside of the support cage. The results of the iron analyses are shown in Figure 4-7.*

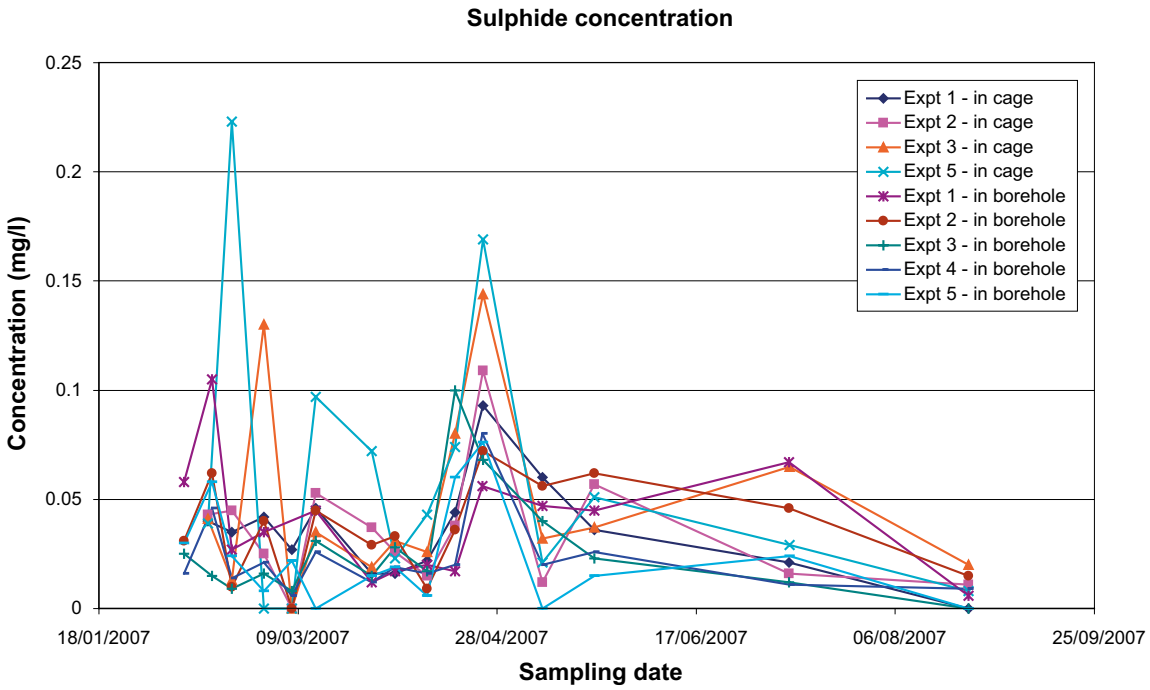

Figure 4-6. *Summary of sulphide concentration in water samples in 2007.*

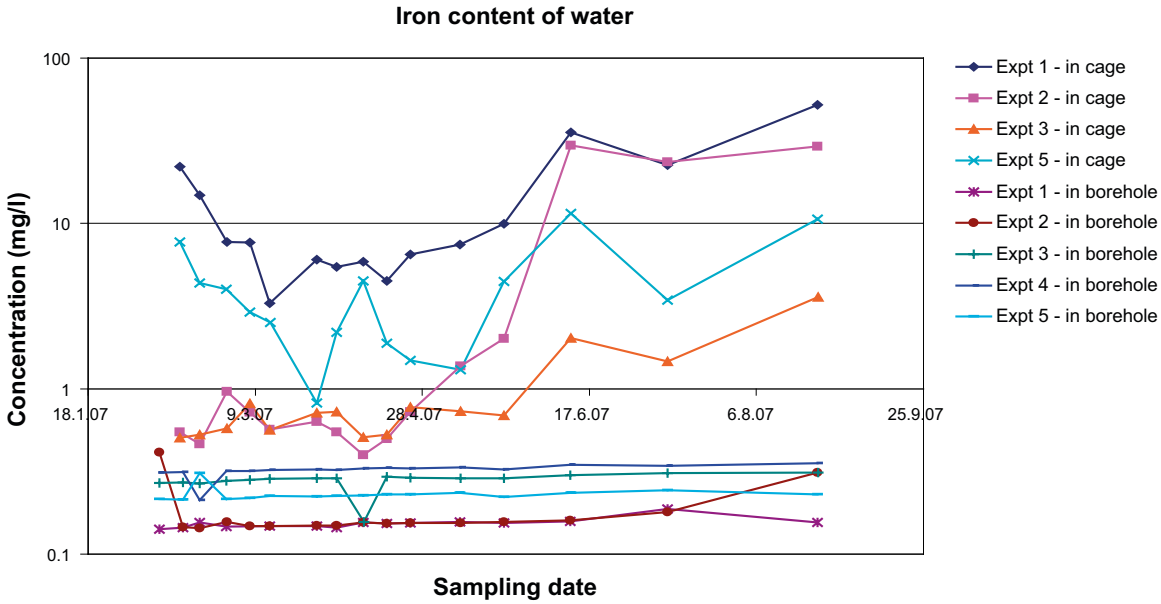

Figure 4-7. *Summary of iron analysis in water samples in 2007.*

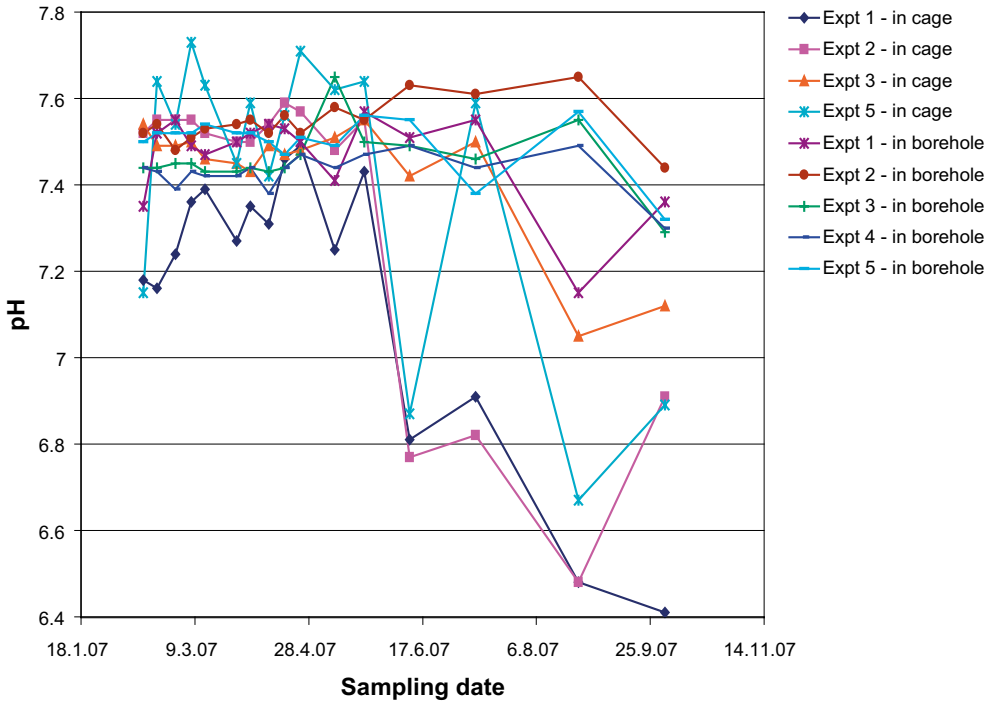

Figure 4-8. *pH of water samples taken from model canister experiments in 2007.*

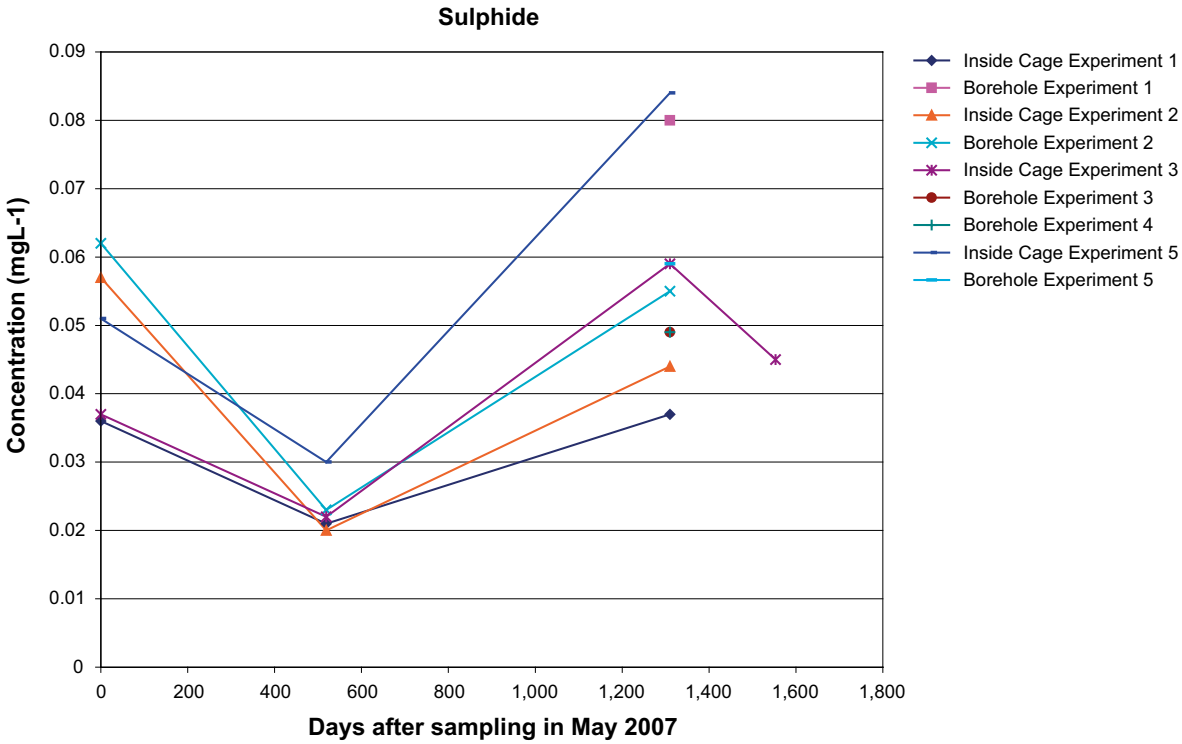

Figure 4-9. *Variation of sulphide concentration with time since the sampling in May 2007 (see Table 4-1).*

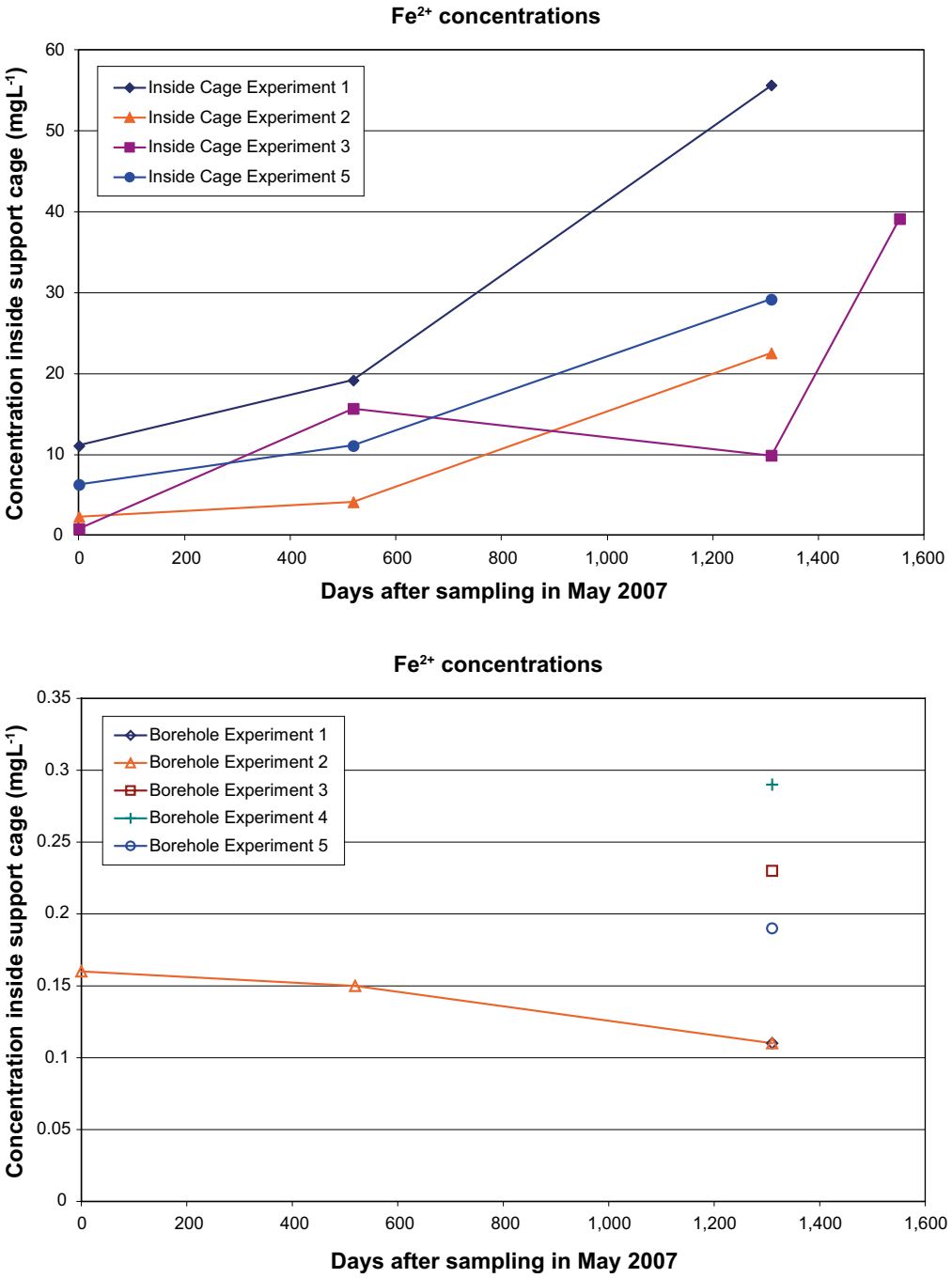

Figure 4-10. *Variation of iron concentration with time since sampling in May 2007: (top) iron concentration inside support cage; (bottom) iron concentration in borehole water (see Table 4-1).*

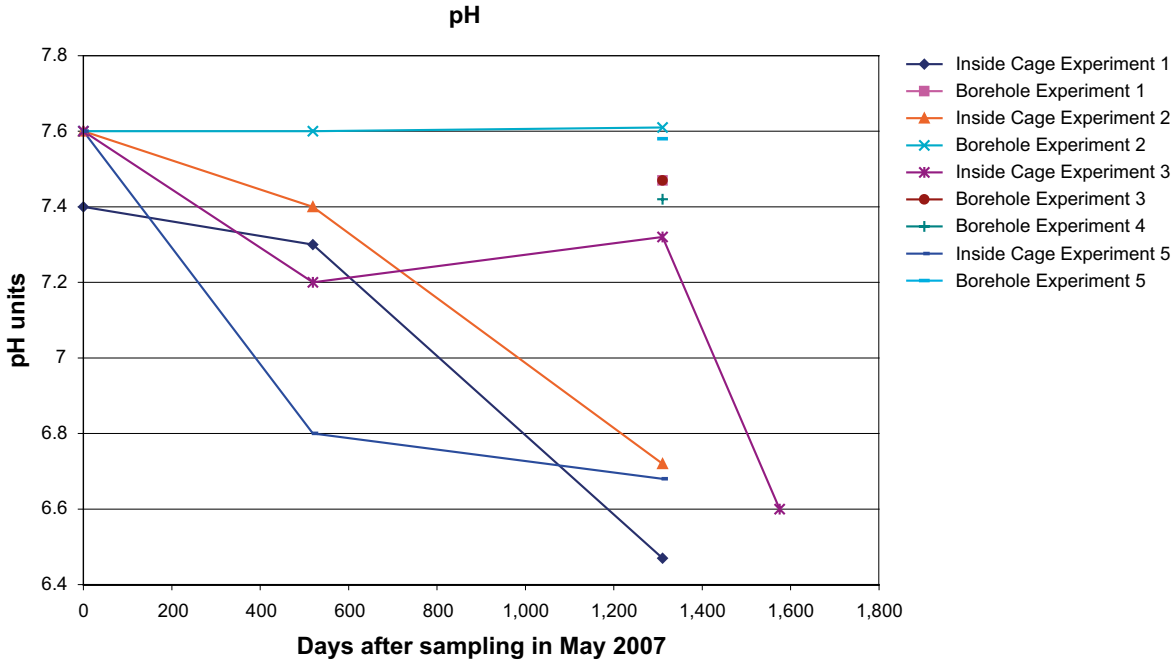

Figure 4-11. *Variation of pH with time since sampling in May 2007 (see Table 4-1).*

4.1.3 pH

The pH values of the water samples taken from inside and outside the support cages are also shown in Table 4-1 and Figure 4-11. These data show a continued decrease in the pH of water inside the support cages compared to the water in the boreholes. The data show pH values of below 7 inside the support cage in the experiments with low density bentonite in the support cage, with Experiment 1 exhibiting a minimum pH of 6.5, compared to the borehole pH value of 7.4–7.6. The most recent pH value for Experiment 3 taken in August 2011 prior to removal of the canister for analysis was 7.0 measured in the field and 6.6 at 25°C in the laboratory (Smart et al. 2012a).

4.1.4 Other elements

Table 4-2 gives the measured concentrations of a range of metallic elements and anions, including those present in trace quantities, together with the total organic content (TOC) and conductivity of the water, for the measurements made in 2008 and 2010. These results show a number of interesting features:

1. It is noticeable that chloride, sodium, calcium, bromide, silicon, total sulphur, manganese, lithium, strontium, barium, cobalt, chromium, nickel and conductivity were all higher in Experiment 5 than in other experiments or in the borehole of Experiment 2. The 2010 data show some distinct differences between the interior and exterior of Experiment 5. The concentrations of nickel and chromium were at least two orders of magnitude greater than in borehole water, suggesting that in Experiment 5 (no bentonite) corrosion of the stainless steel support cage was occurring, as well corrosion of the cast iron insert. Low concentrations of nickel and chromium were observed in Experiments 1, 2 and 3, indicating that most of the increased concentration of iron in these experiments was due to corrosion of the cast iron insert rather than the stainless steel support cage (unless any nickel and chromium released had precipitated as an insoluble corrosion product). The higher concentrations of chloride, sodium, calcium, bromide, silicon, total sulphur, manganese, lithium, strontium and barium in the Experiment 5 borehole indicate that there are local variations in water chemistry, but the reasons for this are currently unknown.
2. There have been changes in the composition of the groundwater since it was analysed in 2008, both internally and externally to the miniature canister experiments. For example, where comparison is possible, it is apparent that the concentrations of the major ions, namely chloride, sodium and calcium, have increased consistently since 2008. This suggests that not only are there local variations in groundwater chemistry (i.e. between boreholes), but that the local composition changes as a function of time, presumably due to changes in flow patterns within the rock mass.

3. The total concentration of sulphur is equivalent to a higher concentration of sulphate than was actually measured (Table 4-1) (the mass of sulphate is 3 × the mass of sulphur) and the difference cannot be accounted for by the measured low concentrations of dissolved sulphide (HS^-) present (Table 4-1), so some sulphur must be present in a form other than sulphate or sulphide. The identity of the missing species is currently unknown. It is also possible that the difference in sulphur content could be due to the presence of iron sulphide colloids or fine particulates; the water was filtered through a 0.45 µm filter when the samples were taken, but it is possible that very small particulates containing sulphur-based species might have passed through and been included in the analyses.
4. The changes in the concentrations of the minor cations, such as magnesium, strontium, potassium, silicon and lithium are small between 2008 and 2010 and probably within the error bands for the analyses. There are slight differences in the strontium concentration in Experiment 5 in 2010 between the internal and external environments.
5. Regarding the elements present in trace amounts (i.e. at µg L^{-1} concentrations) it is noteworthy that the concentration of manganese is higher internally than externally and that manganese is present as a component of the cast iron insert (~0.09 wt%) and the stainless steel (~2 wt%). For example the dissolved concentration internally has increased in some experiments since 2008 (e.g. Experiments 1 and 2) and is higher internally than externally in Experiments 1, 2 and 5. The concentrations of nickel and chromium inside the support cage for Experiment 5 are significantly higher internally than externally and this is assumed to be due to release from the stainless steel support cage; this appears to be more of a feature for the experiment with no bentonite present in the support cage (Experiment 5). The concentration of dissolved copper is extremely small in all experiments (0.0005 µg L^{-1}) and appears to have fallen since 2008.
6. The total organic carbon content has fallen since 2008 in all measurements where comparison is possible.
7. The conductivity has increased since 2008 and this is in agreement with the increased dissolved concentration of the major ions.

4.1.5 Gas analysis

The results of the dissolved gas analyses are shown in Table 4-3 and more details about the sampling and analysis techniques, and the results from analyses in 2007, 2008 and 2010, are given in Lydmark and Hallbeck (2011). The dissolved oxygen concentration in the groundwater was essentially zero (Smart and Rance 2009). The dominant dissolved gas was nitrogen, with significant quantities of helium, argon, carbon dioxide and methane also present. The hydrogen pressure increased in those experiments that can be considered as closed systems (i.e. Experiments 1–3, which had bentonite clay in the steel cage). The concentration of hydrogen was particularly high in Experiment 5 in 2007 (215 µL L^{-1}), much lower (7.3 µL L^{-1}) in 2008 but it increased again in 2010 (> 54 µL L^{-1}). The levels of both carbon dioxide and the alkalinity were lower in 2008 but increased again inside Experiments 1, 2 and 5. Further interpretation of the results of the gas analysis is presented in Lydmark and Hallbeck (2011).

4.1.6 Microbial analysis

The results of the microbial analyses performed in 2007, 2008, and 2010 are summarised in Table 4-4 to 4-6. The details of the measurements and the analyses, which were provided by Microbial Analytics AB, are given in Lydmark and Hallbeck (2011). The general presence and activity of microorganisms was monitored by measuring the total number of cells (TNC), the levels of adenosine-tri-phosphate (ATP) and the number of cultivable heterotrophic aerobic bacteria (CHAB). The only microorganisms analysed specifically were autotrophic acetogens (AA) and sulphate reducing bacteria (SRB), since these are known to influence the corrosion of metals.

To summarise the findings reported in Lydmark and Hallbeck (2011), there has been a succession in the microbial populations; from a complex composition of CHAB, AA and SRB in 2007, towards a composition with higher numbers of SRB and low or undetectable levels of CHAB and AA in 2010. During the period 2007 to 2010, the MPN of SRB from water samples taken inside the steel cages increased.

It should be noted that the microbiological data were obtained on only one sampling occasion per year and because there was not enough water for repeated samples the variations in the measured parameters were difficult to assess. A further set of microbial analyses was carried out when retrieving Experiment 3 in 2011 and the results from these measurements are presented in Hallbeck et al. (2011).

Table 4-2. Chemical composition of the water from inside and outside the support cage around the model canister experiments, as sampled in October 2008 and December 2010 (measurement uncertainty ~ ± 12% unless otherwise noted). Note: a blank cell indicates that no measurement was made.

	Date	Experiment 1	Experiment 1 (borehole)	Experiment 2	Experiment 2 (borehole)	Experiment 3	Experiment 3 (borehole)	Experiment 4 (borehole)	Experiment 5	Experiment 5 (borehole)
Cl (mg L^{-1}) (± 5%)	2008	7,887		7,674	7,926	6,895			11,362	
	2010	8,599.0	8,524	8,373	8,572	7,968	7,973	7,656	11,420	8,905
Na (mg L^{-1})	2008	2,350		2,350	2,330	2,130			2,930	
	2010	2,480	2,470	2,470	2,510	2,340	2,280	2,320	3,100	2,500
Ca (mg L^{-1})	2008	1,910		2,470	2,460	1,930			3,840	
	2010	2,620.0	2,640.0	2,640	2,650	2,430	2,490	2,260	3,910	2,810
Total S (mg L^{-1})	2008	129		186	188	157	156	233		
	2010	132	184	169	182	156	160	152	223	172
Br (mg L^{-1})	2008	49.8		44.7	48.3	35.7			71.3	
	2010	53.3	52.8	53.5	48.90	48.6	48.6	45.4	75.6	55.1
Mg (mg L^{-1})	2008	47.9		51.9	51.3	76.0			42.9	
	2010	51.8	49.1	50.6	49.3	62.7	64.2	66.3	44.6	56.9
Sr (mg L^{-1})	2008	36.7		46.6	46.6	37.8			73.2	
	2010	45.7	46.5	46.6	47.2	41.8	42.9	40.4	66.9	48.6
K (mg L^{-1})	2008	9.0		11.6	11.4	11.0			13.5	
	2010	10.6	10.7	10.8	11.2	10.7	11.3	10.9	12.4	10.9
Si (mg L^{-1})	2008	4.01		6.00	6.04	5.91			9.28	
	2010	4.07	5.8	5.01	5.83	5.96	6.10	6.39	6.95	5.89
F (mg L^{-1})	2008	1.83		1.83	1.75	1.23			1.87	
	2010	1.35	1.53	1.43	1.48	1.43	1.48	1.46	1.56	1.49
Li (µg L^{-1})	2008	1410		1820	1750	1360			2670	
	2010	1860	1880	1920	1850	1660	1670	1530	2830	1960
Mn (µg L^{-1})	2008	362		387	370	490			678	
	2010	691	351	468	349	452	455	485	525	408
Ba (µg L^{-1})	2008	89.0		80.3	78.3	89.8			101	
	2010	135	80.5	89.7	80.6	90.9	85.6	85.2	86.8	100

Table 4-2 continued.

	Date	Experiment 1	Experiment 1 (borehole)	Experiment 2	Experiment 2 (borehole)	Experiment 3	Experiment 3 (borehole)	Experiment 4 (borehole)	Experiment 5	Experiment 5 (borehole)
Mo (µg L^{-1})	2008	54.0		60.1	57.4	60.5			53.4	
	2010									
Zn (µg L^{-1})	2008	1.08		4.03	1.19	< 0.8			4.33	
	2010									
Ni (µg L^{-1})	2008	0.866		2.87	< 0.2	0.971			322	
	2010	0.5830	< 0.5	1.33	< 0.5	< 0.5	< 0.5	< 0.5	74.6	< 0.5
Cu (µg L^{-1})	2008	0.251		0.767	< 0.2	< 0.2			0.283	
	2010	0.0005	0.0005	0.0005	0.0005	0.0005	0.0005	0.0005	0.0005	0.0005
V (µg L^{-1})	2008	0.199		0.275	0.291	0.215			0.0455	
	2010	0.010	0.1600	0.2240	0.0533	0.1810	0.1440	0.3620	0.1430	0.0854
Pb (µg L^{-1})	2008	0.179		0.383	0.152	0.174			0.220	
	2010									
Cr (µg L^{-1})	2008	0.169		1.80	0.159	0.191			248	
	2010	0.1	0.1	0.100	0.100	0.1000	0.1980	0.1000	55.70	0.1000
Co (µg L^{-1})	2008	0.0391		0.152	0.0526	0.022			8.12	
	2010									
NO_2^- (mg L^{-1})	2008	0.0013		0.0006	< 0.0002	0.0008			0.0012	
	2010	0.0003	0.0002	0.0002	0.0002	0.0003	0.0002	0.0002	0.0003	0.0003
NO_3^- (mg L^{-1})	2008	0.0010		< 0.0003	0.0015	0.0021			0.0006	
	2010	0.0007	< 0.0003	< 0.0003	< 0.0003	< 0.0003	< 0.0003	< 0.0003	0.0006	< 0.0003
PO_4^{3+} (mg L^{-1})	2008	<0.0005		< 0.0005	< 0.0005	< 0.0005			< 0.0005	
	2010	<0.0005	< 0.0005	< 0.0005	< 0.0005	< 0.0005	0.0007	< 0.0005	0.0010	< 0.0005
TOC (mg L^{-1})	2008	3.2		1.9	1.3	3.6			1.2	
	2010	1.7	1.1	1.2	1.1	1.5	1.5	1.4	1.0	1.1
Conductivity, mS m^{-1}	2008	2230		2178	2197	1975			2960	
	2010	2,347	2,353	2,336	2,342	2,196	2,193	2,115	3,033	2,422

Table 4-3. Dissolved gas in the water from the model canister experiments sampled in September 2007, October 2008 and August 2010 (bd = below detection level).

Gases	Date	Experiments				
		1	2	2 G	3	5
Gas/water (mL L^{-1})	09-07	68	128	76	69	112
	10-08	90	109	103	53	86
	08-10	69.7	74.4	70.2	67.9	83.5
H_2 (µL L^{-1})	09-07	0.22	0.52	0.22	0.10	215
	10-08	90.1	0.57	0.52	0.55	7.3
	08-10	> 18.5	4.5	1.1	17.2	> 54.1
CO (µL L^{-1})	09-07	0.58	1.08	3.39	0.72	1.14
	10-08	0.52	0.53	0.70	0.69	6.8
	08-10	0.28	0.26	0.26	0.25	0.43
CH_4 (µL L^{-1})	09-07	326	317	210	245	117
	10-08	500	593	344	215	216
	08-10	329	387	271	167	183
CO_2 (µL L^{-1})	09-07	913	786	186	1,850	843
	10-08	338	284	338	568	394
	08-10	664	799	66.1	465	679
C_2H_6 (µL L^{-1})	09-07	0.33	0.20	0.09	0.12	0.65
	10-08	bd	018	bd[a]	0.28	1.08
	08-10	0.24	0.32	0.04	0.1	0.44
C_2H_{2-4}* (µL L^{-1})	09-07	0.14	0.17	bd	0.02	bd
	10-08	bd	bd	bd	bd	bd
	08-10	< 0.1	< 0.1	< 0.1	< 0.1	< 0.1
C_3H_8 (µL L^{-1})	09-07	bd	bd	bd	bd	bd
	10-08	bd	bd	bd	0.05	0.05
	08-10	< 0.1	< 0.1	< 0.1	< 0.1	< 0.1
C_3H_6 (µL L^{-1})	09-07	bd	bd	bd	bd	bd
	10-08	bd	bd	bd	bd	bd
	08-10	< 0.1	< 0.1	< 0.1	< 0.1	< 0.1
Ar (µL L^{-1})	09-07	838	1,060	649	849	710
	10-08	1,110	1,190	740	185	bd
	08-10	626	425	589	773	1,120
He (µL L^{-1})	09-07	7,980	8,420	8,110	4,920	14,200
	10-08	9,990	9,100	9,070	6,600	14,900
	08-10	8,670	9,180	8,800	7,030	12,500
N_2 (µL L^{-1})	09-07	57,800	118,000	67,100	61,100	95,600
	10-08	77,400	91,900	98,200	44,900	71,200
	08-10	59,400	63,600	60,400	59,500	68,900
O_2 (µL L^{-1})	09-07	bd	bd	bd	bd	bd
	10-08	bd	bd	bd	bd	bd

* i.e. C_2H_2 + C_2H_4

Table 4-4. The microbial composition inside and the outside (2G) the model canister experiments sampled in 05-2007.

Experiment	ATP (amol mL^{-1})	TNC (mL^{-1})	Q-PCR 16S DNA (mL^{-1})	CHAB (mL^{-1})	MPN SRB (mL^{-1})	Q-PCR active SRB (relative activity)	Q-PCR total SRB (mL^{-1})	MPN AA (mL^{-1})	Q-PCR AA (relative activity)	Acetate (mg L^{-1})
1	2,400 ± 450 [a]	130,000 ± 16,000 [a]	na [b]	227 ± 42 [a]	5,000 (2,000–17,000) [c]	10	na [b]	30,000 (2,000–17,000) [c]	631	8.5
2	2,800 ± 240 [a]	95,000 ± 39,000 [a]	na [b]	200 ± 57 [a]	1,400 (600–3,600) [c]	2	na [b]	50,000 (20,000–200,000) [c]	10	8
2 G	3,300 ± 710 [a]	31,000 ± 11,000 [a]	na [b]	20 ± 35 [a]	3 (1–12) [c]	3	na [b]	3 (1–12) [c]	3	6.9
3	15,500 ± 810 [a]	150,000 ± 61,000 [a]	na [b]	530 ± 28 [a]	230 (90–860) [c]	2	na [b]	7,000 (3,000–21,000) [c]	336	6.9
5	3,000 ± 680 [a]	13,000 ± 4,900 [a]	na [b]	17 ± 12 [a]	300 (100–1,100) [c]	1	na [b]	bd [c]	1	11

[a] ± standard deviation
[b] not analysed
[c] 95% confidence interval

Key

ATP	adenosine triphosphate
TNC	total number of cells
CHAB	number of cultivable heterotrophic aerobic bacteria
MPN	most probable numbers
AA	autotrophic acetogens
SRB	sulphate-reducing bacteria
Q-PCR	quantitative real time polymerase chain reaction
DNA	deoxyribonucleic acid

Table 4-5. The microbial composition inside and outside (2G) the model canister experiments sampled in October 2008.

Experiment	ATP (amol mL^{-1})	TNC (mL^{-1})	Q-PCR 16S DNA (mL^{-1})	CHAB (mL^{-1})	MPN SRB (mL^{-1})	Q-PCR active SRB (mL^{-1})	Q-PCR total SRB (mL^{-1})	MPN AA (mL^{-1})	Q-PCR active AA (mL^{-1})	Acetate (mg L^{-1})
1	17,400 ± 2,500 [a]	180,000 ± 4,600 [a]	6,700,000	bd [b]	5,000 (2,000–17,000) [c]	5,500	540,000	1.7 (0.7–4) [c]	bd [b]	1.7
2	10,400 ± 690 [a]	180,000 ± 18,000 [a]	4,500,000	3 ± 6 [a]	800 (300–2,500) [c]	31	37,000	17 (7–48) [c]	bd [b]	1.6
2G	4,400 ± 570 [a]	2,500 ± 880 [a]	8,000,000	bd [b]	2.3 (0.9–8.6) [c]	bd [b]	bd [b]	0.4 (0.1–1.7) [c]	bd [b]	2.9
3	27,400 ± 1,820	200,000 ± 22,000 [a]	5,000,000	bd [b]	70 (30–210) [c]	350	74,000	90 (30–290) [c]	bd [b]	1.8
5	18,600 ± 1,270 [a]	71,000 ± 11,000 [a]	14,000,000	bd [b]	110 (40–300) [c]	bd [b]	11,000	2,700 (1,200–6,700) [c]	bd [b]	2.3

[a] ± standard deviation
[b] below detection limit
[c] 95% confidence interval

Key

ATP adenosine triphosphate
TNC total number of cells
CHAB number of cultivable heterotrophic aerobic bacteria
MPN most probable numbers
AA autotrophic acetogens
SRB sulphate-reducing bacteria
Q-PCR quantitative real time polymerase chain reaction
DNA deoxyribonucleic acid

Table 4-6. The microbial composition inside and outside (2G) the model canister experiments sampled in August 2010.

Experiment	ATP (amol mL^{-1})	TNC (mL^{-1})	CHAB (mL^{-1})	MPN SRB (mL^{-1})	MPN AA (mL^{-1})	Acetate (mg L^{-1})
1	3,100 ± 1,710[a]	72,000 ± 10,000[a]	bd[b]	24,000 (10,000 – 94,000)[c]	bd[c]	3.5
2	5,800 ± 1,220[a]	320,000 ± 52,000[a]	bd	8,000 (3,000 – 25,000)	bd[c]	2.9
2G	27,700 ± 3,770[a]	4,400 ± 1,100[a]	bd	< 2	bd[c]	1.8
3	6,800 ± 2,330[a]	120,000 ± 7,800[a]	bd	800 (300 – 2,500)	bd[c]	1.8
5	3,700 ± 840[a]	22,000 ± 1,500[a]	bd	7,000 (3,000 – 21,000)	bd[c]	2.8

[a] ± standard deviation
[b] below detection limit
[c] 95% confidence interval

4.1.7 Pressure

The results from the pressure gauges in the boreholes are shown in Figure 4-12. Unfortunately there was a loss of data due to a fault with the datalogging system during the winter of 2007/8 and due to breakdown of the computer during the winter of 2011 and 2012. The data show that there is a general tendency for the pressure to fall with time, although the rate of decrease has fallen and the pressures have stabilised and increased slightly in recent months. The low pressure is mainly due to water loss through the rock face surrounding the boreholes.

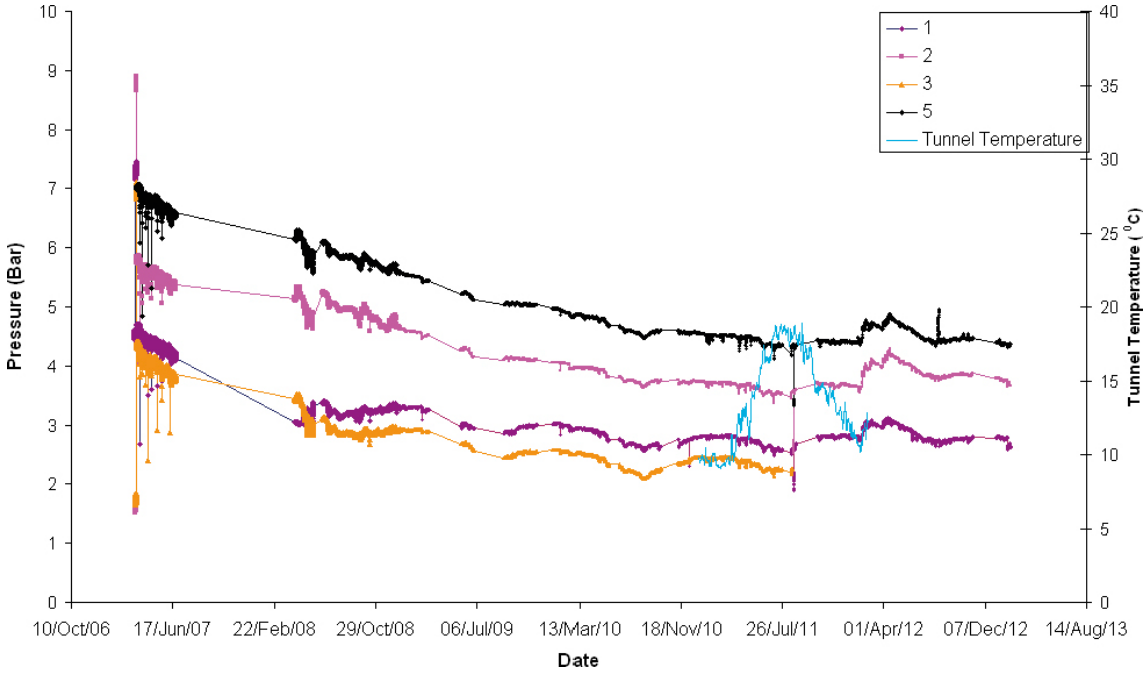

Figure 4-12. *Pressure reading for borehole 1 to 5 (pressure inside support cage, no measurements possible for Experiment 4 because of presence of compacted bentonite). Temperature of tunnel is also shown to illustrate pressure.*

4.2 Electrochemical potential measurements

This section presents the electrochemical potential measurements for each of the model canister experiments. Some of the figures also include the results of corrosion rate measurements (see Section 4.3). The exposure period for all experiments up to the end of the data shown in this report was ~54,000 hours (i.e. ~6.2 years). All electrochemical potentials are reported with respect to the Normal Hydrogen Electrode (NHE), which is taken in this report as being equivalent to the Standard Hydrogen Electrode (SHE).

4.2.1 Experiment 1: Low density bentonite

In this experiment the defect in the outer copper shell (located near the top cap weld), is pointing vertically upwards. Figure 4-13 shows the results from the potential measurements for gold, platinum, E_h probe and the miniature canister. These data show the E_h values using the gold and platinum electrodes, which are inside the support cage, and the E_h measured using the mixed-metal oxide electrode outside the support cage. Initially the internal silver-silver chloride reference electrodes were used for measuring the potential of the Au and Pt electrodes, but these failed and it was necessary to switch to the Silvion reference electrode, which was mounted in the borehole outside the support cage (see change at 4,000 hours). Therefore, the Au, Pt and MiniCan potential data up to 4,000 hours should be discounted. At the time, it was not clear why the Ag-AgCl disc electrodes failed in these experiments, since they had behaved satisfactorily during the laboratory autoclave tests (Smart and Rance 2009); however recent examination of Experiment 3 (Smart et al. 2012a) has shown that the internal silver-silver chloride reference electrodes had become covered with a layer of black deposit composed of iron sulphide, which had probably disabled the reference electrodes. To date, the Silvion reference electrodes mounted in the boreholes have performed satisfactorily.

The mixed metal oxide E_h values are reliable and show a decrease in the E_h with time. This is expected, since oxygen is consumed by microbial activity, mineral reactions and corrosion. Until recently, the E_h value was lower inside the cage than outside, indicating more reducing conditions, possibly due to the ongoing corrosion reactions. In 2010 (26,220–34,834 hours exposure) there were some fluctuations in the E_h values measured using the metal-oxide probe; the reasons for these are not clear at present but during 2011 (34,835–43,595 hours exposure) and 2012 (43,596–51,050 hours exposure) the potentials stabilised and the E_h value became more negative, so that the values are now similar to the values measured on the gold and platinum electrodes inside the MiniCan support cage.

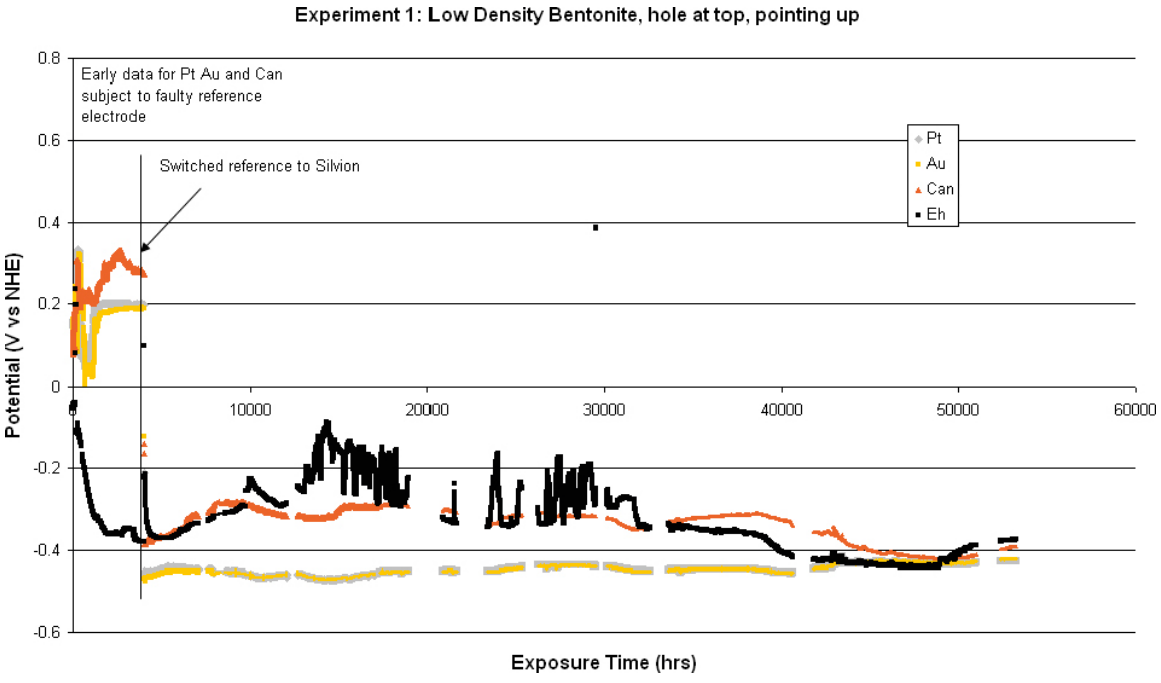

Figure 4-13. *Results of E_h and canister potential measurements from Experiment 1 (low density bentonite).*

The electrochemical potential for the model canister represents a mixed potential for the copper canister itself and the inner cast iron insert, which would have been partially wetted by water passing through the 1 mm defect in the outer copper canister. The copper canister was electrically insulated from the stainless steel support cage to avoid any galvanic coupling between the copper and stainless steel.

Figure 4-14 shows the potentials for the iron and copper coupons inside Experiment 1, up to the end of 2012. Again, there was a problem with the reference electrodes up to 27 June 2007, but after that date the measurements were changed to be with respect to the Silvion reference electrode, at which point reasonable values of about –450 mV vs NHE were obtained, for both iron and copper. The iron and copper potentials are consistent with anoxic conditions existing in the boreholes. These potentials have now been stable for a period of approximately five years.

4.2.2 Experiment 2: Low density bentonite

In this experiment the defect in the outer copper shell is at the top end of the canister (i.e. near the lid) but pointing downwards. Figure 4-15 shows the results from the potential measurements for gold, platinum, E_h probe and the model canister.

With Experiment 2, as for Experiment 1, there was a problem with the small Ag-AgCl reference electrodes mounted inside the support cages, but when the measurements were carried out against the external Silvion reference electrode reasonable values were obtained. The E_h value is again slightly more reducing inside the support cage than outside. The electrochemical potential values measured for the canister and E_h probe in this experiment were slightly lower than in Experiment 1.

The electrochemical potential values for iron and copper are shown in Figure 4-16. As for Experiment 1 it was necessary to measure the values against the Silvion reference electrode because the internal silver-silver chloride electrodes failed. This correction was made after June 2007. The potentials have been stable since the reference electrode system was changed; they are consistent with anoxic reducing conditions and are similar to those for Experiment 1 in Figure 4-14.

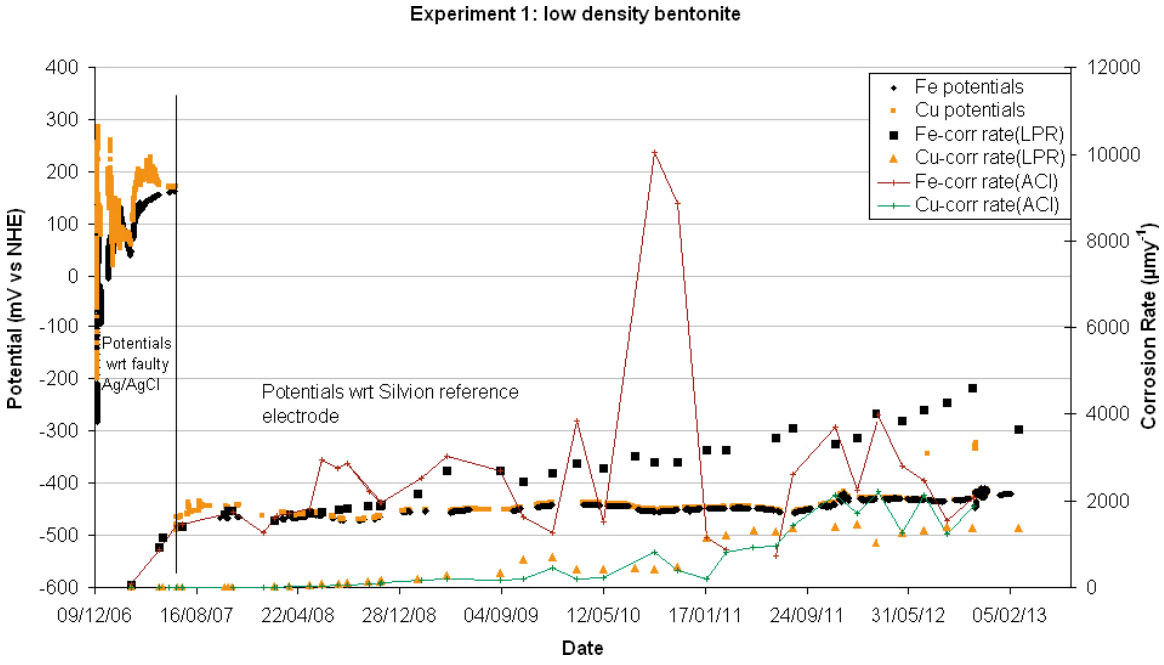

Figure 4-14. *Results of corrosion potential and corrosion rate measurements for cast iron and copper electrodes in Experiment 1 (low density bentonite).*

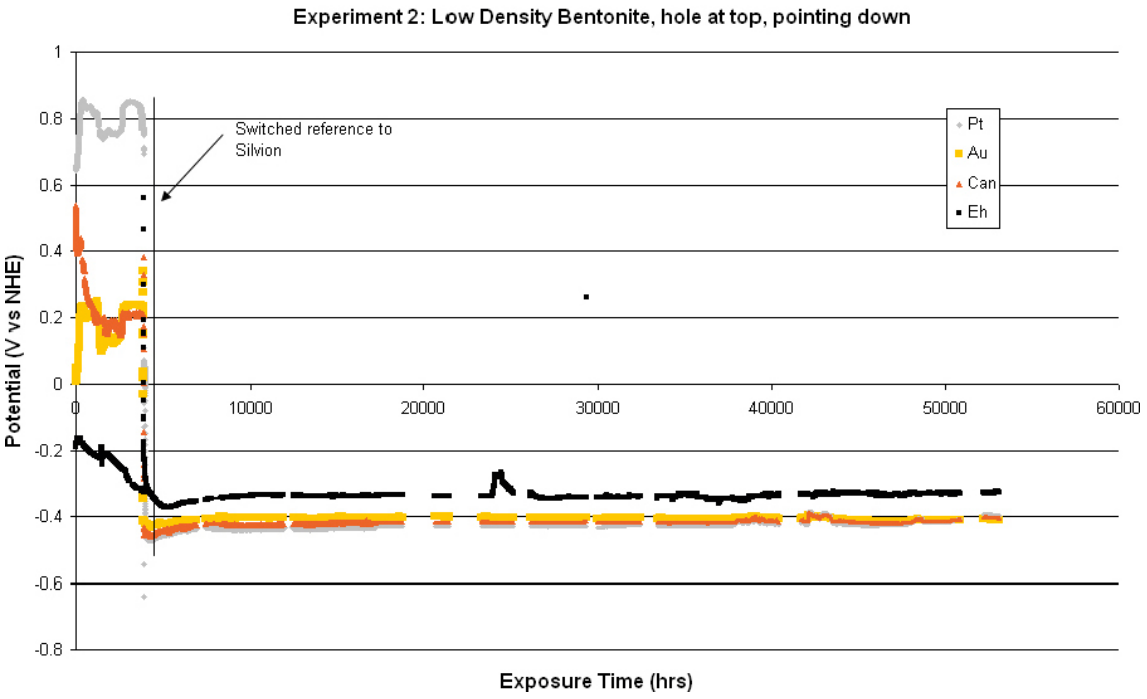

Figure 4-15. *Results of E_h and can potential measurements from Experiment 2 (low density bentonite).*

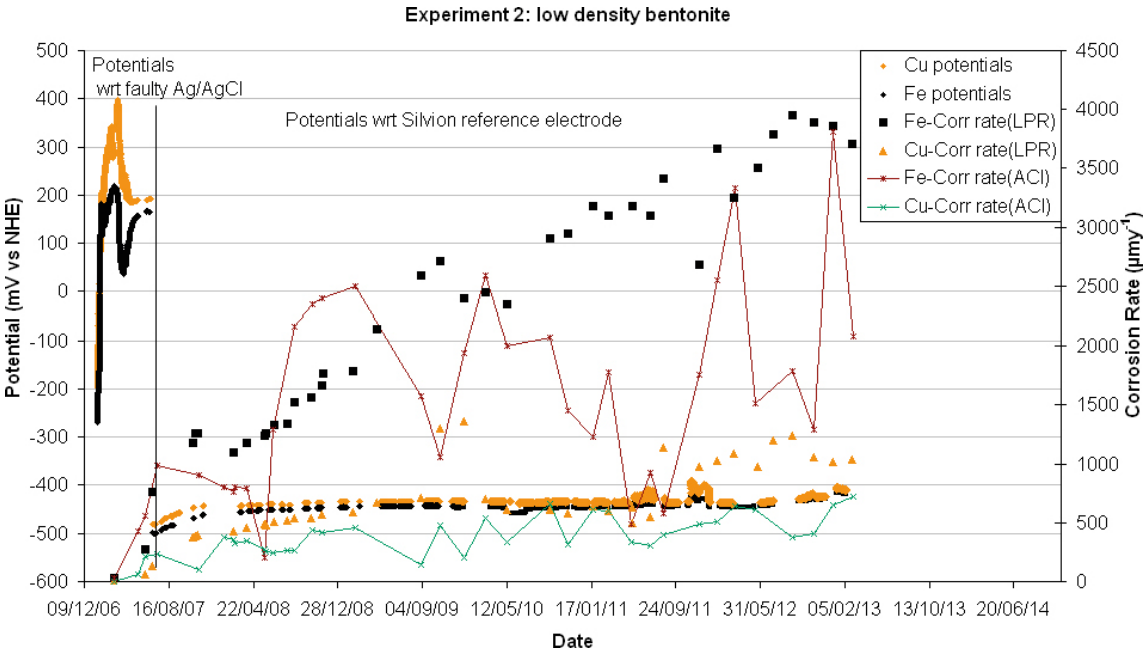

Figure 4-16. *Results of corrosion potential and corrosion rate measurements for cast iron and copper electrodes in Experiment 2 (low density bentonite).*

4.2.3 Experiment 3: Low density bentonite

This experiment was removed in August 2011 for analysis and the results of the examination are reported separately (Smart et al. 2012a). In this experiment there were two defects present in the outer copper shell; the defect near the top lid was pointing upwards, while the defect near the bottom cap was pointing downwards. Figure 4-17 shows the results from the potential measurements for gold, platinum, E_h probe and the model canister up until the point of removal. In Experiment 3 the internal Ag-AgCl electrodes appear to have worked properly until approximately 8,000 hours had elapsed, when it was necessary to change to the Silvion reference electrode outside the support cage. As mentioned previously this failure of the internal reference electrodes appears to have been due to the build up of deposit on the surface of the reference electrodes (Smart et al. 2012a). The early fluctuations in E_h inside the support cage appear to be genuine. The E_h value external to the support cage stabilised at ~–300 mV after 3,500 hours.

The electrochemical potential values for iron and copper in Experiment 3 are shown in Figure 4-18. These data show a decrease in the corrosion potential of the copper initially, stabilising at highly negative values. The potentials were subsequently measured against the Silvion reference electrode after failure of the internal silver-silver chloride reference electrodes after approximately 7,500 hours. The potentials were stable for the remainder of the experiment but attained more positive values than initially (~–430 mV NHE); they were similar to those measured in Experiments 1 and 2.

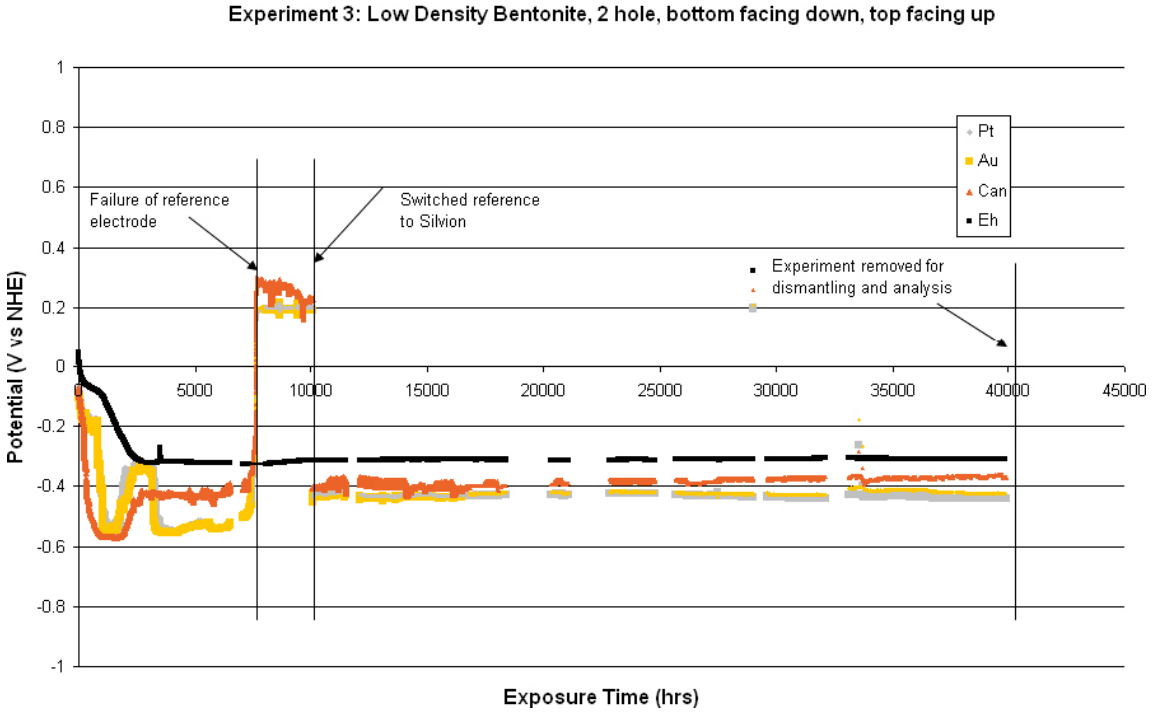

Figure 4-17. *Results of E_h and can potential measurements from Experiment 3 (low density bentonite).*

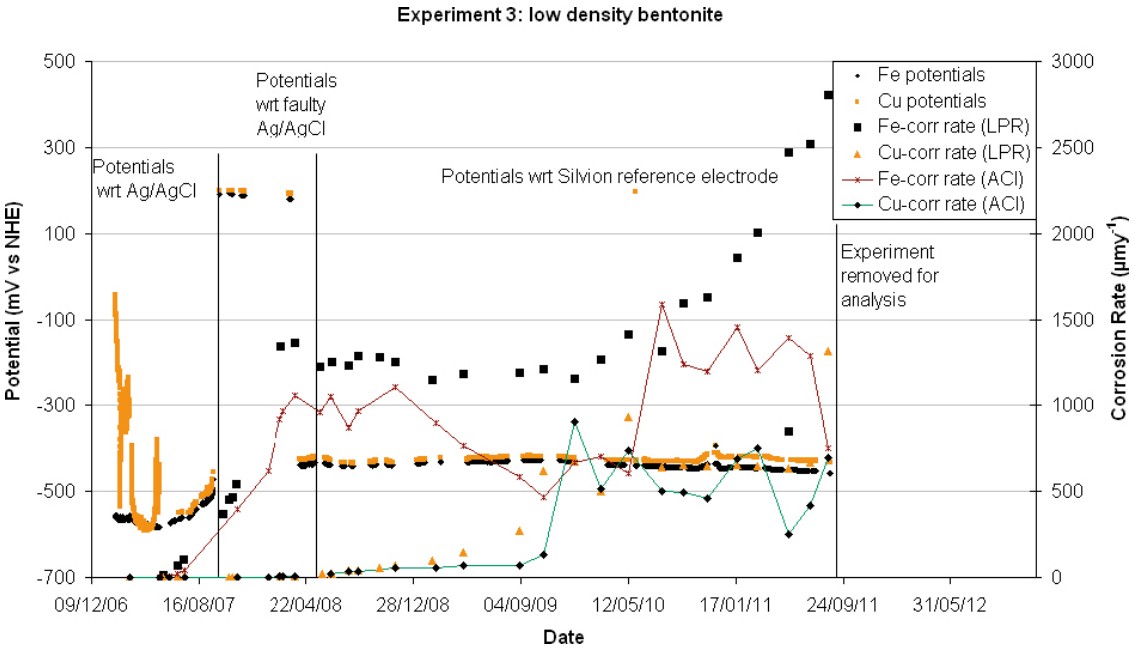

Figure 4-18. *Results of corrosion potential and corrosion rate measurements for cast iron and copper electrodes in Experiment 3 (low density bentonite).*

4.2.4 Experiment 4: Compacted bentonite

In Experiment 4 the defect in the outer copper shell is near the top lid but pointing downwards. The whole model canister is surrounded by compacted bentonite, with the test electrodes placed in slots cut into the compacted bentonite. Figure 4-19 shows the results from the potential measurements for gold, platinum, E_h probe and the model canister. The potentials for the platinum exhibited a considerable amount of noise. It was necessary to use the external Silvion reference electrodes to measure the potentials after about 3,500 hours. It is noticeable that the E_h values measured on the gold electrode were not as negative as in the low density bentonite tests (Experiments 1–3). The E_h probe values were similar to the other experiments.

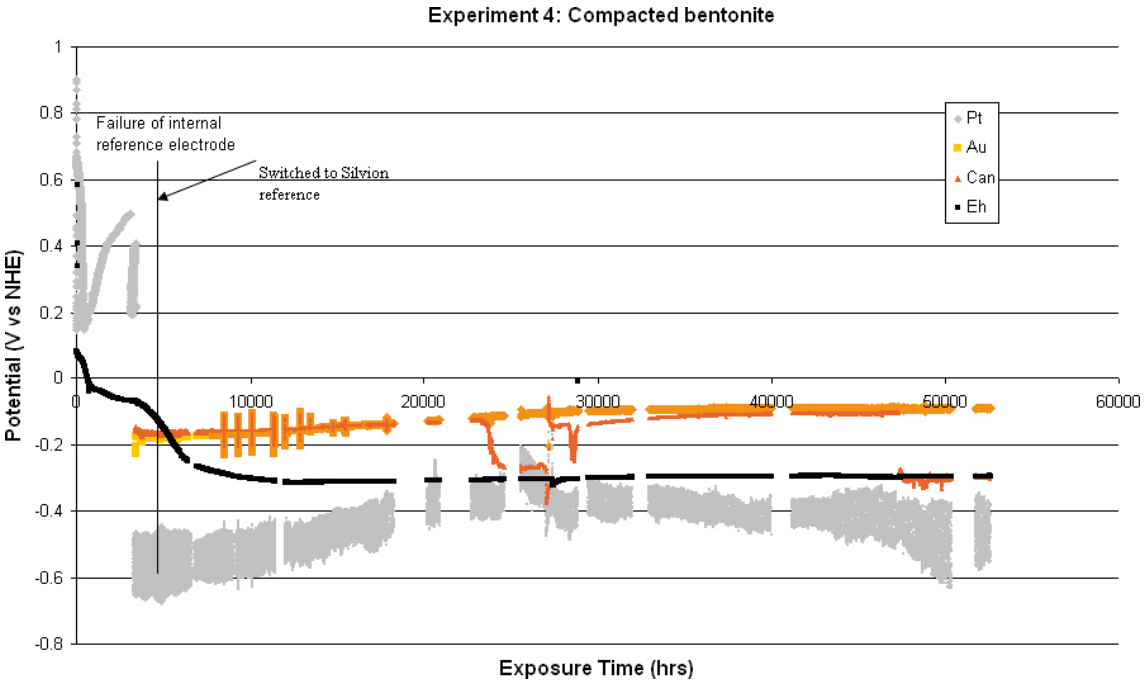

Figure 4-19. *Results of E_h and can potential measurements from Experiment 4 (compact bentonite).*

The electrochemical potential values for copper and iron in Experiment 4 are shown in Figure 4-20 and Figure 4-21 respectively. Contact has now been lost with the iron electrode in this experiment (it appears that both iron electrodes and the auxiliary electrode are shorted to the stainless steel flange but it is not clear when this shorting occurred.). This may have been caused by expansion of the compact bentonite leading to crushing of the electrical connections. The data for the iron electrode are included for completeness, but the data should be treated with caution (i.e. they are not valid and are only included for completeness).

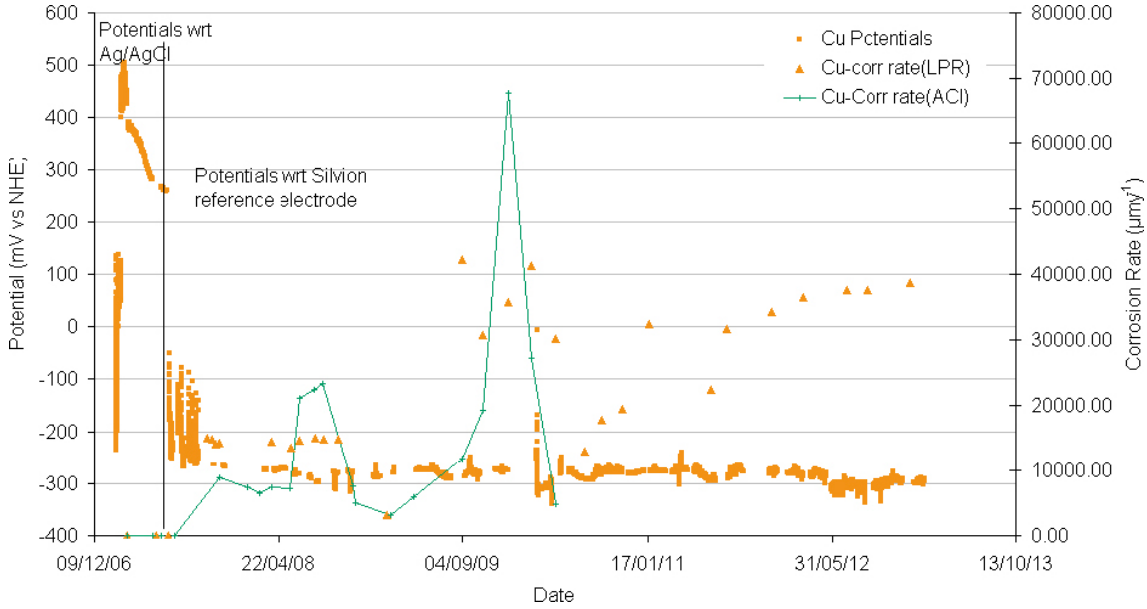

Figure 4-20. *Results of corrosion potential and corrosion rate measurements for copper electrodes in Experiment 4 (compacted bentonite).*

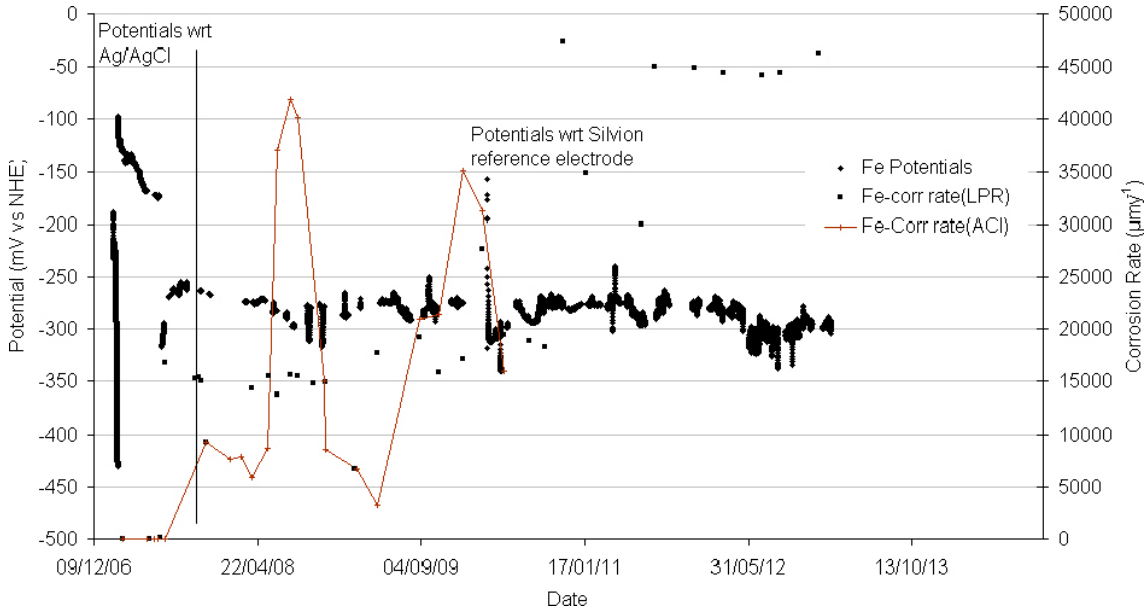

Figure 4-21. *Results of corrosion potential and corrosion rate measurements for cast iron electrodes in Experiment 4 (compacted bentonite).*

4.2.5 Experiment 5: No bentonite

In this experiment there are two defects in the outer copper shell, both of which are near the top lid. One defect is pointing vertically upwards, the other is pointing downwards. In this experiment there is no bentonite around the model canister (i.e. it is in direct contact with the Äspö groundwater). Figure 4-22 shows the results from the potential measurements for gold, platinum, E_h probe and the model canister. In this experiment there was a problem with both the internal silver-silver chloride reference electrodes and the external E_h probe and the Silvion electrode and so it was necessary to set up an external reference electrode (a Clarke's silver-silver reference electrode) and E_h probe, mounted on the borehole flange. This would not have affected the values of the potentials measured and all the data were normalised to the Normal Hydrogen Electrode (NHE). The iron and copper potentials in this experiment are shown in Figure 4-23. Again there were problems with the small internal Ag-AgCl reference electrodes up to June 2007, after which it was necessary to switch to using the stainless steel flange as a pseudo reference electrode and then switch to an external reference electrode. The potentials of the reference electrodes and the stainless steel pseudo-reference electrode were checked against a calibrated reference electrode, so all the data are directly comparable. The E_h probe data and the recent (i.e. 2012) iron and copper potentials are unusually high and there was some doubt about the reliability of the external Clarke's silver-silver chloride reference electrode system. In May 2010 the external reference electrode was replaced with a Silvion external reference electrode and this appears to be operating satisfactorily, although it is noticeable that there appeared to be an equilibration period after the new reference electrode was installed (see Figure 4-22), for the E_h potentials, and the copper and iron potentials. This probably corresponds to a period when there was a spike of oxygen entering the borehole after the external reference electrode was changed. It is also noticeable that this period corresponded to an increase in the electrochemically measured corrosion rate.

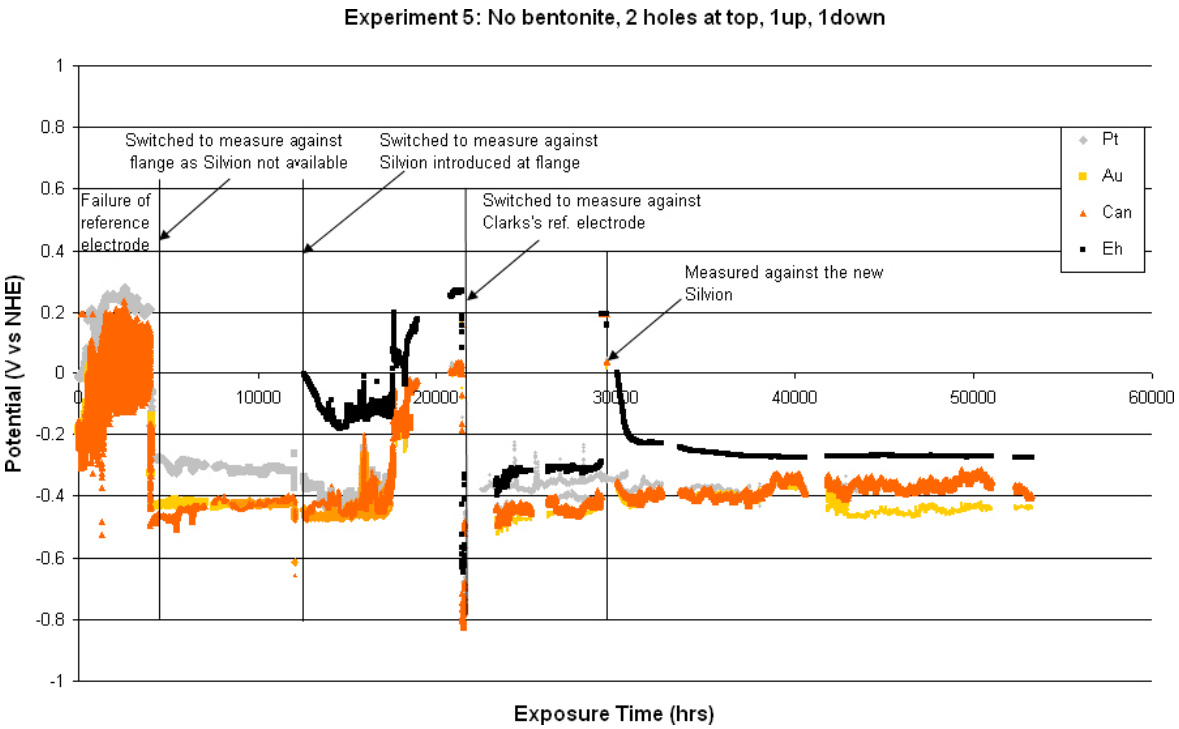

Figure 4-22. *Results of E_h and can potential measurements from Experiment 5 (no bentonite).*

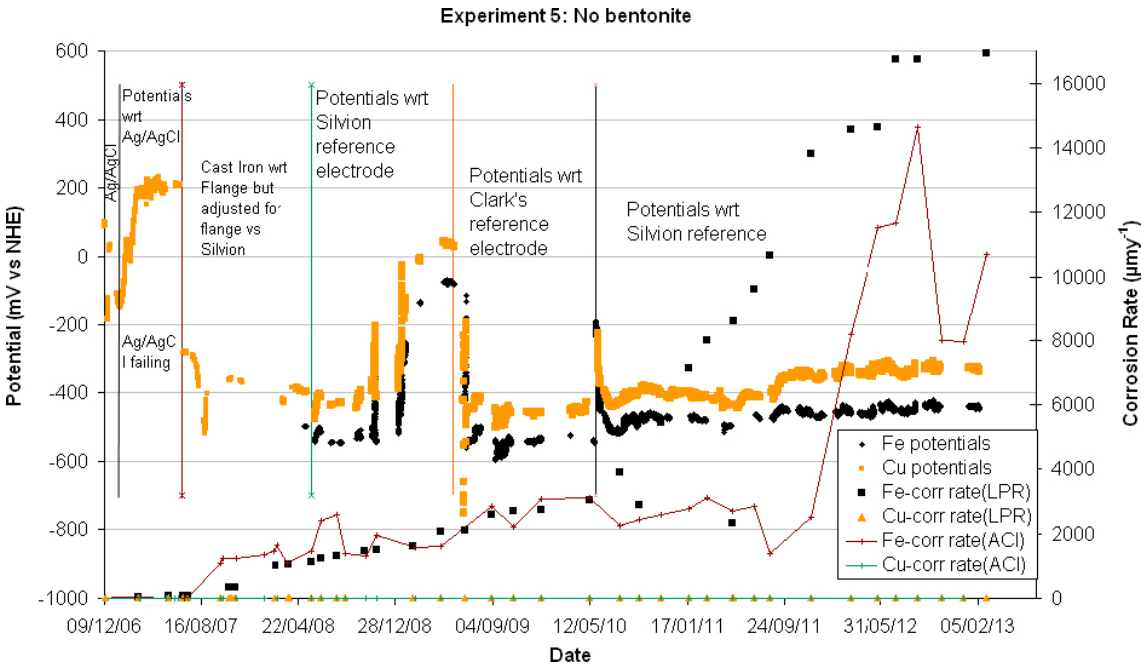

Figure 4-23. *Results of corrosion potential and corrosion rate measurements for cast iron and copper electrodes in Experiment 5 (no bentonite).*

4.3 Electrochemical corrosion rate measurements

Examples of typical LPR and AC impedance measurements for copper and iron electrodes in Experiment 1 are shown in Figure 4-24 and Figure 4-25. All the raw data obtained during 2012 for Experiments 1–3 and 5 are given in Appendix 1 and the raw data obtained for Experiment 4 are given in Appendix 2; the raw data acquired during previous reporting periods are presented in Smart et al. (2011a, 2012b). The plots in the appendices show how the LPR data and the AC impedance data in Nyquist and Bode format have evolved with exposure time. An increasing slope in the LPR plots corresponds to an increasing corrosion rate. Similarly, a decrease in the diameter of the AC impedance Nyquist plots corresponds to an increase in corrosion rate. It is possible to see some fine structure in the Nyquist plots at the high frequency end of the scans, which probably represents, the development of features in the surface films rather than instrumental artefacts.

Summaries of the measured corrosion rate data for copper and cast iron are presented in Figure 4-26 to Figure 4-29. The measured corrosion rates are also shown on the plots of corrosion potential against time for each of the five experiments (i.e. Figure 4-14, 4-16, 4-18, 4-20 and 4-22). Generally speaking, good agreement was obtained between the corrosion rates derived from the two techniques, although it should be noted that they essentially measure the same parameter (i.e. charge transfer resistance) so that agreement does not necessarily mean that the corrosion rates are accurate. There is a peculiarity about the corrosion rate data for cast iron from Experiment 4 because it appears that the electrode is currently in contact with the stainless steel flange. Figure 4-29 shows that up to June 2007 the corrosion rate was less than 100 µm yr^{-1} but thereafter there was a sudden change in behaviour. This seems unlikely to be a genuine change in corrosion rate and the most likely explanation is that swelling of the bentonite clay caused damage to the electrical connections and forced the electrodes up into contact with the stainless steel flange. This would have had the effect of producing a much larger electrode surface area and hence the measured currents would have increased sharply.

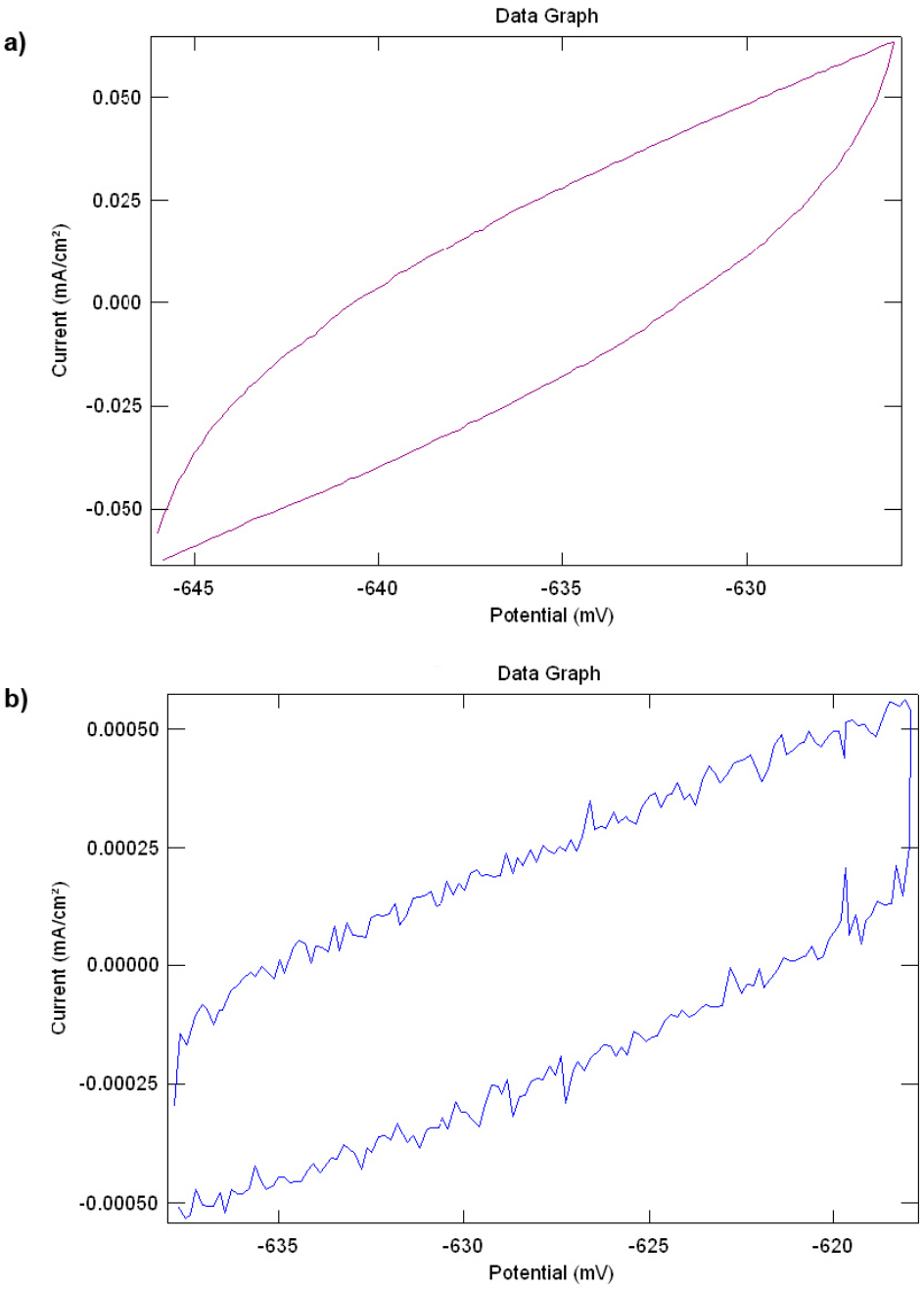

Figure 4-24. *Typical examples of linear polarisation resistance (LPR) measurements on Experiment 1: (a) cast iron, (b) copper.*

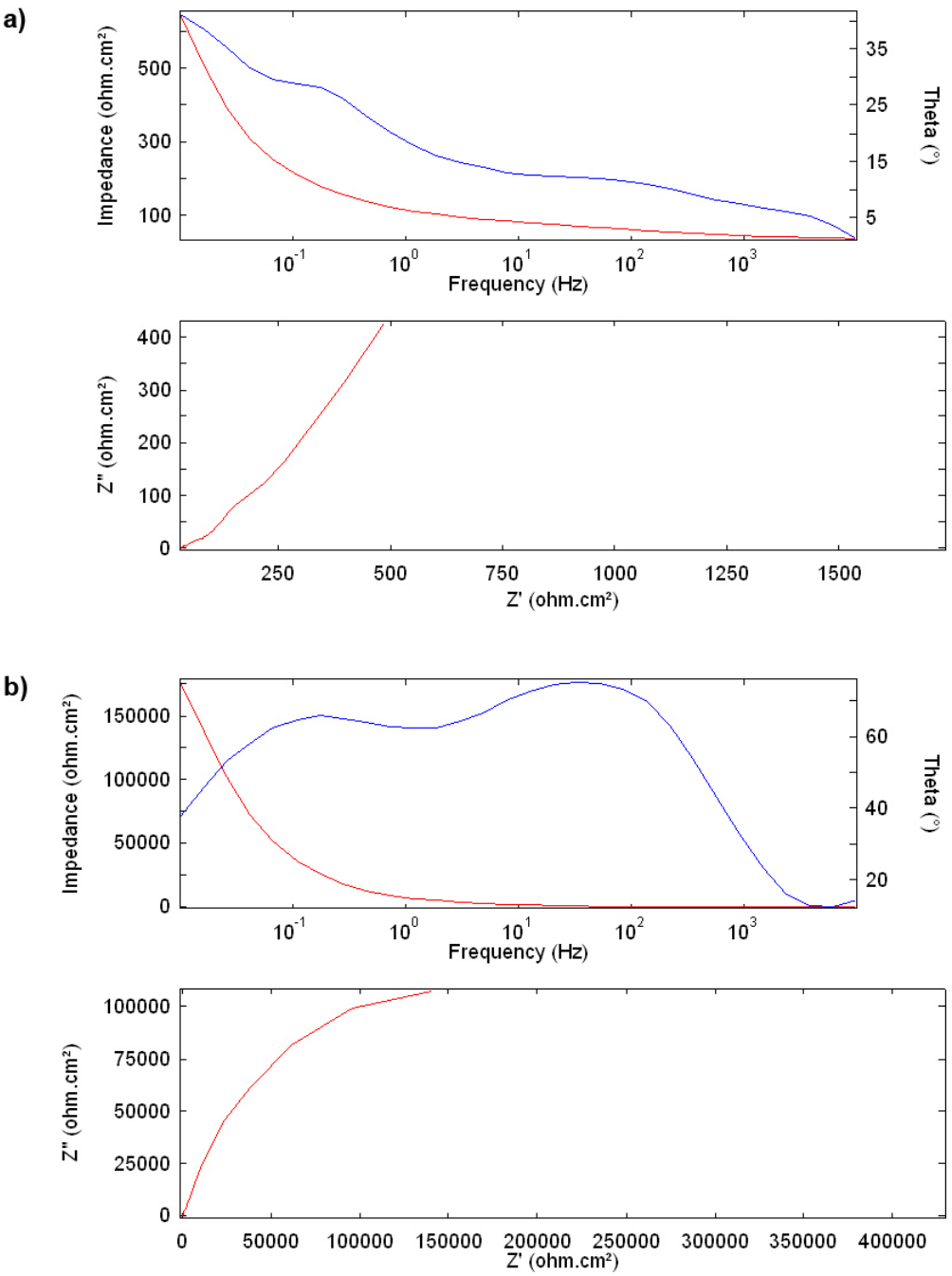

Figure 4-25. *Typical examples of AC impedance measurements (ACI) on Experiment 1: (a) cast iron, (b) copper. Blue line = theta plot; red line = impedance plot.*

The corrosion rate values obtained for copper in Experiments 1, 2, 3 and 5 are summarised in Figure 4-26 and the values from electrochemical measurements on cast iron in Experiments 1, 2, 3 and 5 are shown in Figure 4-28. The corrosion rate data for copper in Experiment 4 are plotted separately for copper in Figure 4-27 because the experiment yielded considerably higher corrosion rate values. The corrosion rates measured for copper in Experiment 4 (Figure 4-27) are impossibly high because if such corrosion rates had actually occurred there would not be any electrode material left to measure (the original dimensions of the copper electrodes were 5×10×20 mm). This suggests that, at least for Experiment 4, the corrosion rates after November 2007 were not being measured accurately and that there must have been some kind of experimental artefact affecting them. It is possible that there has been some disruption of the electrodes and the connections due to the swelling pressure exerted by the compacted bentonite. This is further supported by the identical readings for the corrosion potential measurement for the cast iron and copper electrodes, as shown Figure A2-5 (Appendix 2). This indicates that the electrodes are touching or that they are touching the same material (e.g. the stainless steel flange). If the electrodes are touching other materials it is not possible to extract valid measurements from them. The most recent AC Impedance data for copper in Experiment 4 are not included in Figure 4-27 because they were clearly not correct and should be discounted. However, for completeness, the raw LPR and AC impedance data from Experiment 4 for both cast iron and copper are plotted in Figure A2-1 to Figure A2-4 (Appendix 2). The very irregular results for Experiment 4 compared to Figures A1-7 to A1-11 for Experiments 1, 2, 3 and 5 indicate that the measurements were not giving valid results. Prior to the step change in the corrosion rate at the end of 2007 the measured corrosion rate of the copper in compacted bentonite was of the order of 1 µm yr^{-1} (Figure 4-27). Data obtained after this date are probably not credible. There is also an unresolved question about whether the high pressure exerted by the swelling bentonite in Experiment 4 could affect the electrochemical response of any corrosion product films.

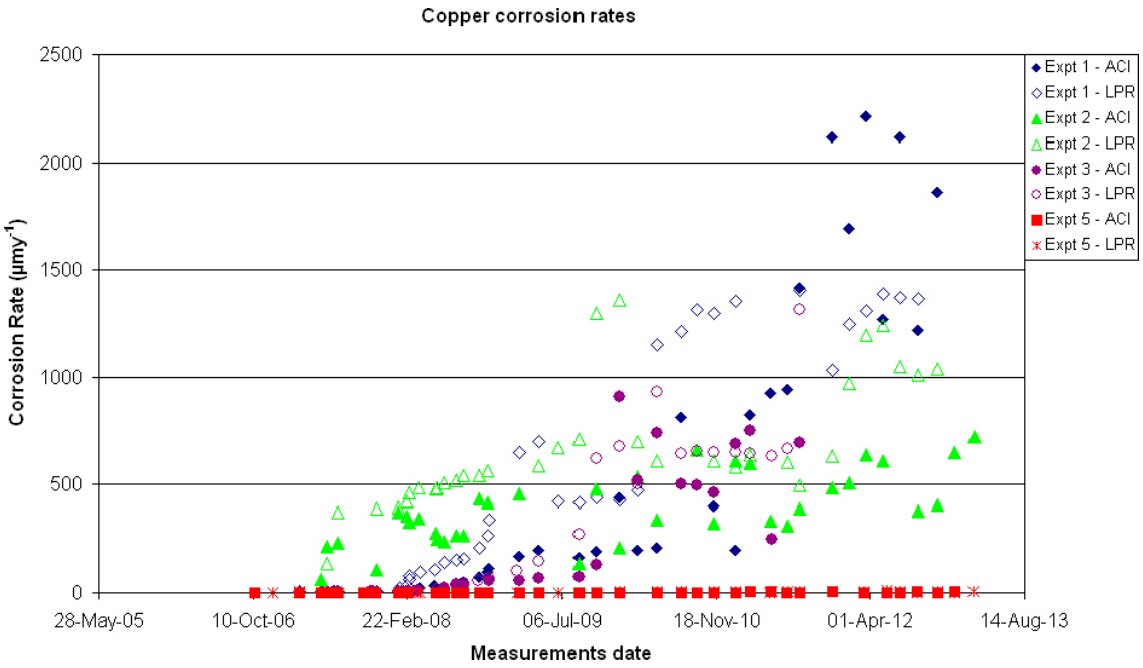

Figure 4-26. *Summary of copper corrosion rates obtained by AC impedance and LPR measurements for Experiments 1, 2, 3 and 5.*

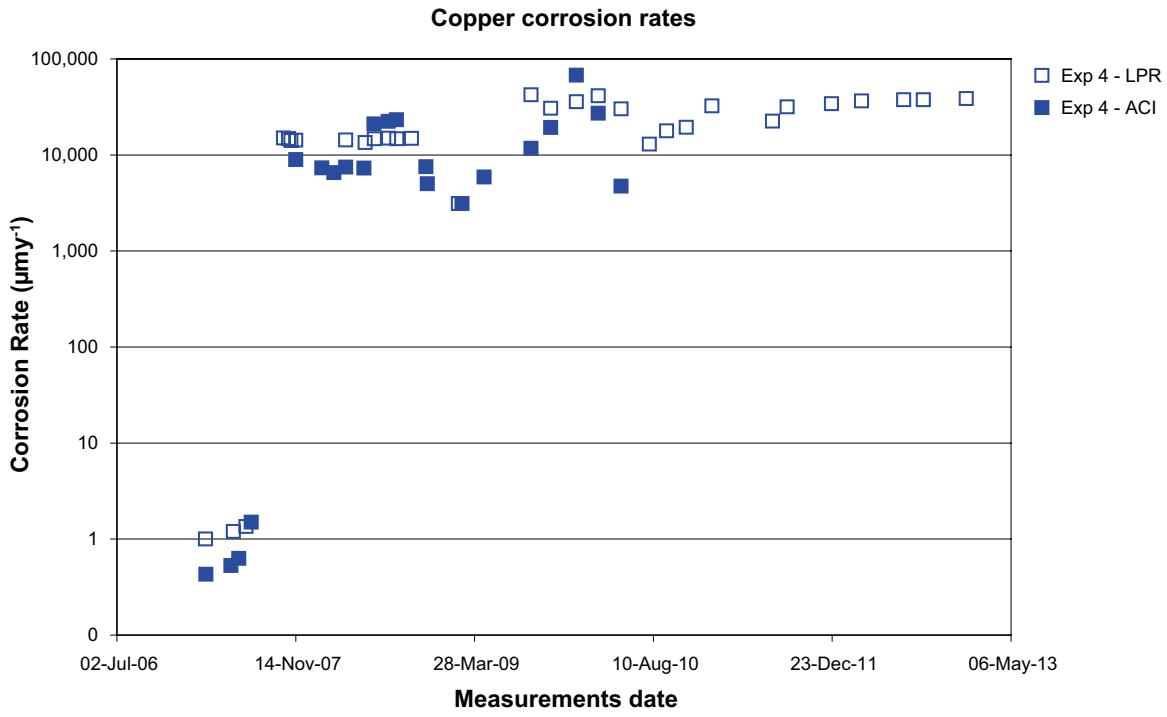

Figure 4-27. *Summary of copper corrosion rates obtained by AC impedance and LPR measurements (Experiment 4). Note that these data are included for completeness, but it is unlikely that the measurements after mid 2007 are valid (i.e. the point at which there is a step change in the measured corrosion rate).*

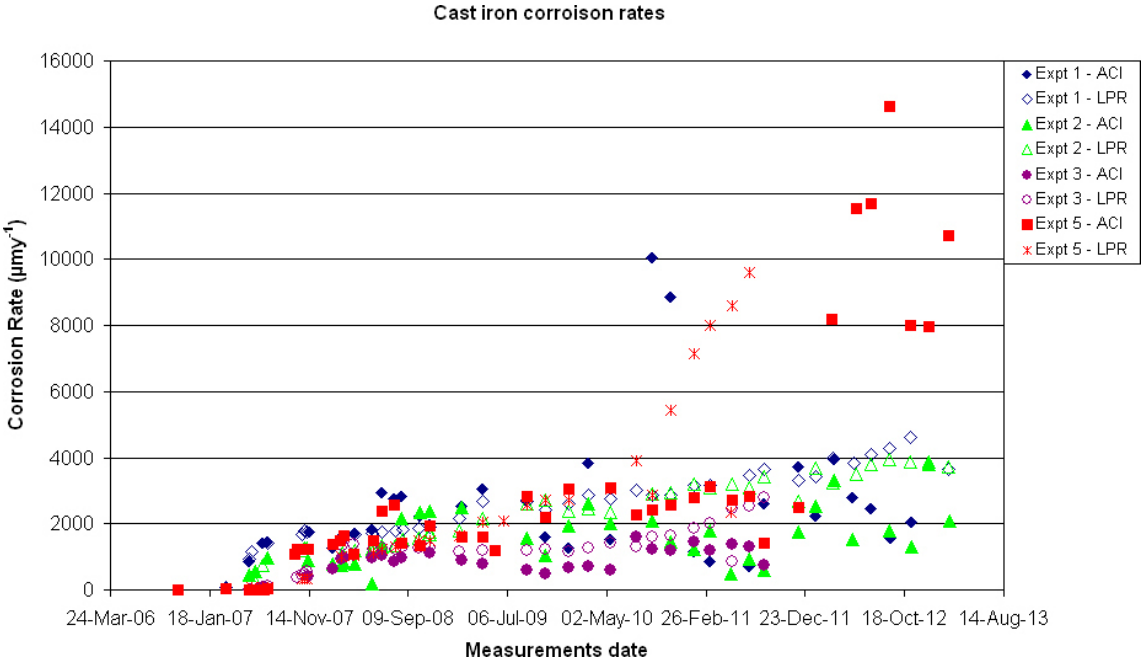

Figure 4-28. *Summary of cast iron corrosion rates obtained by AC impedance and LPR measurements for Experiments 1, 2 3, and 5.*

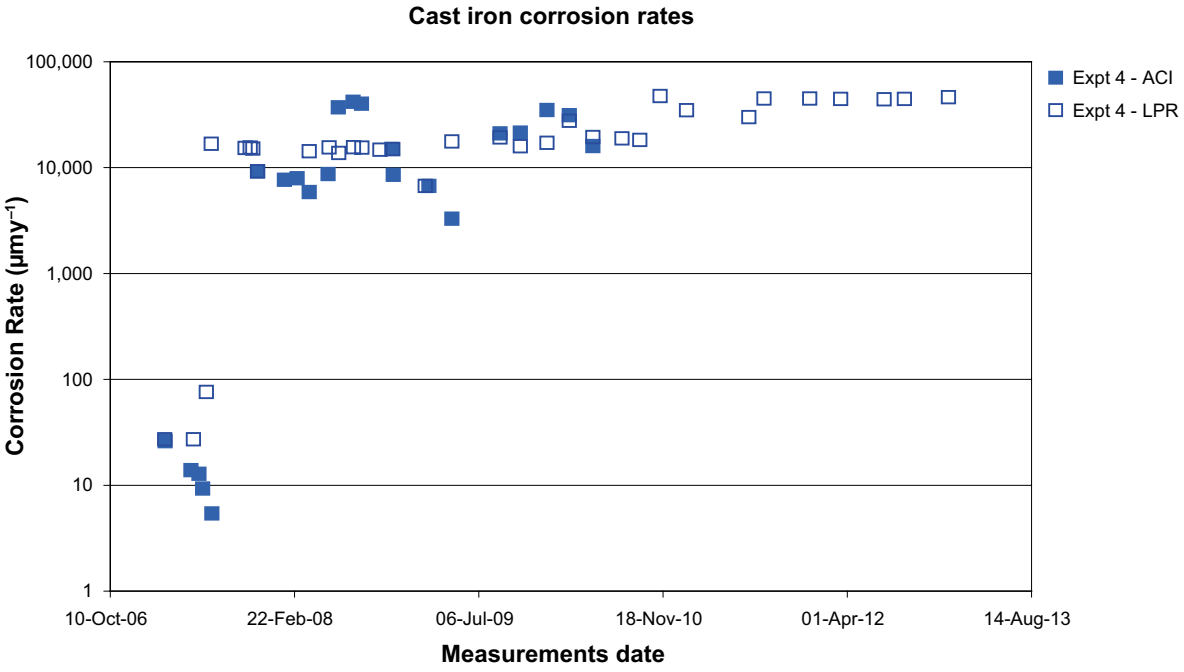

Figure 4-29. *Summary of cast iron corrosion rates obtained by AC impedance and LPR measurements (Experiment 4). Note that these data are included for completeness, but the iron electrode is touching the stainless steel flange and it is unlikely that the measurements after mid 2007 are valid (i.e. the point at which there is a step change in the measured corrosion rate).*

The data in Figure 4-26 show that initially the measured corrosion rate of copper in Experiments 1 to 3, with low density bentonite was < 10 µm yr^{-1}, but after an incubation period, which varied in duration between the experiments, the electrochemically measured corrosion rate increased by several orders of magnitude. The measured corrosion rate of copper in Experiment 5, where no bentonite was present, has remained at < 6 µm yr^{-1} based on LPR measurements and < 3 µm yr^{-1}, based on AC impedance measurements for the duration of the experiment. This indicates that the presence of low density bentonite has either (i) increased the corrosion rate of the copper, or (ii) changed the surface of the copper electrode so that the electrochemical properties indicated an increased, but inaccurate, corrosion rate. One possible explanation is that the microbial activity is enhanced in the presence of low density bentonite, leading to a greater production of sulphide by SRB activity, which is known to increase the corrosion rate of copper (King et al. 2001). Analysis of Experiment 3 (Smart et al. 2012a) has shown that all the surfaces inside the support cage were covered in a black layer of iron sulphide and, since this material is conductive, this could have increased the measured current and produced a misleadingly high value of corrosion rate. This is supported by the fact that the corrosion rate measured using the weight loss technique gave a much lower corrosion rate for the copper in Experiment 3 (0.15 ± 0.02 µm yr^{-1}). It is interesting to note that the lowest corrosion rates for both iron and copper, corresponded to the time when water samples were being extracted most frequently (e.g. see Figure 4-1 for dates of water sampling) and it is possible that the increase in corrosion rate corresponded to the time when microbial activity was least disturbed by drawing water out of the support cage. In situ studies by Hallbeck and Pedersen at a location near to the MiniCan experiment in the Äspö laboratory have shown that closure of a groundwater test loop can lead to an increase in the concentration of sulphide in the groundwater (Pedersen 2012a) due to SRB activity. It should be noted that these experiments did not contain any bentonite in the test loop, showing that the SRB activity can be sustained even in the absence of an additional source of nutrients such as the organic material in bentonite.

The data in Figure 4-28 indicate that the measured corrosion rate of the cast iron in Experiments 1, 2, 3 and 5 has increased but then stabilised at values of several thousand µm yr^{-1}. However, based on values published in the literature there is reason to believe that the corrosion rate measured using electrochemical methods may overestimate the true value because of the nature of the iron sulphide

film formed in the presence of SRB activity; this is discussed further in Section 5.3. On the other hand results from analysis of Experiment 3 (Smart et al. 2012a) show that the corrosion rate of cast iron, based on examination of the weight loss coupon, was indeed very high and of the order of at least 500 µm yr^{-1}, which is approximately the value measured electrochemically for the cast iron electrodes (e.g. see October 2009 measurements in Figure 4-28).

During 2010 the possibility that changes in the reference electrode configuration might have affected the corrosion rate measurements was investigated. Normally, in an electrochemical cell, the reference electrode would be placed near to the working electrode to minimise any potential drop effects (known as IR drop effects) caused by the resistance of the solution to the current passing through it during the electrochemical measurement. However, because of the failure of the internal Ag-AgCl electrodes it was necessary to use an external Silvion reference electrode, which was further from the working electrode and so the IR drop would have been greater. The groundwater has a high conductivity and so this effect is unlikely to be large, but in order to be able to eliminate the possibility a series of experiments was carried out in which the gold electrode was used as a pseudo-reference electrode. The gold electrode was close to the working electrode and so this would have reduced any IR drop effects. The results from this set of measurements are given in Table 4-7. In summary, the results indicate that the measured corrosion rates were not significantly affected by the choice of reference electrode. This view is supported by the fact that the measured corrosion rates did not exhibit a step change when the reference electrode was changed (e.g. see Figure 4-18).

Other possible reasons considered for the measured increased corrosion rates are that localised attack is occurring on the electrodes, or that crevice corrosion has occurred around the polymeric sheathing on the electrodes. These issues are considered further in a separate companion report (Smart et al. 2012a) on the removal and analysis of Experiment 3.

Table 4-7. Comparison of the LPR corrosion rate data (µm yr^{-1}) obtained on the copper and cast iron coupons using different reference electrodes: Reference electrode A (external Silvion electrode) and Reference electrode B (gold as pseudo-reference electrode inside compacted bentonite). Note: the iron electrode in Experiment 4 is shorted to the outer flange.

Experiment	Cast Iron	Copper	Cast Iron	Copper
	Reference Electrode A		Reference Electrode B	
1 (low density bentonite)	1,519	211	2,800	407
2 (low density bentonite)	2,000	337	2,960	586
3 (low density bentonite)	604	741	1,500	1,009
4 (compacted bentonite)	16,000	4,742	8,900	7,005
5 (no bentonite)	3,097	1.5	2,400	1.3

4.4 Copper wire resistance measurements

The results from the electrical resistance measurements on coils of copper wire are shown in Figure 4-30 (Experiment 2) and Figure 4-31 (Experiment 5). The resolution of these measurements is expected to increase with increasing measurement duration. It appears that the long-term corrosion rate for copper is close to zero in these measurements, but the signal is rather noisy. The manufacturers of the measuring equipment (ACM instruments) advised that an average value for the corrosion rate from the electrical resistance data should be taken. It is also possible to smooth the data using a built-in function of the ACM control software (based on a running average), as shown in Figure 4-32. The averaged values based on the electrical resistance data for copper are 0.25 µm yr^{-1} for Experiment 2 (low density bentonite) and 0.39 µm yr^{-1} for Experiment 5 (no bentonite). These values did not change during 2011.

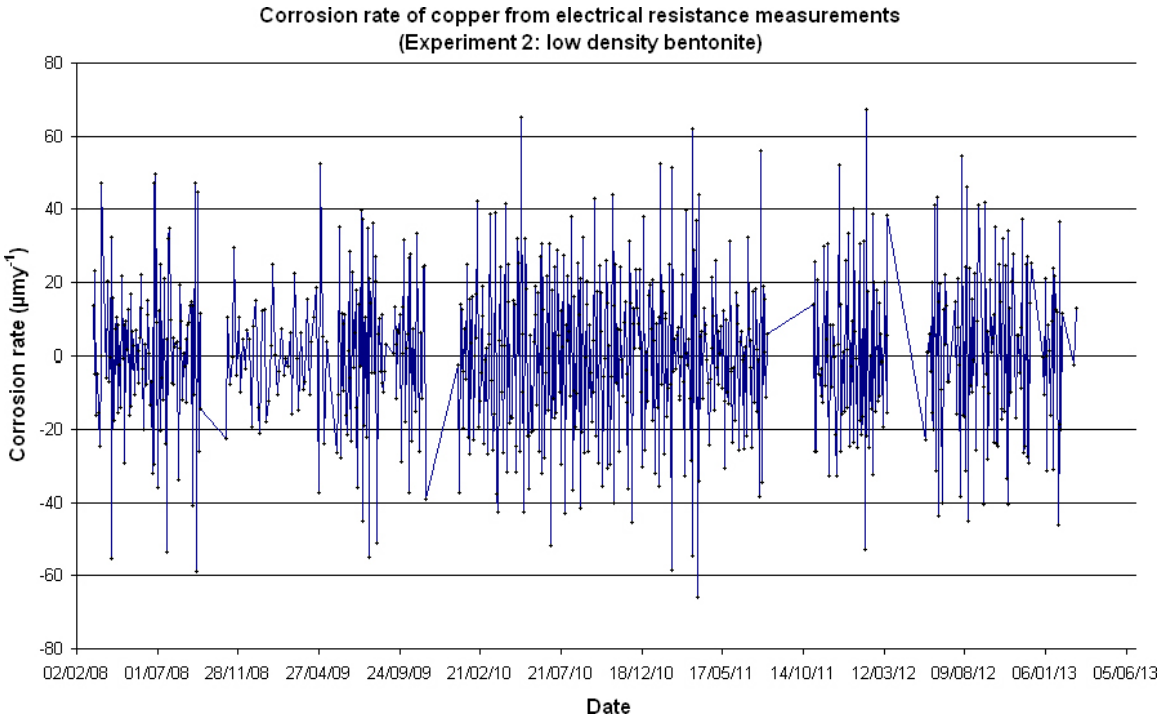

Figure 4-30. *Results of corrosion measurement from copper wire electrical resistance measurement (Experiment 2: low density bentonite).*

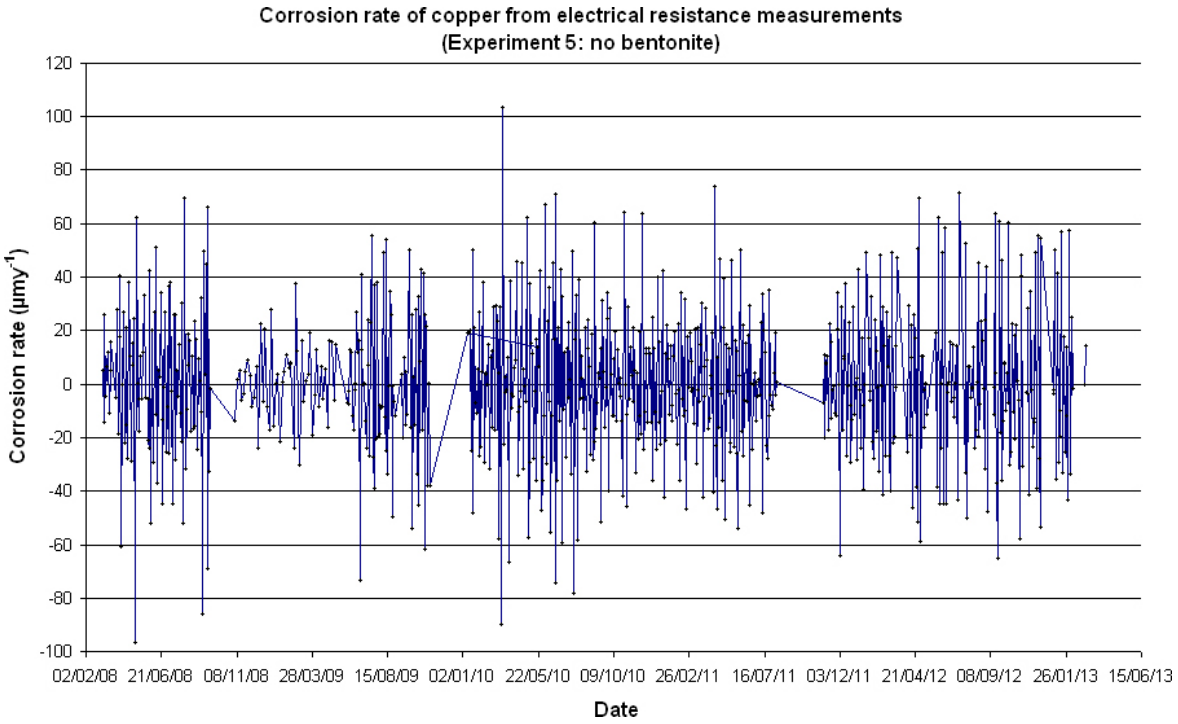

Figure 4-31. *Results of corrosion measurement from copper wire electrical resistance measurement (Experiment 5: no bentonite).*

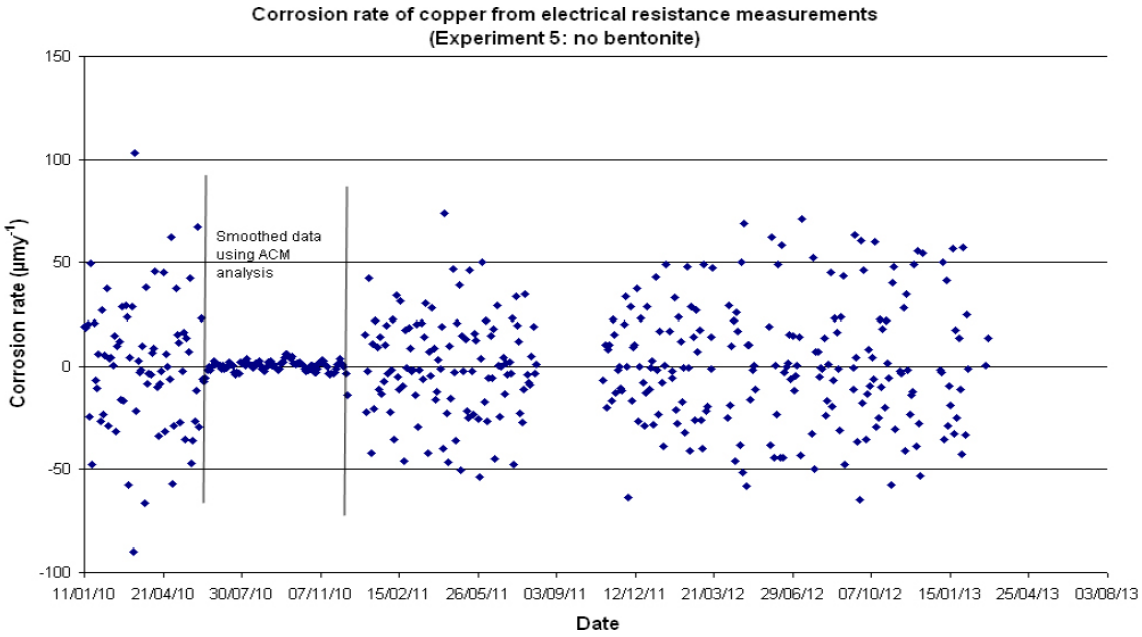

Figure 4-32. *Example of smoothed corrosion rate data obtained from copper wire electrical resistance measurement.*

4.5 Strain gauge data

The strain gauge results for Experiments 1 and 4 are shown in Figure 4-33. Element 4a failed after ~1,000 hours and element 4b failed after ~6,000 hours. Gauges 1a and 1b showed an initial increase in tensile strain and the explanation for this behaviour is not clear. It seems to be too early to be due to expansion caused by a corrosion process and also the gauges 1c and 1d did not show a comparable change in dimensions. This would suggest that for Experiment 1 there was a rapid, greater, non-uniform change in dimensions near the top of the canister compared to the middle of the canister, during the first few weeks after the experiment was installed. The fact that the 1a and 1c elements exhibited a larger deformation than the 1b and 1d elements indicates that there were small directional variations in the degree of deformation on Experiment 1.

It is possible that the cyclic variation in the response of the strain gauges was caused by small local temperature fluctuations, particularly as all the strain gauges show small synchronised changes, which are probably due to temperature fluctuations affecting the measuring equipment, as it is unlikely that there would be any significant temperature fluctuations inside the boreholes. It is also noticeable that the peaks in the response appear to be on an annual timescale so it is possible that there is an effect of seasonal variation on the local temperatures, either the water temperature, which would affect the sensor output, and/or the air temperature which could affect the electronic instrumentation readings. A similar pattern can be seen in the water pressure measurements (Figure 4-12), which are also based on strain gauge technology. Data obtained for the variation in the air temperature in the vicinity of the MiniCan experiments (Figure 4-34) show that there is a seasonal variation in air temperature and relative humidity, which correspond with the variation in the pressure gauge and strain gauge readings. It seems most likely that this behaviour is due to the effect of temperature on the electronic control equipment (an Agilent datalogger used for both pressure and strain measurements) and the pressure sensor, rather than a genuine effect on the pressure or strain, since the electronic components were not housed in a temperature-controlled environment. It is also possible that there may have been some small temperature fluctuations inside the borehole, but no data on this parameter are currently available.

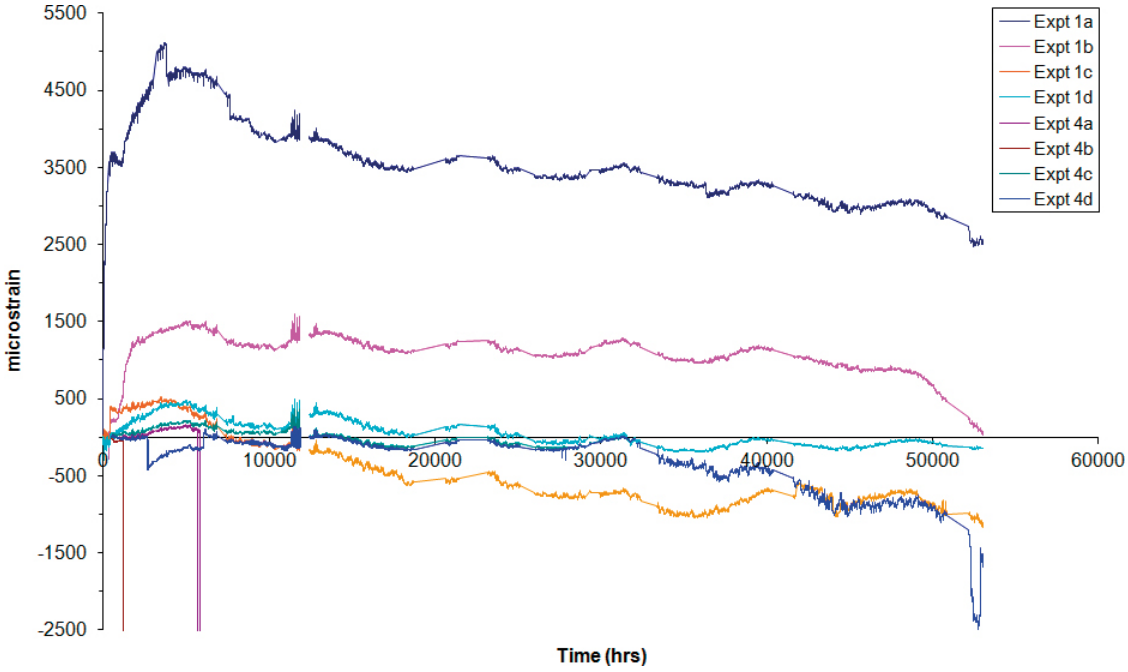

Figure 4-33. *Strain gauge results from Experiments 1 and 4.*

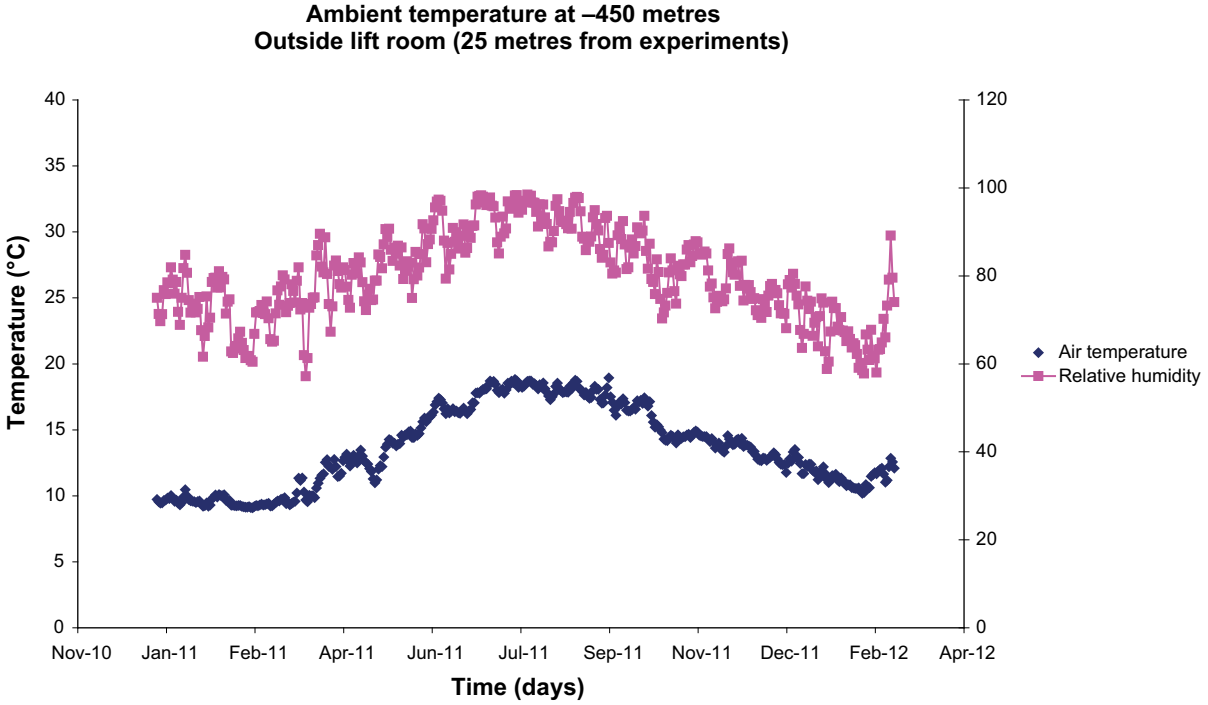

Figure 4-34. *Variation in air temperature and relative humidity at a location 25m from the MiniCan experiments in the Äspö URL*

4.6 Evolution of electrochemical noise data

Electrochemical noise is a technique used to detect indications of localised corrosion; an example of the data acquired to date is shown in Figure 4-35 and Figure 4-36. These data were obtained by coupling two copper electrodes together and measuring the current and potential noise between them. If localised corrosion were occurring transients would be expected in the results. To date, there have been no indications of localised corrosion occurring on the MiniCan corrosion coupons (e.g. sharp

transients lasting 10s of seconds), for either cast iron or copper. It is also possible to calculate the corrosion rate of the coupled electrodes by applying the software using a pre-defined B coefficient provided by ACM Instruments Ltd (26 mV, which is consistent with the value used for the LPR and ACI measurements). This software calculates the charge transfer resistance by dividing the root mean square of the potential noise by the root mean square of the current noise. These results were checked by exporting the raw data to a spreadsheet and carrying out further analysis. The results of the corrosion rates derived from the electrochemical noise measurements are shown graphically in Figure 4-37. It can be seen that the measured corrosion rate values are significantly lower than those measured by the LPR and AC impedance techniques.

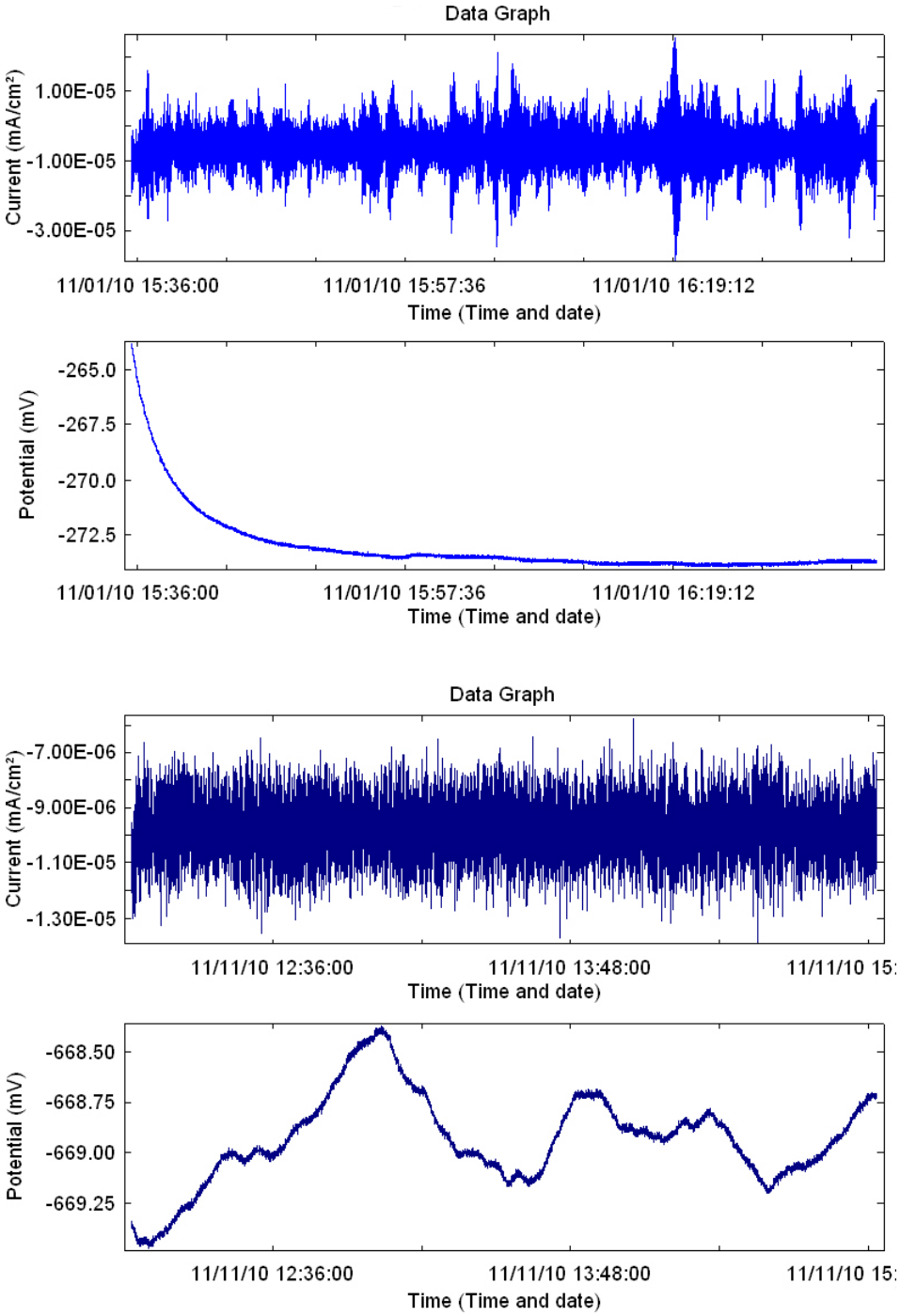

Figure 4-35. *Example of electrochemical noise measurements for cast iron electrode in Experiment 5 (no bentonite).*

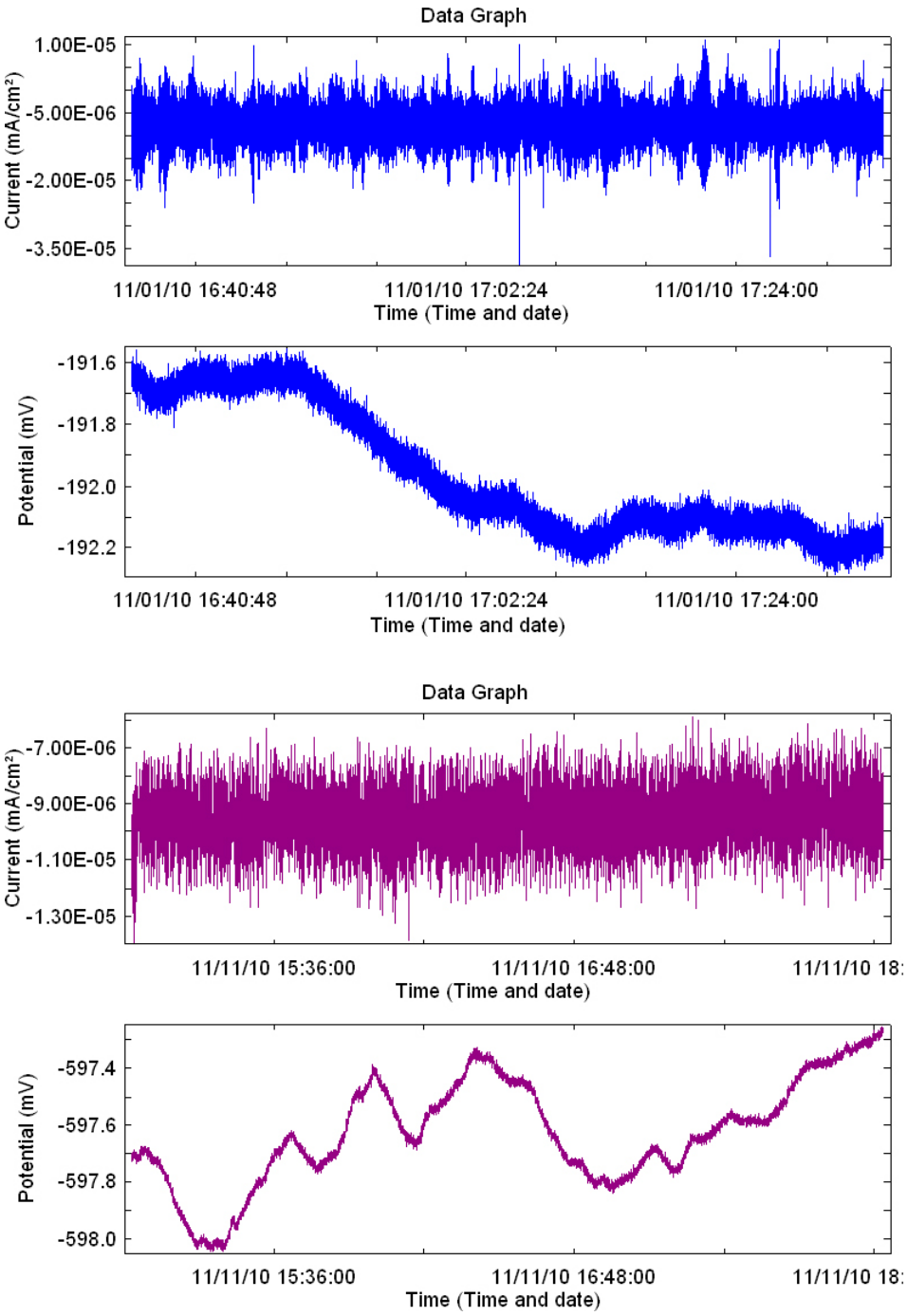

Figure 4-36. *Example of electrochemical noise data from for copper electrode in Experiment 5 (no bentonite).*

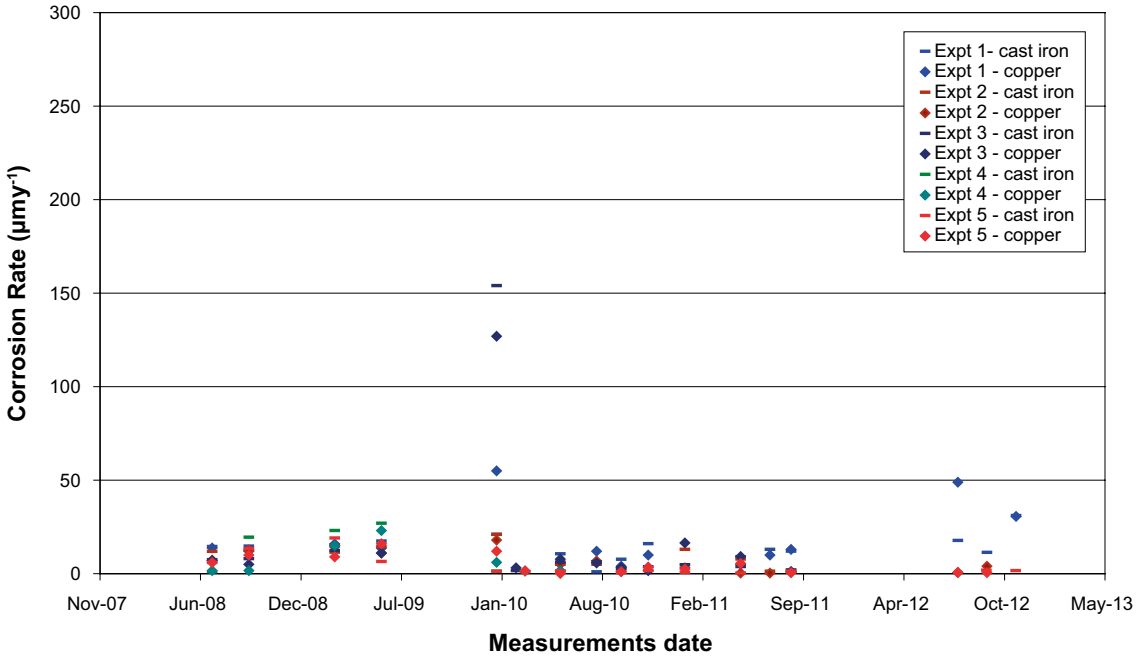

Figure 4-37. *Corrosion rates for copper and cast iron calculated from electrochemical noise data using ACM analysis software*

5 Discussion

5.1 Water analysis and microbial activity

There are a number of interesting features regarding the results of the water analysis from the model canister experiments. In general, the groundwater composition outside the support cages does not vary significantly between boreholes, with the exception of the Experiment 5 borehole, which had a consistently higher concentration of, for example, chloride and calcium compared to the other boreholes.

The first major observation is that there is a marked increase in the iron concentration inside the model canister support cages compared to the surrounding water in the borehole, as shown in Figure 4-7, Figure 4-10 and Table 4-1. This is accompanied by an increase in the concentration of nickel and chromium, particularly in Experiment 5, where there is no bentonite present. On the basis of the observations made when Experiment 3 was dismantled it is clear that the increase in dissolved iron concentration is predominantly due to corrosion of the cast iron coupons and the cast iron insert itself, which was in contact with groundwater as a result of the defect in the outer copper canister. The concentration of chromium and nickel is much lower than the concentration of iron, suggesting that most of the iron results from corrosion of the cast iron, rather than stainless steel (the Fe to Cr/Ni ratio is far greater in the water analysis than in the composition of stainless steel). Figure 4-10 shows that the rate of increase in the iron concentration appears to be accelerating in Experiments 1, 2, 3 and 5. No indications of corrosion of the stainless steel components of Experiment 3 were observed when the experiment was dismantled (Smart et al. 2012a).

Table 4-1, Figure 4-8 and Figure 4-11 show that there has been a decrease of around one pH unit inside the support cages compared to outside the support cages. This could be a result of microbial activity inside the support cages (Table 4-5), although the exact mechanisms for the fall in pH are not currently known. Microbial production of CO_2 could be involved, but abiotic mechanisms could also be responsible (e.g. hydrolysis of metal ions). The gas analysis data (Table 4-3) show the very low oxygen content of the groundwater and the presence of helium and methane from geological sources.

The enhanced corrosion of the iron as shown by the high concentrations of dissolved metals and the results from dismantling Experiment 3 (Smart et al. 2012a), would not be expected in anoxic near-neutral water at low temperature, even with the high concentrations of chloride present, based on the results of laboratory experiments in the absence of microbial activity (Smart et al. 2004b). This result suggests that the corrosion is enhanced by microbial activity.

The microbial analysis indicates that autotrophic acetogens (AA) and sulphate reducing bacteria (SRB) are active in the vicinity of the model canisters. The key metabolic reaction for AA is:

$$4H_2 + 2CO_2 \rightleftarrows CH_3COO^- + H^+ + 2H_2O$$

The acetate produced by AA can cause stress corrosion cracking (SCC) of copper, if sufficient concentrations are reached and combined with tensile stress in the material.

SRB can use organic material (e.g. acetate) as an electron source:

$$Fe + CH_3COO^- + SO_4^{2-} + H_2O \rightleftarrows FeS + 2HCO_3^- + H_2 + OH^-$$

However, SRB can also utilise cathodic hydrogen emanating from the anaerobic corrosion of iron (Little and Lee 2007):

$$4Fe + SO_4^{2-} + 4H_2O \rightleftarrows FeS + 3Fe(OH)_2 + 2OH^-$$

Hydrogen produced by the anaerobic corrosion of iron can be utilised by both acetogens and sulphate reducers, provided the hydrogen pressure reaches a critical value (Pedersen 2012b), which it did in the Minican experiment (Lydmark and Hallbeck 2011). Hence there is a possibility of synergistic behaviour between anaerobic corrosion of iron and microbial activity (see Smart et al. 2010b, Appendix 1 for further discussion). The processes summarised above are consistent with the decrease in the sulphate concentrations and the high corrosion rate and release of iron observed during these experiments. During the period 2007 to 2010, the MPN of SRB, as well as the concentration of

ferrous iron inside the steel cages increased, suggesting causality between SRB activity and iron corrosion. The concentration of sulphate decreased in all experiment cages and the hydrogen pressure increased in those experiments, which can be considered as being closed systems (i.e. Experiments 1–3, which have bentonite clay in the steel cage). Thus, the rapid corrosion of cast-iron observed electrochemically (and gravimetrically for Experiment 3 when it was retrieved) appears to be explained by microbial activity. It is noteworthy that there was a fall in the total organic content of the water inside the canisters between 2008 and 2010 (Table 4-2); the reasons for this are not clear but one possibility is the consumption of organic material in the bentonite by microbial activity. As mentioned above the reasons for the fall in pH are not well understood. Acetogenic metabolism alone does not explain the observed decrease in pH since both the MPN of AA and the concentration of acetate decreased over time (Tables 4-3 to 4-5).

5.2 Electrochemical measurements

5.2.1 E_h measurements

The electrochemical potential values for the gold and platinum inside the support cages, and the E_h probe outside the support cages in the borehole, show that after sealing the boreholes the E_h fell from initial values of the order of 0 mV vs NHE, which correspond to oxic conditions in the groundwater, to values of the order of –300 mV, as any residual oxygen was consumed by reaction with rock minerals, microbial activity and/or corrosion processes. It is notable that the E_h values inside the support cages (e.g. Experiment 3 in Figure 4-17) fell more rapidly than outside the support cage, suggesting that residual oxygen was consumed more rapidly due to the increased surface area on which corrosion reactions could take place.

The long-term electrochemical potentials of the gold, platinum and the miniature canisters are indicative of very low oxygen concentrations. The electrochemical potential values obtained for the gold in the MiniCan experiments are comparable to the electrochemical potential values obtained during laboratory investigations of galvanic corrosion of iron-copper couples in anoxic conditions (Smart et al. 2004a, c), and the anaerobic corrosion of iron (Peat and al. 2001, Smart et al. 2001). They are also comparable to E_h values reported in the literature for deep Swedish groundwaters (Kind et al. 2001, Puigdomenech et al. 2001). The data show that for Experiments 1 to 3 (Figure 4-13, Figure 4-15 and Figure 4-17), with low density bentonite, the long-term E_h outside the cage is slightly higher than inside the cage, whereas for Experiment 4 (Figure 4-19), with compacted bentonite the situation is reversed.

It should be noted that the increase in corrosion rate for both copper and iron (for example see Figure 4-15 and Figure 4-16 for Experiment 2), began when the E_h had reached its minimum value. Since SRB are organisms that only proliferate under anoxic conditions it is possible that the increase in corrosion rate corresponded to the time when SRB became active and started to generate sulphide, which then caused an increase in the corrosion rate of both the copper and the iron electrodes.

5.2.2 Corrosion potential of copper and iron

The corrosion potential of the copper and the model canisters can be compared with other measurements and modelling activities (King et al. 2001); for example the predicted long-term corrosion potential of a copper canister in initially aerated compacted bentonite has been reported previously (King et al. 2001). The modelling calculations showed that the predicted short-term corrosion potential for a copper canister is of the order of –300 mV vs SCE (i.e. c. –50 mV vs NHE). This is more positive by approximately 100 mV than the value measured in Experiment 4 for the model canister embedded in compact bentonite under anoxic conditions (Figure 4-19). However, it should be noted that the corrosion potential of copper is a strong function of chloride concentration, oxygen concentration and mass-transport conditions (King et al. 2001) and direct comparisons with the results from the MiniCan experiment are not therefore possible because the environmental conditions considered in the modelling were not necessarily the same as those in the MiniCan experiment as there are number of factors that are unknown in the current experiments. The rest potential of the canister in Experiment 4 became more negative towards the end of 2009. The potential of the copper electrode in the same experiment was similar to that of the copper canister (Figure 4-20).

The long-term corrosion potentials of the copper electrodes in Experiments 1–3 (low density bentonite) generally fell in the range –400 to –500 mV vs NHE (Figure 4-14, Figure 4-16, Figure 4-18), the corrosion potential for copper in Experiment 4 (compact bentonite) was about –300 mV vs NHE (Figure 4-20) and the potential for Experiment 5 (no bentonite) was approximately –500 mV vs NHE (Figure 4-23). The corrosion potentials of the model canisters themselves in Experiments 1–5 were generally approximately 100 mV more positive than the potentials of the copper electrodes, but it should be noted that the potential of the copper canisters represents a mixed potential of the copper-cast iron couple, assuming that wetting of the cast iron insert had occurred by water penetration through the 1 mm defect in the copper shell. These corrosion potential values can be compared to published Pourbaix diagrams (Puigdomenech and Taxén 2000) for copper in pure water (Figure 5-1), in the presence of carbonate and high concentrations of chloride (Figure 5-2) and in the presence of sulphide (Figure 5-3). In pure water, copper is regarded as being thermodynamically immune to corrosion at the temperature of the MiniCan experiment and the measured corrosion potentials (Figure 5-1). In high concentrations of chloride, the measured corrosion potentials for the MiniCan experiments also show that copper is immune to corrosion by the formation of copper chlorides (Figure 5-2). However, in the presence of sulphide, Figure 5-3 indicates that for Experiments 1–4 the potential of the copper is in the domain of stability of copper sulphide. Experiment 5 exhibited a more negative copper corrosion potential which was nearer the region of thermodynamic stability of copper and this may account for the lower corrosion rate measured in this experiment.

Pourbaix diagrams in Figure 5-1 to Figure 5-3 should only be used as a guide for interpreting the MiniCan experiments, because they were calculated for a specific set of conditions (i.e. defined concentrations of dissolved species such as chloride, sulphur, carbonate and copper at 25°C) that were not exactly the same as those in the MiniCan experiment, which was at an ambient temperature of 15°C. The calculations of thermodynamic stability for copper could be extended to take account of the measured chemical conditions inside the support cages of the MiniCan experiments.

The potentials of the iron electrodes are below the hydrogen evolution potential at pH 7 and are consistent with the occurrence of anaerobic corrosion, with the resulting formation of hydrogen. The measured corrosion potentials for the cast iron electrodes are also consistent with the domain of stability of iron sulphide (Macdonald and Syrett 1979, Smart 2011).

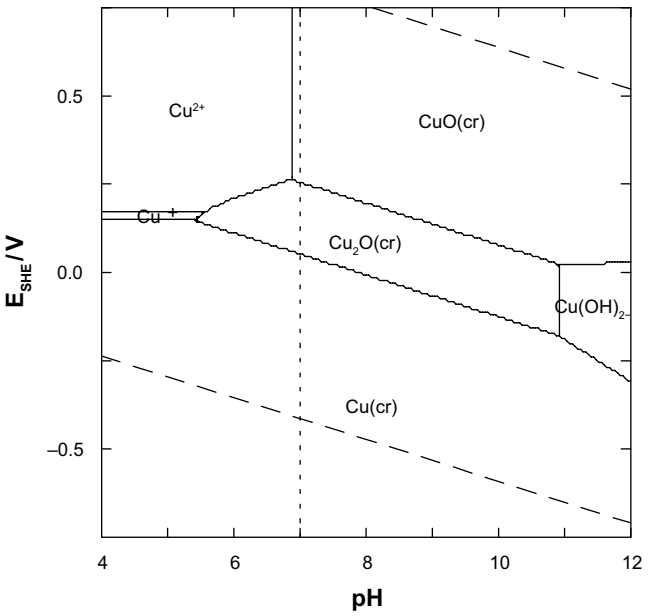

Figure 5-1. *Pourbaix diagram for copper in pure water $[Cu]_{TOT} = 10^{-6}$ mol/kg at 25°C (Puigdomenech and Taxén 2000).*

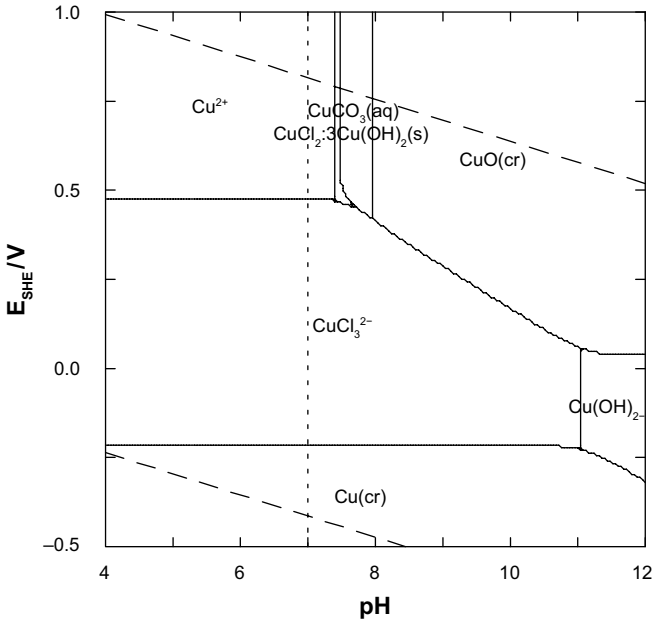

Figure 5-2. *Pourbaix diagram for copper at $[Cu]_{TOT} = 10^{-6}$ mol/kg at 25°C in solution containing $[CO_3^{2-}]_{TOT}$ = 2 mmol/kg and $[Cl]_{TOT}$ = 1.7 mol/kg (Puigdomenech and Taxén 2000).*

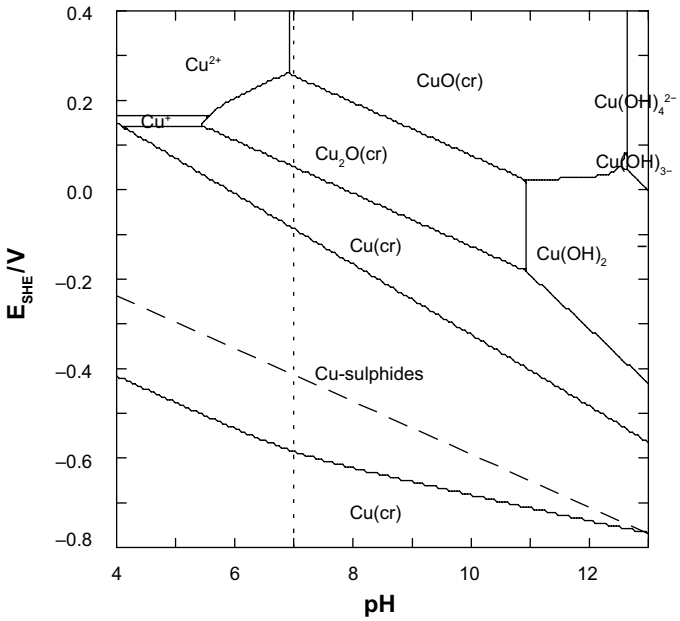

Figure 5-3. *Pourbaix diagram for copper in solutions containing $[HS^-]_{TOT}$ = 0.2 mmol/kg and $[Cu]_{TOT} = 10^{-6}$ mol/kg at 25°C (Puigdomenech and Taxén 2000).*

5.3 Corrosion rate measurements

5.3.1 Iron corrosion rates

The corrosion rates for iron are high but in Experiments 1, 2, 3 and 5 they appear to have stabilised (Figure 4-28). They are considerably higher than would be expected from laboratory experiments on the anaerobic corrosion on iron (Smart et al. 2002a, b). However, the values of corrosion rates should be treated with some caution as electrochemical measurements tend to overestimate the true values, since they only provide an instantaneous measure of corrosion rate, which is based on a number of assumptions about the nature of the electrochemical interface. The overall corrosion rate from the cast iron weight loss specimen from Experiment 3 (i.e. the long-term integrated measurement of corrosion rate) was at least 500 μm yr^{-1} on the basis that the weight loss sample had been completely converted to a mass of residual graphite, silicon and oxide. It is not known at what point the weight loss sample was completely consumed but based on the initial dimensions of the sample it is possible to estimate that the minimum corrosion rate was at least 500 μm yr^{-1}. This can be compared to an electrochemically measured value for Experiment 3 of up to 2,500 μm yr^{-1} (Figure 4-28). Examination of the electrodes from Experiment 3 showed that there had not been crevice corrosion around the sheathing on the iron electrodes (Smart et al. 2012a). The high corrosion rates reported here support the observation of increased iron concentrations in the water analyses and it seems most likely that the high rates are a result of microbial activity inside the support cage, particularly sulphate reducing bacteria (see Section 4.1.6 and Lydmark and Hallbeck 2011).

Hilbert et al. (2005) investigated the use of the LPR and ACI techniques to measure corrosion rates of steel in anoxic environments containing sulphide produced by SRB activity. Their conclusion was that under these conditions the formation of porous reactive sulphide films dominates the electrochemical response, leading to misleadingly high values of corrosion rate by a factor of 10–100 times. It is therefore probable that the high corrosion rates measured for cast iron in the MiniCan experiment by LPR and ACI are an overestimate of the true corrosion rate and based on the weight loss measurements from Experiment 3 (Smart et al. 2012a) it appears that the overestimate is of the order of 5×. The cast iron corrosion rate for Experiment 4 (Figure 4-29) is not clear because of the probable difficulties with the connections and electrodes damaged by the swelling of the compacted bentonite. The corrosion rates derived from the electrochemical noise experiments are considerably lower than the measurements from the LPR and ACI measurements, by a factor of ×100 for the cast iron and ×10 for the copper.

5.3.2 Copper corrosion rates

The electrochemical measurements of the initial corrosion rate gave values for copper below 5 μm yr^{-1} (Smart and Rance 2009). This is based on a Stern-Geary constant of 26 mV, whereas other authors (e.g. Rosborg et al. 2004) have used lower values. Thus the figures reported here are conservative values (i.e. they may exaggerate the corrosion rate). The derived corrosion rate values can be compared with values given in the literature for experiments on copper in compacted bentonite; for example values of up to 2.5 μm yr^{-1} have been reported by Rosborg et al. (2004) for measurements during the LOT experiment and 4.7 μm yr^{-1} by Saario et al. (2004) for weight loss measurements on copper in compacted bentonite in laboratory tests.

More recent measurements (e.g. Figure 4-26) suggest that higher corrosion rates of copper may be occurring. However, the electrochemically measured corrosion rate for copper in Experiment 2 is much higher than that measured using the copper coil electrical resistance method (see Figure 4-26 and Figure 4-30), which suggests that there were some experimental difficulties associated with the electrochemical corrosion rate measurements. When Experiment 3 was opened it was found that the majority of the surfaces inside the support cage were covered in a layer of black deposit, which was found by analysis to be predominantly iron sulphide. This layer is likely to have caused the high corrosion rates measured on the copper electrodes, because the iron sulphide is electronically conducting and it therefore allows a higher current to be measured for the electrode during the electrochemical measurements than would otherwise be the case on a bare copper surface. A weight loss analysis on the copper weight loss specimen from Experiment 3 gave a corrosion rate of 0.15 μm yr^{-1}, so it can be concluded that the later electrochemical measurements for the copper corrosion rate were a significant overestimate (particularly the AC impedance and LPR measurements; the noise measurements gave lower values) and that the electrical resistance measurements were nearer to the true,

gravimetric, corrosion rate for the copper. It is possible that the electrical resistance measurements were affected by a thin layer of copper sulphide on the surface of the wire; copper sulphide was observed on the surface of the copper samples taken from Experiment 3. The AC impedance plots for copper (see Appendix 1) show some structure in the results that is similar to that observed for coated surfaces (e.g. Macdonald and McKubre 2005). It is noticeable that the ACI plots for Experiment 5 do not show the same structure.

5.3.3 Implications of corrosion rate results for a KBS-3 repository

It should be recognised that the environmental conditions within Experiments 1, 2, 3 and 5 are not fully representative of the conditions that will be experienced in a repository because the containers are in contact with low density bentonite (Experiments 1 to 3) or raw groundwater (Experiment 5), rather than fully compacted bentonite. It should also be noted that in the repository situation the temperatures will be higher than in the MiniCan experiments for a very long period. In both these environments (i.e. low density bentonite and no bentonite) it is likely that microbial activity would be different to that expected in the fully compacted bentonite that would be used in the repository situation, since fully compacted bentonite is expected to inhibit microbial activity (Motamedi et al. 1996). Experiment 4 therefore represents the closest analogy to the proposed SKB design since it uses fully compacted bentonite (however the thickness of the bentonite layer in this experiment is less than one tenth of the thickness of the actual bentonite buffer in the KBS-3 concept). Unfortunately, the corrosion rates measured electrochemically in Experiment 4 appear to be unreliable, probably because swelling of the bentonite has led to deformation or damage to the electrical connections. The true average corrosion rate of copper in compacted bentonite will not be confirmed until Experiment 4 is dismantled.

It should also be noted that in the repository situation the temperatures would be higher than in the MiniCan experiments. This could have the effect of increasing the corrosion rate, if it is due to abiotic corrosion processes, or it may affect the viability of microbial populations and hence reduce the rate of any microbially influenced corrosion processes. In fact, for the geological and hydrogeochemical conditions at the chosen site for the Swedish repository, the rate of corrosion has been shown to be controlled by the supply of sulphide external to the compacted bentonite so that the corrosion rate will be controlled by the rate of transport of sulphide through the bentonite layer, as discussed by King et al. (2001), and the rate of production of sulphide by sulphate reducing bacteria in the vicinity of the external surfaces of the bentonite buffer. Recent work by Masurat et al. (Masurat et al. 2010) suggests that the rate of production of sulphide by microbial activity within compacted bentonite is very limited and that the amount of sulphide that can be produced by microbial activity is insufficient to sustain significant degrees of corrosion of the copper canister. Their work also showed that the rate of growth of SRB is two orders of magnitude higher in lower density bentonite (1.5 g cm^{-3}) compared to that in compacted bentonite with a density of 2 g cm^{-3}. For comparison, the density of the bentonite used in Experiments 1 to 3 of the MiniCan project was 1.16 to 1.36 g cm^{-3}, whereas the density of the compacted bentonite in Experiment 4 was ~2 g cm^{-3}.

The electrochemical measurements from Experiment 5 (no bentonite) indicate that the corrosion rate of copper in raw groundwater is significantly lower than in the experiments with low density bentonite present. However, analysis of the copper coupon removed from Experiment 3 indicates that the electrochemical measurements overstated the actual corrosion rate (Smart et al. 2012a) and the high results from the electrochemical measurements are probably an artefact caused by the presence of conductive sulphide films that precipitated on the surface of the copper. The electrochemically measured corrosion rate of the iron in Experiment 5 is similar to the values recorded in the presence of low density bentonite and significantly higher than those values measured in laboratory experiments under anoxic conditions, in the absence of sulphur. Analysis of the weight loss coupon from Experiment 3 (Smart et al. 2012), showed that the corrosion rate of the cast iron was at least 500 μm yr^{-1} and this is the same order of magnitude as the later electrochemical measurements.

The dissolved iron concentrations in Experiment 5 are the highest measured for any of the experiments. This suggests that even if the available sulphide concentration is lower than in Experiments 1 to 3 there is still sufficient sulphide present in Experiment 5 for iron sulphide production to occur. This could be a result of SRB activity supported by the metabolism of hydrogen produced by the anaerobic corrosion of the cast iron components of the experiment (Masurat et al. 2010). Based on

the results of analysing Experiment 3 it is probable that the inside of Experiment 5 is also covered by iron sulphide, but for some reason this did not lead to an increase in the electrochemically measured corrosion rate of the copper. One explanation for this may be that the flow of water through the support cage is greater because there are no restrictions from bentonite in the annulus of the support cage and therefore the iron precipitate is distributed differently inside the support cage, with less on the surface of the copper electrodes, but this remains speculation until Experiment 5 is examined in more detail.

5.4 Strain gauge measurements

It is clear that the small fluctuations in the responses from the strain gauges attached to Experiments 1 and 4 (Figure 4-33) are most probably due to seasonal changes in the local temperatures in the vicinity of the experiments.

Since the unexplained increase in tensile strain for one of the sensors on Experiment 1 (strain gauge elements 1a and 1b near the top of the canister), there has been a slow decrease in the strain, suggesting a slow compression of the canister. The largest fall in the measured strain occurred on sensors 1a and 1c, which exhibited a change of ~1,000–1,500 microstrain over a 5-year period. The other sensors exhibited changes of a few hundred microstrain over a five year period. Over the complete length of the model canister (i.e. 300 mm length) a microstrain of 1,000 (i.e. 1 milli-strain) corresponds to a change in length of the canister of 300 μm. This is well within the elastic region for the deformation of copper under load.

Strain gauge measurements are very sensitive to small changes in dimensions and the results show that no significant expansion of Experiment 1 (low density bentonite) or Experiment 4 (compacted bentonite) occurred as a result of corrosion of the cast iron insert. This is consistent with the observations made on Experiment 3 when it was dismantled (Smart et al. 2012a) and no changes were found when the external dimensions of the canister were measured and compared to the original machined dimensions.

6 Future work

The following suggestions are made for future activities on the MiniCan experiment:

- Consider dismantling other MiniCan experiments to confirm the observations from Experiment 3 under different operating conditions, for example for fully compacted bentonite (Experiment 4).
- Consider placing a new experiment in Borehole for Experiment 3, to investigate other parameters that may affect corrosion behaviour (e.g. higher temperatures).
- Carry out thermodynamic calculations to define Pourbaix diagrams for copper and iron in the environments measured for the interior of the support cages in the MiniCan experiments.

7 Conclusions

The main conclusions from the MiniCan project to date are as follows:

1. Water analysis has shown that there are compositional differences between the water inside the support cages compared to the external borehole water. These can be explained on the basis of corrosion of the iron and microbial activity inside the support cages. There has been a large increase in the concentration of dissolved iron, which is mainly present in the form of Fe^{2+}, and a parallel decrease in the pH from the groundwater pH value of ~7.6 to a value inside the support cage of ~6.6.
2. Microbial analysis has demonstrated that SRB are active in the experimental boreholes.
3. E_h measurements have shown that the test conditions within the support cages around the MiniCan experiments became reducing over a period of a few thousand hours at the start of the experiments.
4. The corrosion potentials of the copper and iron electrodes in the experiments with low density bentonite (Experiments 1 to 3) are consistent with the formation of copper sulphide and iron sulphide corrosion products.
5. The electrochemically measured corrosion rates increased for both copper and iron. Analysis of the weight loss sample in Experiment 3 has confirmed that the corrosion rate for iron is at least 500 μm yr^{-1}. However, the corrosion rates measured for iron and copper by LPR and ACI are probably overestimated due to the electrochemical properties of the sulphide films that accumulated on the surface as a result of SRB activity.
6. High corrosion rates have been measured electrochemically for copper in low density bentonite and unconditioned groundwater, but these values are very likely to have been overestimated due to the surface precipitation of iron sulphide produced by corrosion of cast iron in the vicinity. The measured values are considerably higher than that measured by weight loss in Experiment 3, where a value of 0.15 ± 0.02 μm yr^{-1} was obtained.
7. Strain gauge measurements showed that no expansion of the copper canister had occurred as a result of corrosion of the cast iron insert.
8. It should be recognised that these test conditions are not directly comparable with the proposed repository conditions. It appears that the low density bentonite is conducive to microbial activity, particularly that of sulphate reducing bacteria (SRB), and this has led to an increase in the corrosion rate of the cast iron. However, the copper corrosion rates measured by the electrical resistance method in low density bentonite and raw groundwater are considerably lower (< 1 μm yr^{-1}).

8 Acknowledgements

The authors gratefully acknowledge assistance provided by the following during the reporting period:

- SKB: Christina Lilja, Lars Werme, Richard Bäck, Mats Lundqvist, Teresita Morales, Siren Bortelid Moen, SKB chemistry laboratory staff at Äspö.
- Microbial Analytics: Karsten Pedersen and Sara Eriksson.

The authors also gratefully acknowledge financial support provided by SKB for conducting this project.

References

SKB's (Svensk Kärnbränslehantering AB) publications can be found at www.skb.se/publications.

Aggarwal S, Addepalli V, Smart N, 2015. Further metallographic analysis of MiniCan SCC test specimens. SKB R-15-11, Svensk Kärnbränslehantering AB.

ASTM, 2003. ASTM G59-97e1: Standard test method for conducting potentiodynamic polarization resistance measurements. West Conshohocken, PA: ASTM International.

Bond A E, Hoch A R, Jones G D, Tomczyk A J, Wiggin R M, Worraker W J, 1997. Assessment of a spent fuel disposal canister. Assessment studies for a copper canister with cast steel inner component. SKB TR 97-19, Svensk Kärnbränslehantering AB.

Hallbeck L, Edlund J, Eriksson L, 2011. Microbial analyses of groundwater and surfaces during the retrieval of Experiment 3, A04, in MINICAN. SKB P-12-01, Svensk Kärnbränslehantering AB.

Hilbert L R, Hemmingsen T, Nielsen L V, Richter S, 2005. When can electrochemical techniques give reliable corrosion rates on carbon steel in sulfide media. NACE Corrosion 2005, Houston, Texas, 3–7 April 2005, Paper 05346.

King F, Ahonen L, Taxén C, Vuorinen U, Werme L, 2001. Copper corrosion under expected conditions in a deep geological repository. SKB TR-01-23, Svensk Kärnbränslehantering AB.

Little B J, Lee J S, 2007. Microbiologically influenced corrosion. Hoboken, NJ: Wiley-Interscience.

Lydmark S, Hallbeck L, 2011. Results report. Sampling and analyses of gases and microorganisms in the water from MINICAN in 2007, 2008 and 2010. SKB P-11-32, Svensk Kärnbränslehantering AB.

Macdonald D D, McKubre M C H, 2005. Coatings. In Barsoukov E, Macdonald J R (eds). Impedance spectroscopy; theory, experiment, and applications. Hoboken, NJ: Willey-Interscience, 419–420.

Macdonald D D, Syrett B C, 1979. Potential-pH diagrams for iron and nickel in high salinity geothermal brine containing low concentrations of hydrogen sulphide. Corrosion 35, 471–474.

Masurat P, Eriksson S, Pedersen K, 2010. Microbial sulphide production in compacted Wyoming bentonite MX-80 under in situ conditions relevant to a repository for high-level radioactive waste. Applied Clay Science 47, 58–64.

Motamedi M, Karnland O, K Pedersen, 1996. Survival of sulfate reducing bacteria at different water activities in compacted bentonite. FEMS Microbiology Letters 141, 83–87.

Peat R, Brabon S, Fennell P A H, Rance A P, Smart N R, 2001. Investigation of Eh, pH and corrosion potential of steel in anoxic groundwater. SKB TR-01-01, Svensk Kärnbränslehantering AB.

Pedersen K, 2012a. Subterranean microbial populations metabolize hydrogen and acetate under in situ conditions in granitic groundwater at 450 m depth in the Äspö Hard Rock Laboratory, Sweden. FEMS Microbiology Ecology 81, 217–229.

Pedersen K, 2012b. Influence of H_2 and O_2 on sulphate-reducing activity of a subterranean community and the coupled response in potential. FEMS Microbiology Ecology 82, 653–665.

Puigdomenech I, Taxén C, 2000. Thermodynamic data for copper. Implications for the corrosion of copper under repository conditions. SKB TR-00-13, Svensk Kärnbränslehantering AB.

Puigdomenech I, Ambrosi J-P, Eisenlohr L, Lartigue J-E, Banwart S A, Bateman K, Milodowski A E, West J M, Griffault L, Gustafsson E, Hama K, Yoshida H, Kotelnikova S, Pedersen K, Michaud V, Trotignon L, Rivas Perez J, Tullborg E-L, 2001. O2 depletion in granitic media. The REX project. SKB TR-01-05, Svensk Kärnbränslehantering AB.

Rosborg B, Eden D A, Karnland O, Pan J, Werme L O, 2004. Real-time monitoring of copper corrosion at the Äspö Laboratory. presented at Eurocorr 2004, Nice, 12–16 September 2004. In Prediction of long term corrosion behaviour in nuclear waste systems: proceedings of the 2nd International Workshop Organized by the Working Party on Nuclear Corrosion (WP4) of the European Federation of Corrosion (EFC), Nice, September 2004, Eurocorr 2004. Châtenay-Malabry: Agence nationale pour la gestion des déchets radioactifs (Andra), 10.

Saario T, Betova I, Heinonen J, Kinnunen P, Lilja C, 2004. Effect of the degree of compaction of bentonite on the general corrosion rate of copper. Presented at Eurocorr 2004, Nice, 12–16 September 2004. In Prediction of long term corrosion behaviour in nuclear waste systems: proceedings of the 2nd International Workshop Organized by the Working Party on Nuclear Corrosion (WP4) of the European Federation of Corrosion (EFC), Nice, September 2004, Eurocorr 2004.Châtenay-Malabry: Agence nationale pour la gestion des déchets radioactifs (Andra), 45.

Smart N R, 2011. The anaerobic corrosion of carbon steel and the potential influence of sulphur species. Presented at the SACNUC workshop, Brussels, 21–23 October 2008. In Féron D, Kursten B, Druyts F (eds). Sulphur-assisted corrosion in nuclear disposal systems. Leeds: Maney. (EFC 59)

Smart N R, Rance A P, 2009. Miniature canister corrosion experiment – results of operations to May 2008. SKB TR-09-20, Svensk Kärnbränslehantering AB.

Smart N R, Fennell P A H, Peat R, Spahiu K, Werme L, 2001. Electrochemical measurements during the anaerobic corrosion of steel. In: Hart K P, Lumpkin G R (eds). Scientific basis for nuclear waste management XXIV: symposium held in Sydney, Australia, 27–31 August 2000. Warrendale, PA: Materials Research Society. (Materials Research Society Symposium Proceedings 663), 487–495.

Smart N R, Blackwood D J, Werme L, 2002a. Anaerobic corrosion of carbon steel and cast iron in artificial groundwaters: Part 1 – Electrochemical aspects. Corrosion 58, 547–559.

Smart N R, Blackwood D J, Werme L, 2002b. Anaerobic corrosion of carbon steel and cast iron in artificial groundwaters: Part 2 – Gas generation, Corrosion 58, 627–637.

Smart N R, Rance A P, Fennell P A H, 2004a. Galvanic corrosion of copper-cast iron couples. SA/EIG/13974/C001, Serco, UK. (Also published as SKB TR-05-06, Svensk Kärnbränslehantering AB.)

Smart R, Rance A P, Werme L O, 2004b. Anaerobic corrosion of steel in bentonite. In Oversby V M, Werme L O (eds). Scientific Basis for Nuclear Waste Management XXVII. Warrendale, PA: Materials Research Society. (Materials Research Society Symposium Proceedings 807), 441–446.

Smart N R, Fennell P A H, Rance A P, Werme L O, 2004c. Galvanic corrosion of copper-cast iron couples in relation to the swedish radioactive waste canister concept. Presented at Eurocorr 2004, Nice, 12–16 September 2004. In Prediction of long term corrosion behaviour in nuclear waste systems: proceedings of the 2nd International Workshop Organized by the Working Party on Nuclear Corrosion (WP4) of the European Federation of Corrosion (EFC), Nice, September 2004, Eurocorr 2004. Châtenay-Malabry: Agence nationale pour la gestion des déchets radioactifs (Andra), 52.

Smart N R, Rance A P, Fennell P A H, 2006. Expansion due to anaerobic corrosion of iron. SKB TR-06-41, Svensk Kärnbränslehantering AB.

Smart N R, Bäck R, Fennell P A H, Knowles G, Lundqvist M, Rance A P, Reddy B, Spencer D, Werme L O, 2007. In situ corrosion testing of miniature copper-cast iron radioactive waste canisters. In Corrosion 2007, Extended abstract, Research in progress Symposium, Nashville, March 2007.

Smart N R, Rance A P, Reddy B, 2010a. Miniature canister (MiniCan) corrosion experiment progress report 1 for 2008–9. SERCO/TAS/E.003110.01/Issue 01, Serco Assurance.

Smart N R, Rance A P, Reddy B, 2010b. Miniature canister (MiniCan) corrosion experiment progress report 2 for 2008–9. SERCO/TAS/E.003110.02/Issue 01, Serco Assurance.

Smart N R, Reddy B, Rance A P, 2011a. Miniature canister (MiniCan) corrosion experiment progress report 3 for 2008–2010. SKB P-11-40, Svensk Kärnbränslehantering AB.

Smart N R, Rance A P, Reddy B, Eriksson S, Pedersen K, Lilja C, 2011b. Further studies of in situ corrosion testing of miniature copper-cast iron nuclear waste canisters. Corrosion Engineering, Science and Technology 46, 142–147.

Smart N R, Rance A P, Reddy B, Fennell P, Winsley R J, 2012a. Analysis of SKB MiniCan Experiment 3. SKB TR-12-09, Svensk Kärnbränslehantering AB.

Smart N, Reddy B, Rance A, 2012b. Miniature Canister (MiniCan). Corrosion experiment progress report 4 for 2008–2011. SKB P-12-13, Svensk Kärnbränslehantering AB.

Smart N, Rose S, Nixon D, Rance A, 2013. Metallographic analysis of SKB MiniCan Experiment 3. SKB R-13-35, Svensk Kärnbränslehantering AB.

Appendix 1

Electrochemical corrosion rate measurements for Experiments 1 to 3 and 5 for January to December 2012

Please note that all potentials shown in the electrochemical measurements are with respect to the reference electrode (i.e. Ag/AgCl), not NHE.

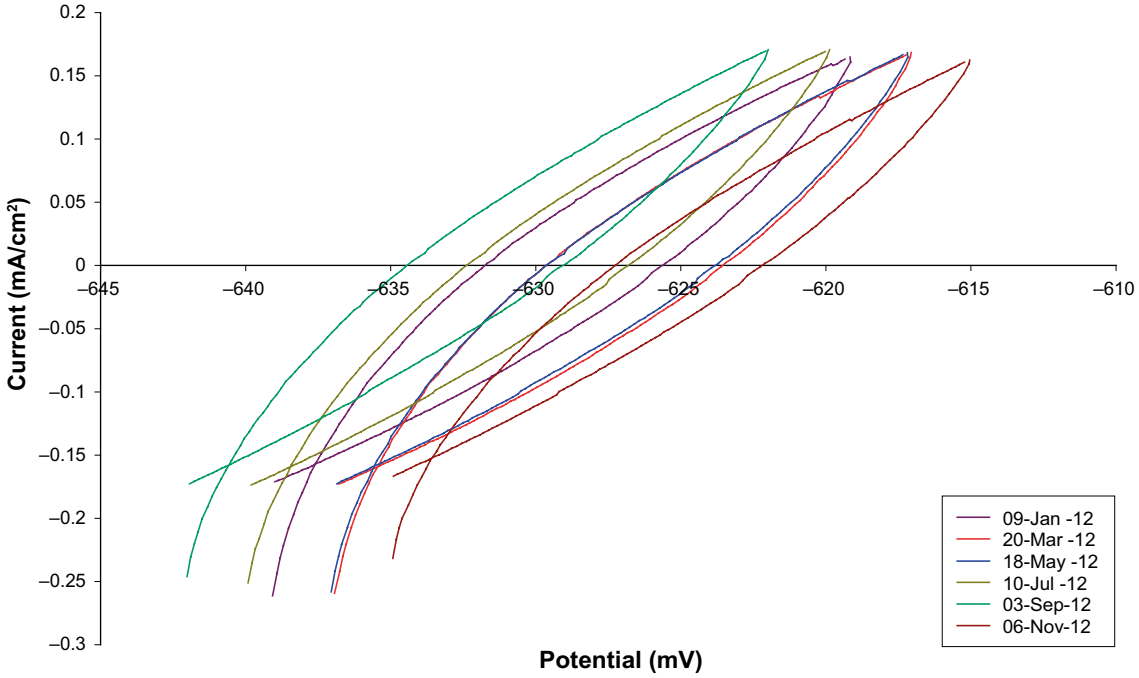

Figure A1-1. *LPR plots of cast iron in Experiment 1 (low density bentonite).*

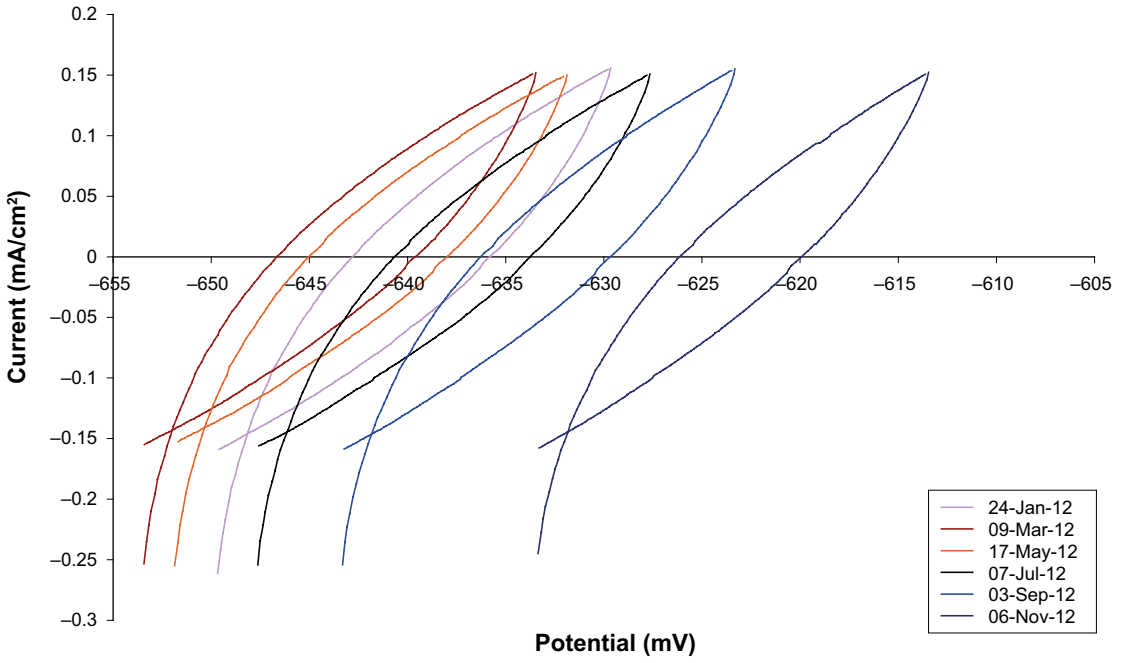

Figure A1-2. *LPR plots of cast iron in Experiment 2 (low density bentonite).*

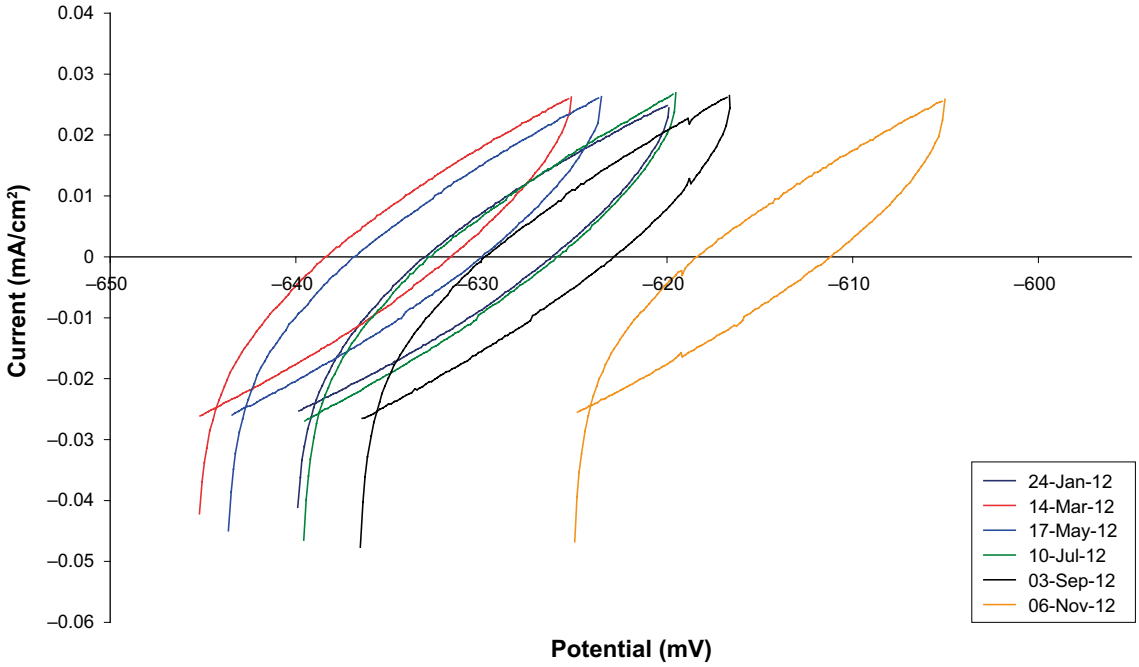

Figure A1-3. *LPR plots of copper in Experiment 2 (low density bentonite).*

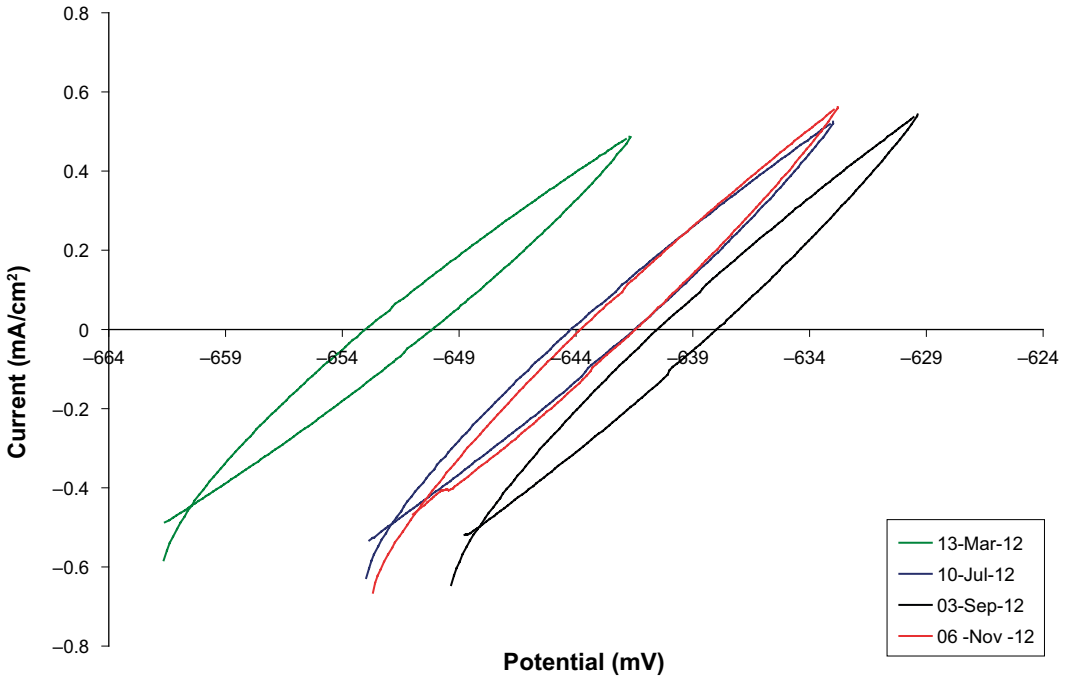

Figure A1-4. *LPR plots of cast iron in Experiment 5 (no bentonite).*

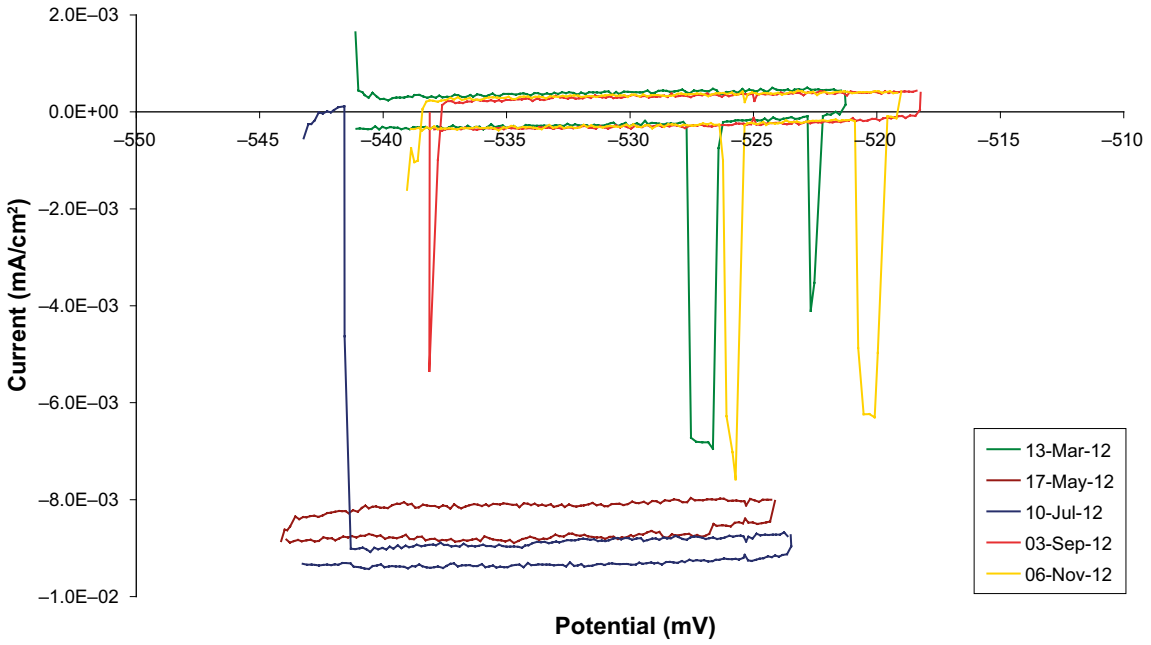

Figure A1-5. *LPR plots of copper in Experiment 5 (no bentonite).*

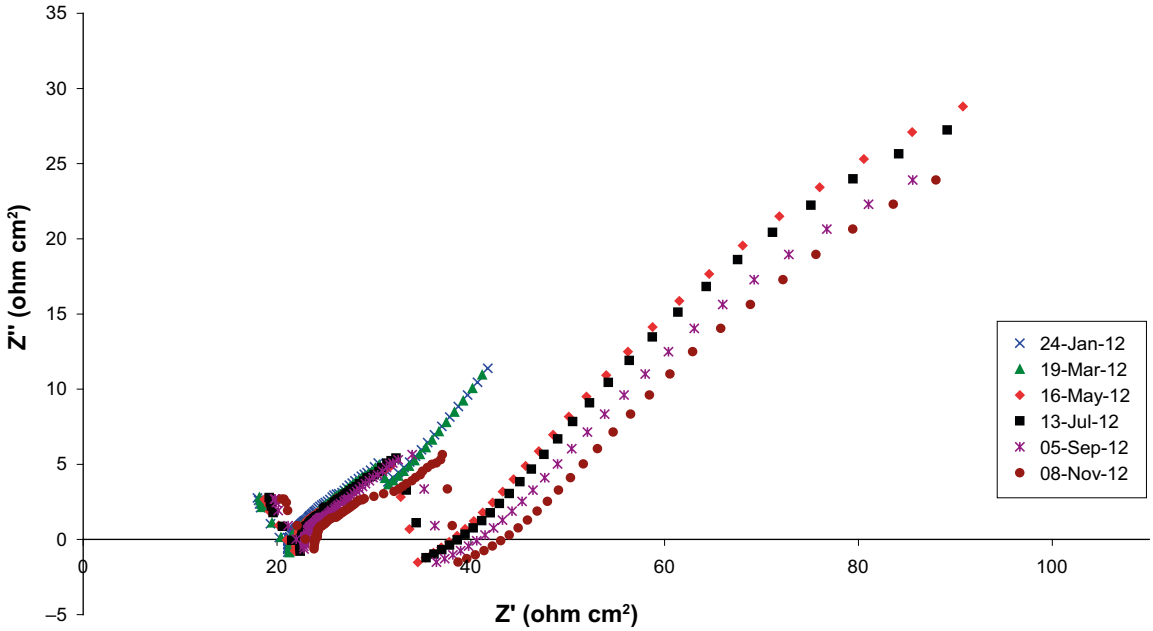

Figure A1-6. *ACI plots of cast iron in Experiment 1 (low density bentonite).*

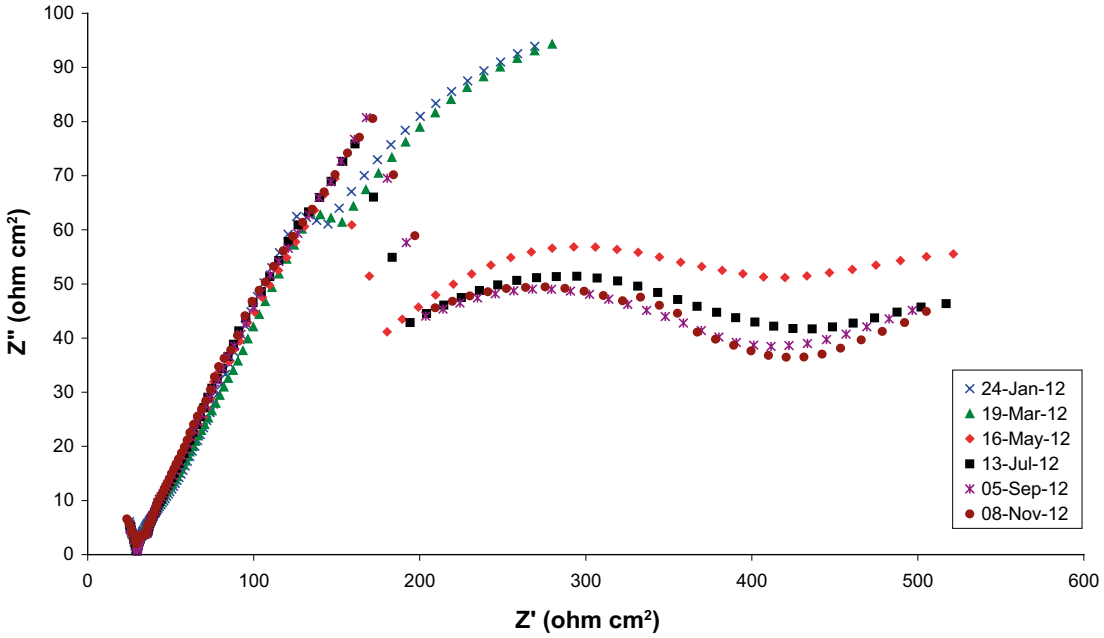

Figure A1-7. *ACI plots of copper in Experiment 1 (low density bentonite).*

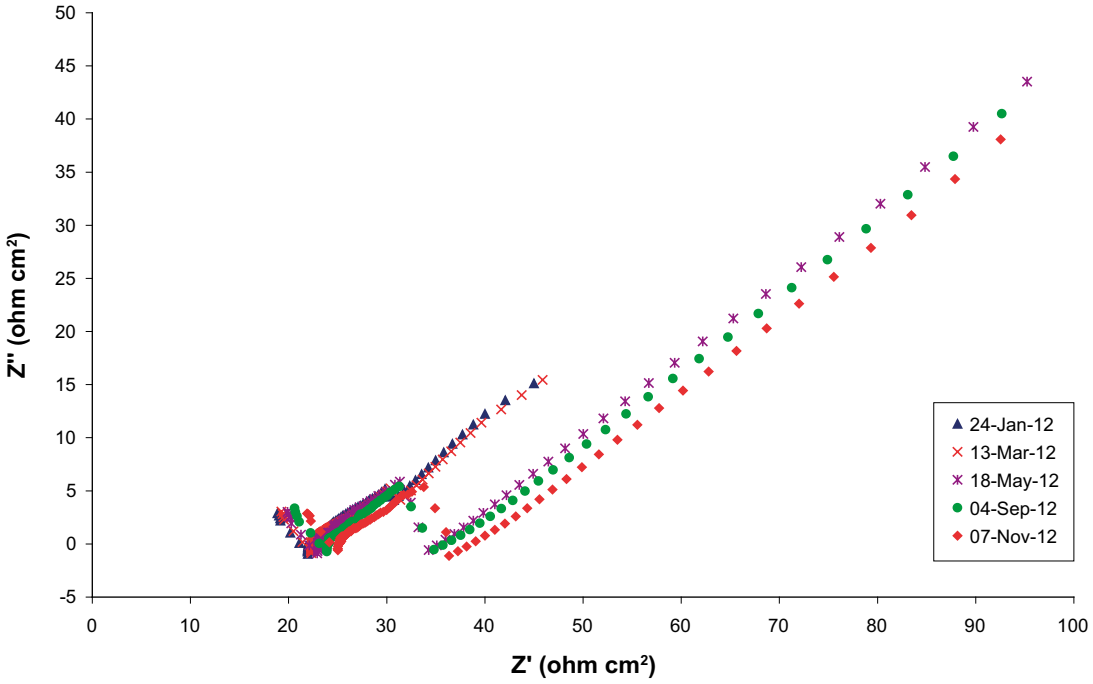

Figure A1-8. *ACI plots of cast iron in Experiment 2 (low density bentonite).*

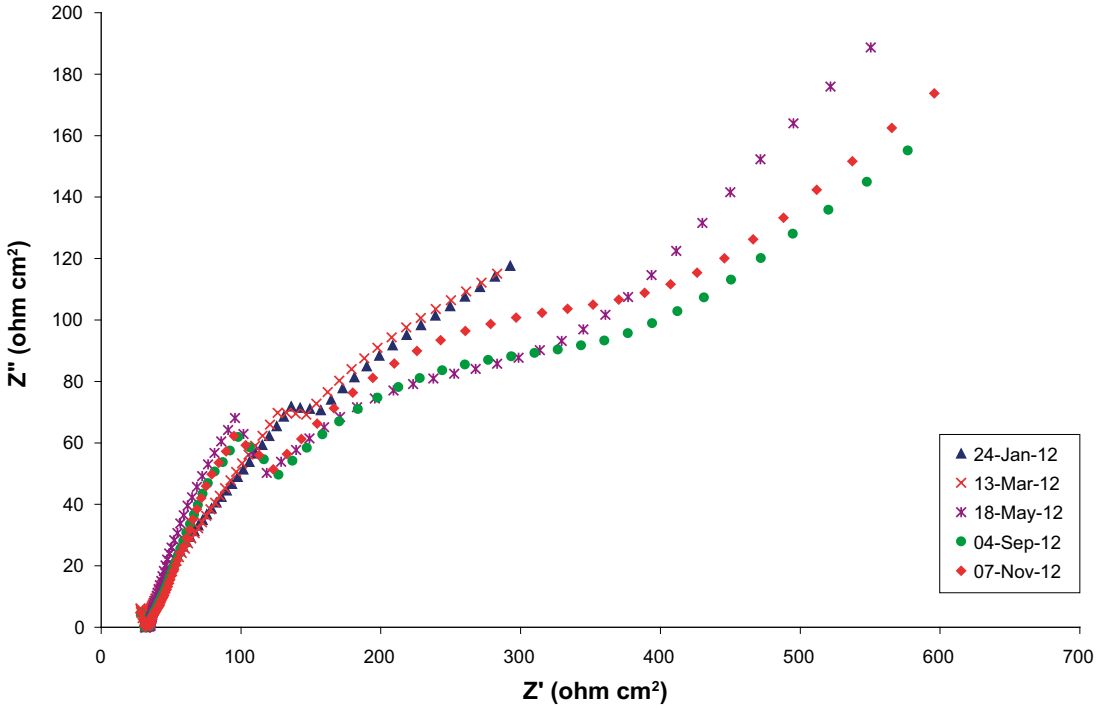

Figure A1-9. *ACI plots of copper in Experiment 2 (low density bentonite).*

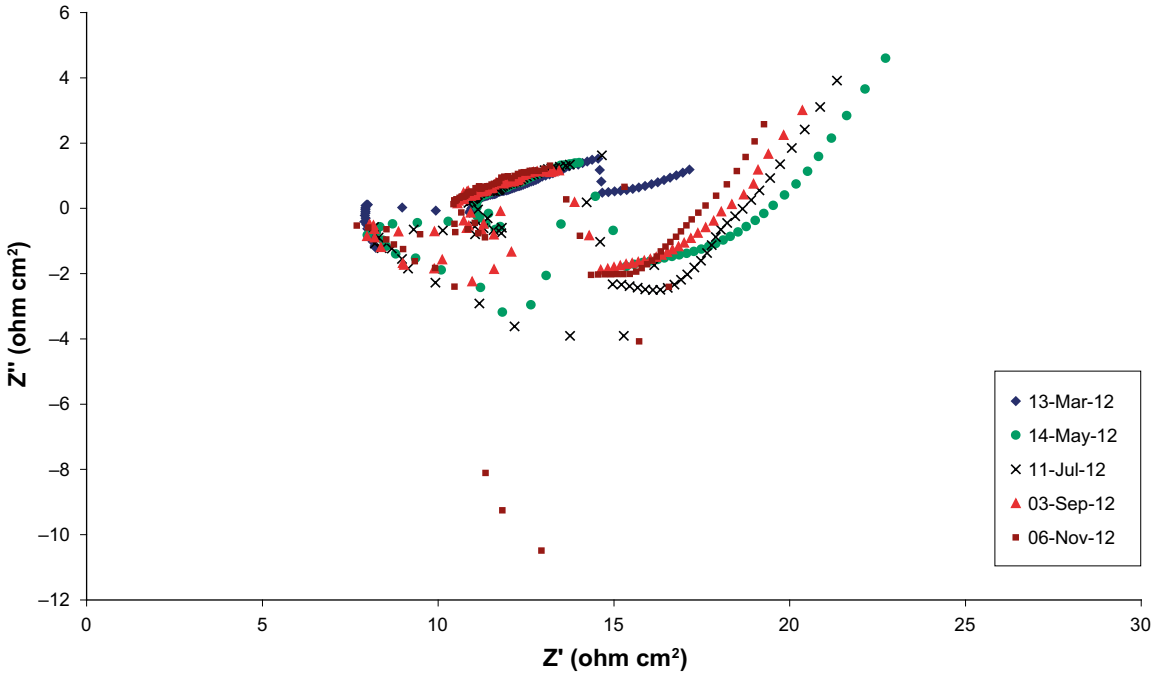

Figure A1-10. *ACI plots of cast iron in Experiment 5 (no bentonite).*

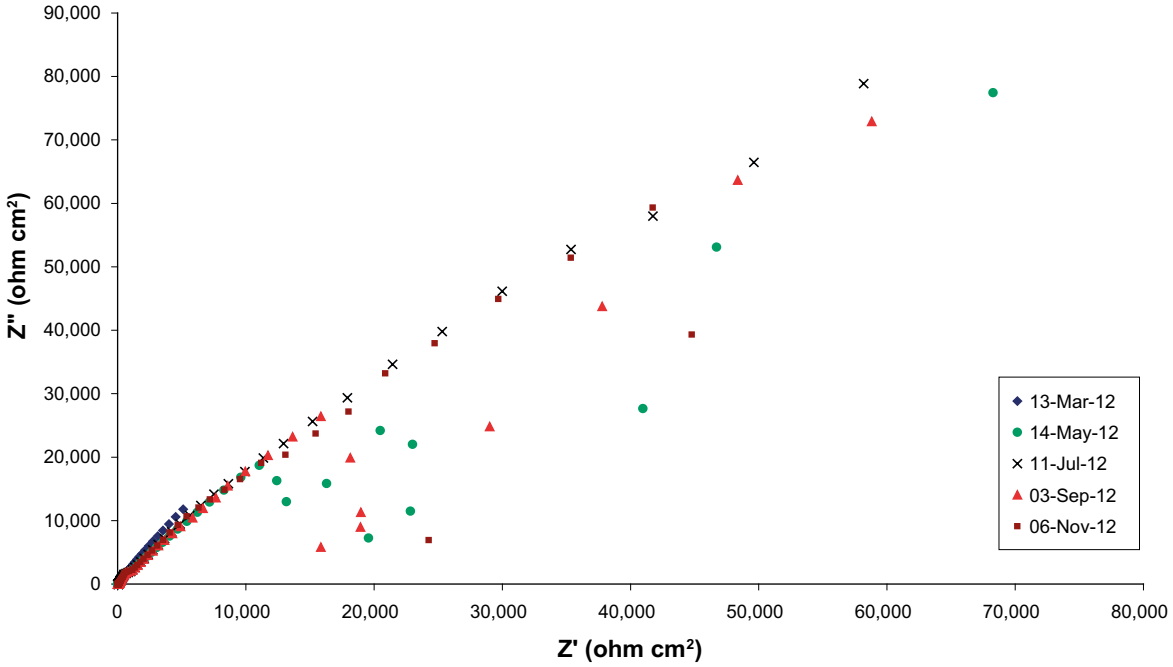

Figure A1-11. *ACI plots of copper in Experiment 5 (no bentonite).*

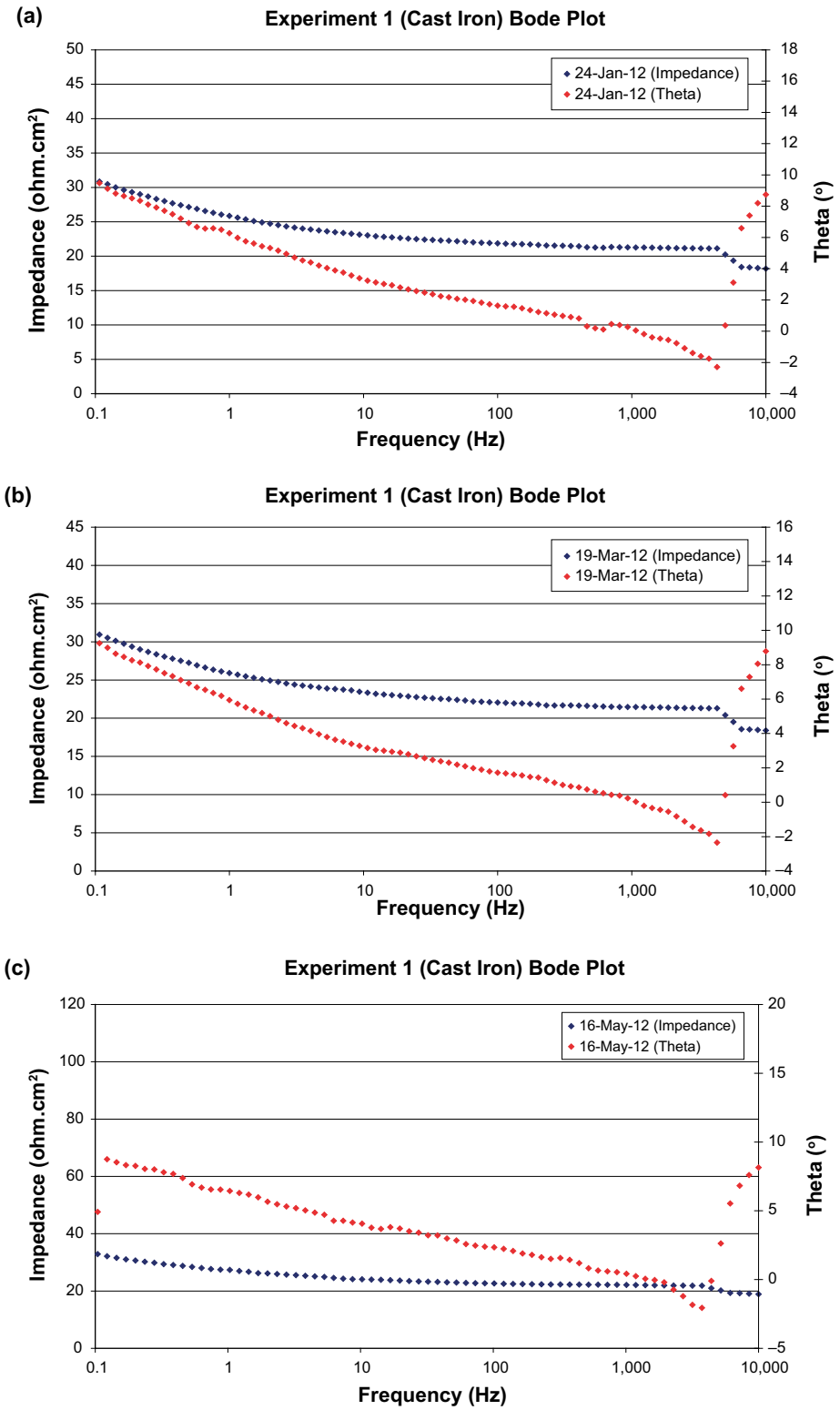

Figure A1-12. *Bode plots of cast iron in Experiment 1 (low density bentonite) in (a) January 2012, (b) March 2012 and (c) May 2012.*

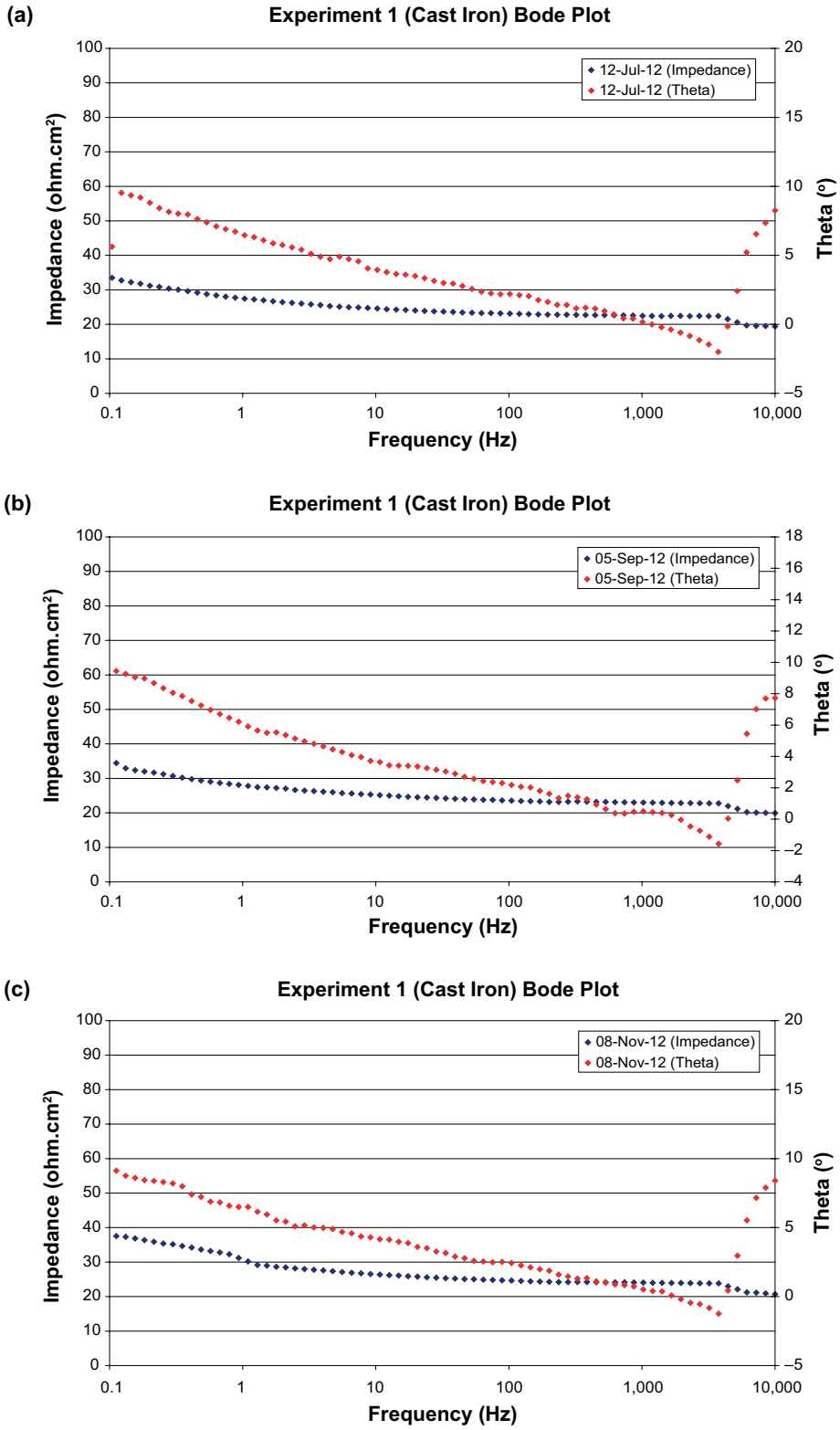

Figure A1-13. *Bode plots of cast iron in Experiment 1 (low density bentonite) in (a) July 2012, (b) September 2012 and (c) November 2012.*

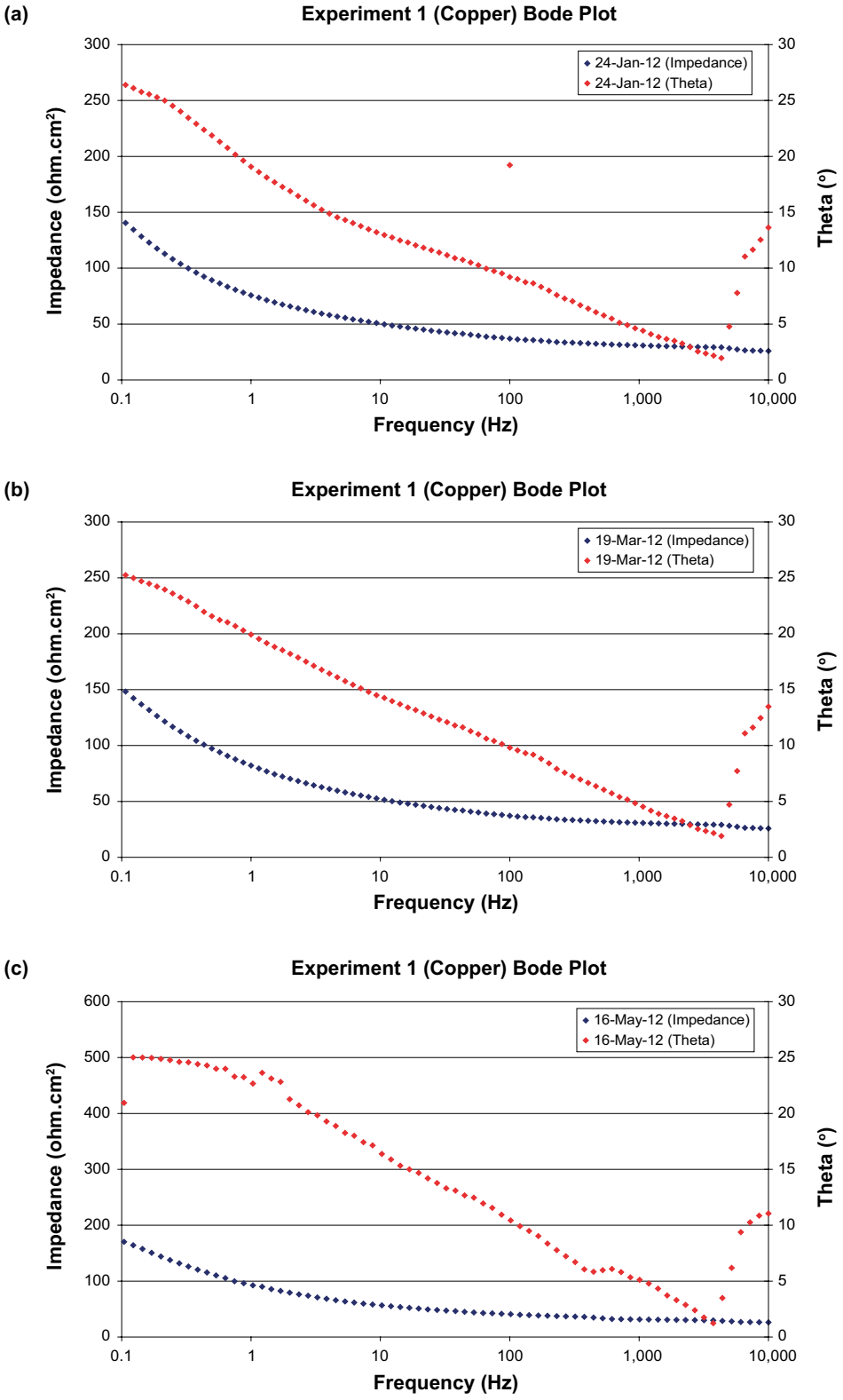

Figure A1-14. *Bode plots of copper in Experiment 1 (low density bentonite) in (a) January 2012, (b) March 2012 and (c) May 2012.*

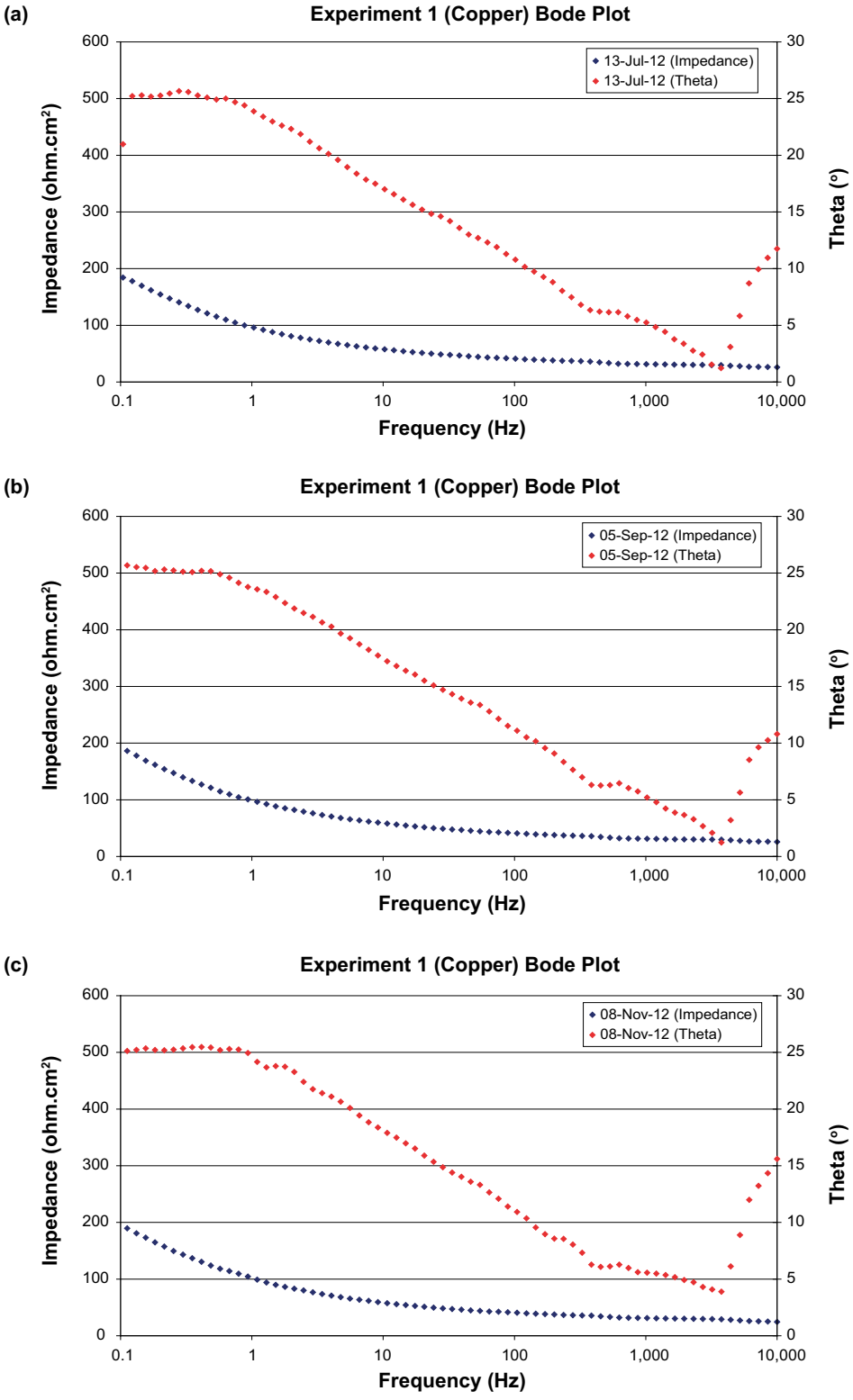

Figure A1-15. *Bode plots of copper in Experiment 1 (low density bentonite) in (a) July 2012, (b) September 2012 and (c) November 2012.*

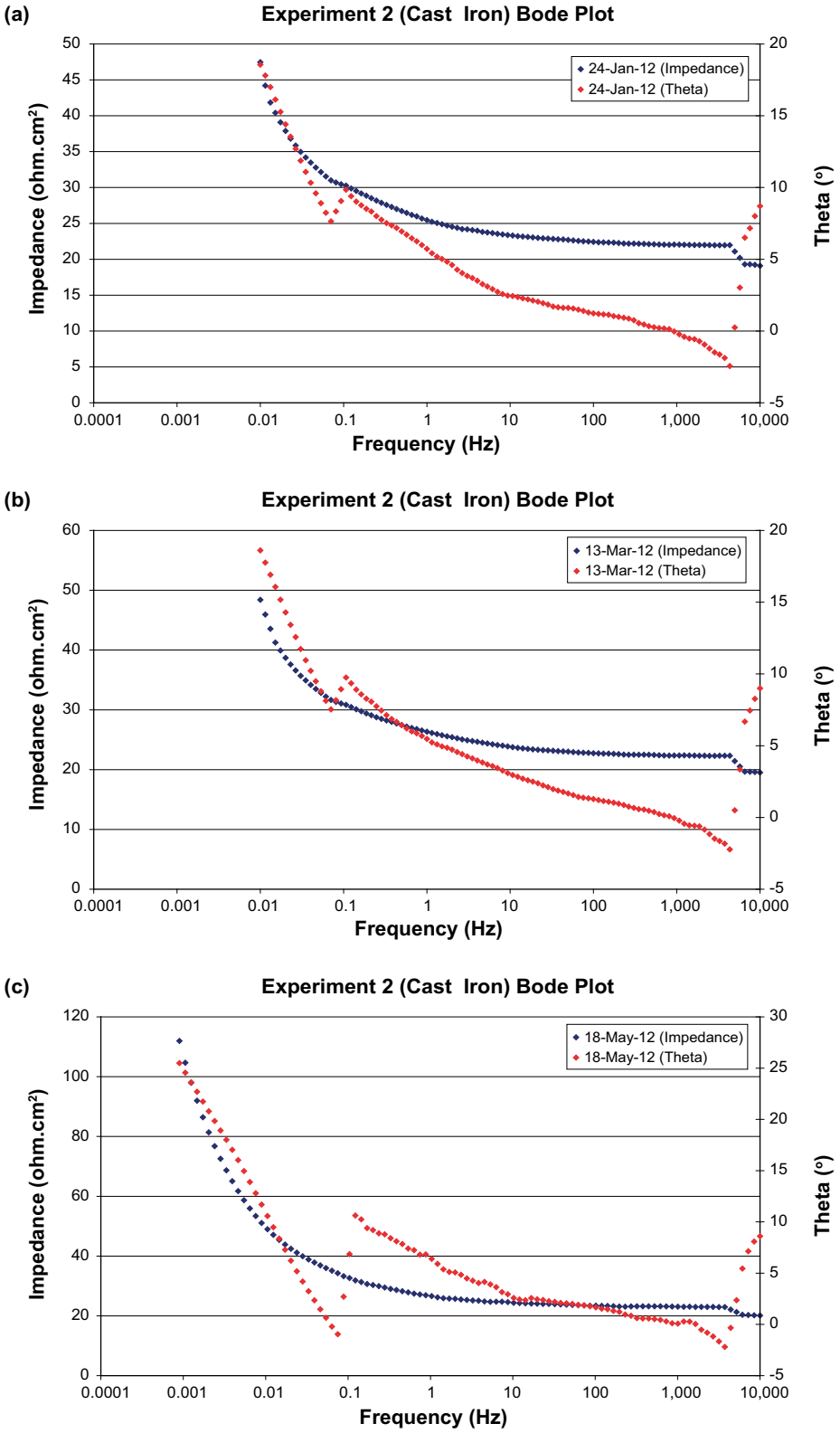

Figure A1-16. *Bode plots of cast iron in Experiment 2 (low density bentonite) in (a) January 2012, (b) March 2012 and (c) May 2012.*

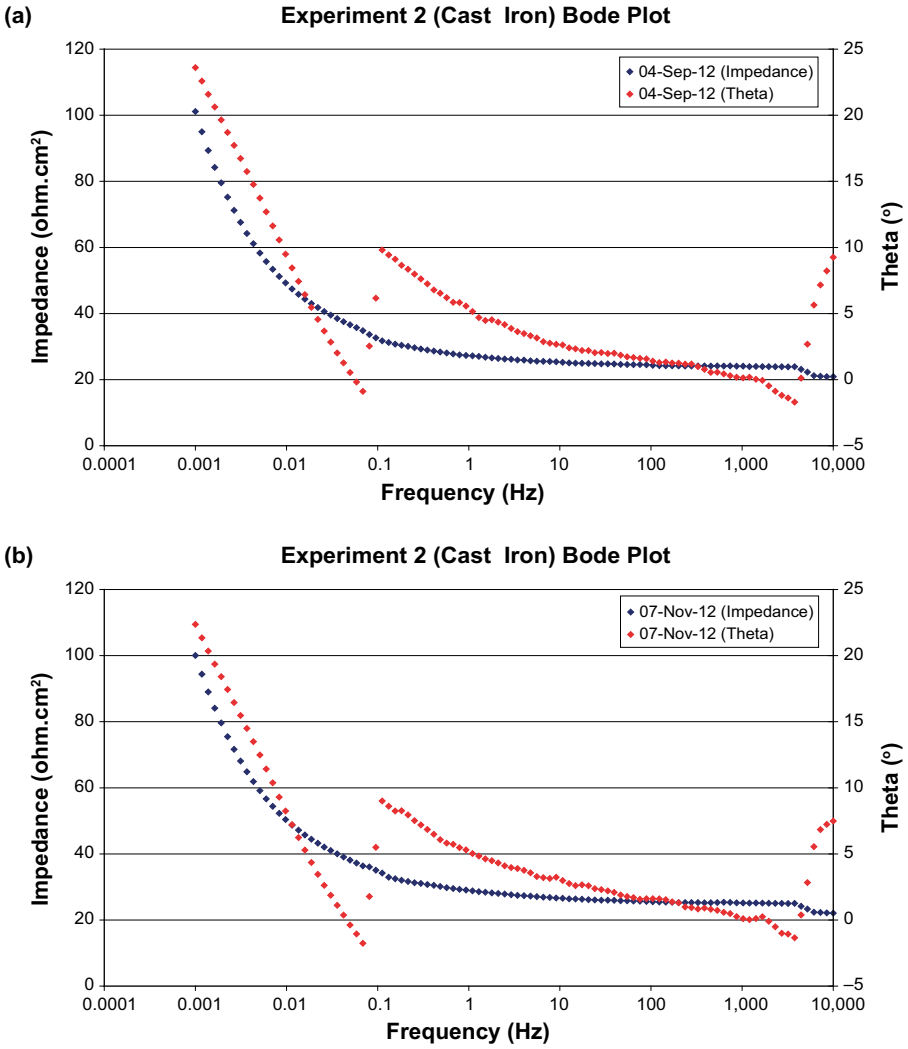

Figure A1-17. *Bode plots of cast iron in Experiment 2 (low density bentonite) in (a) September 2012 and (b) November 2012.*

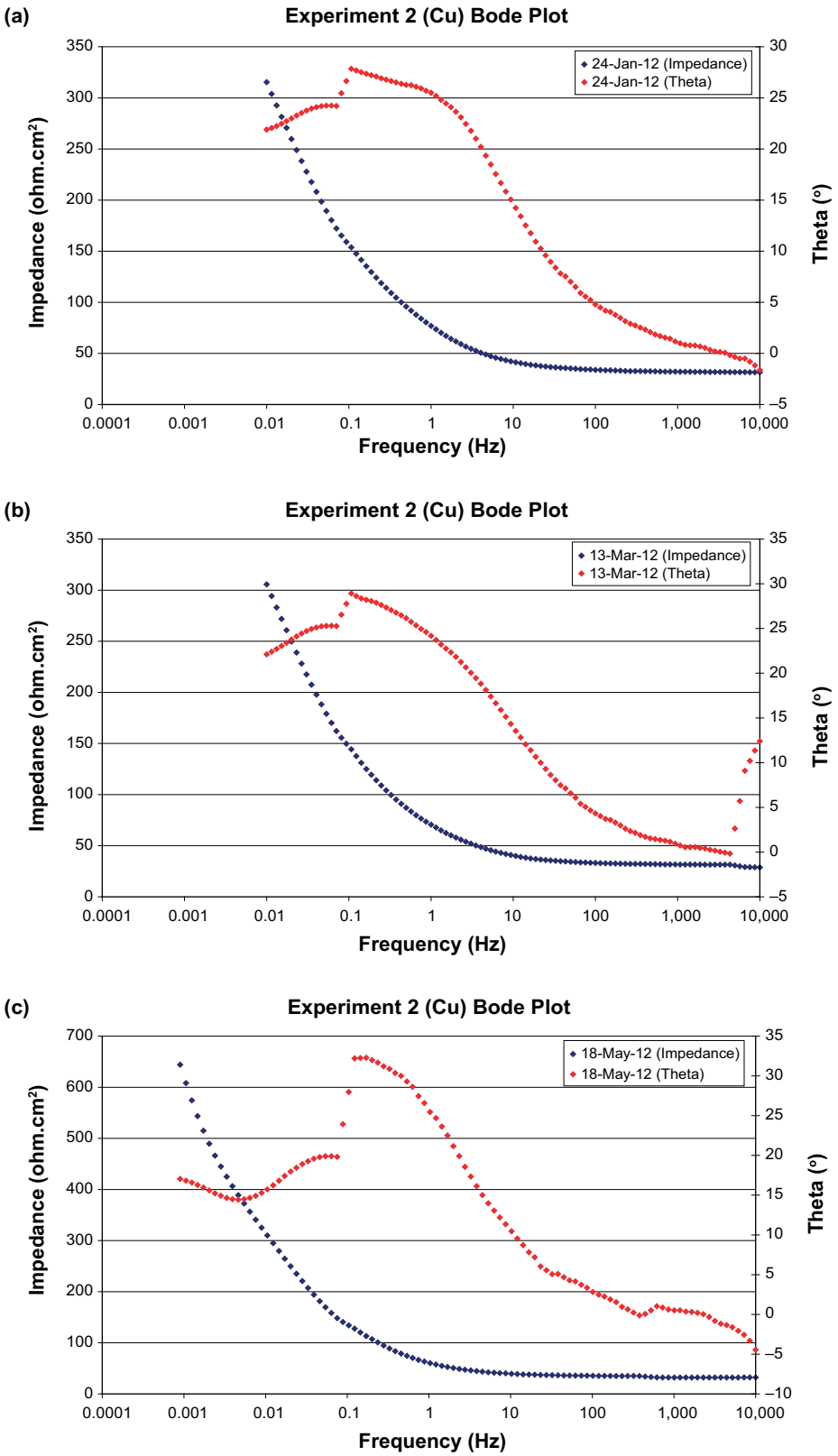

Figure A1-18. *Bode plots of copper in Experiment 2 (low density bentonite) in (a) January 2012, (b) March 2012 and (c) May 2012.*

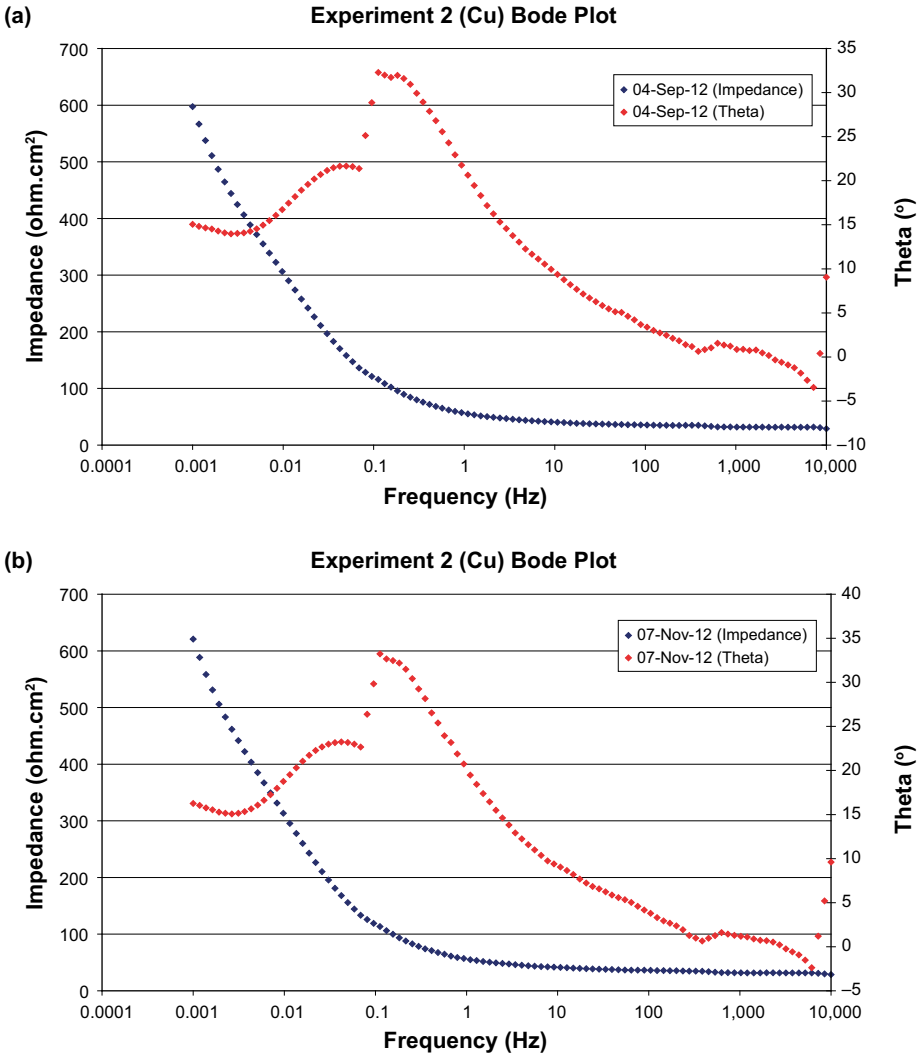

Figure A1-19. *Bode plots of copper in Experiment 2 (low density bentonite) in (a) September 2012 and (b) November 2012.*

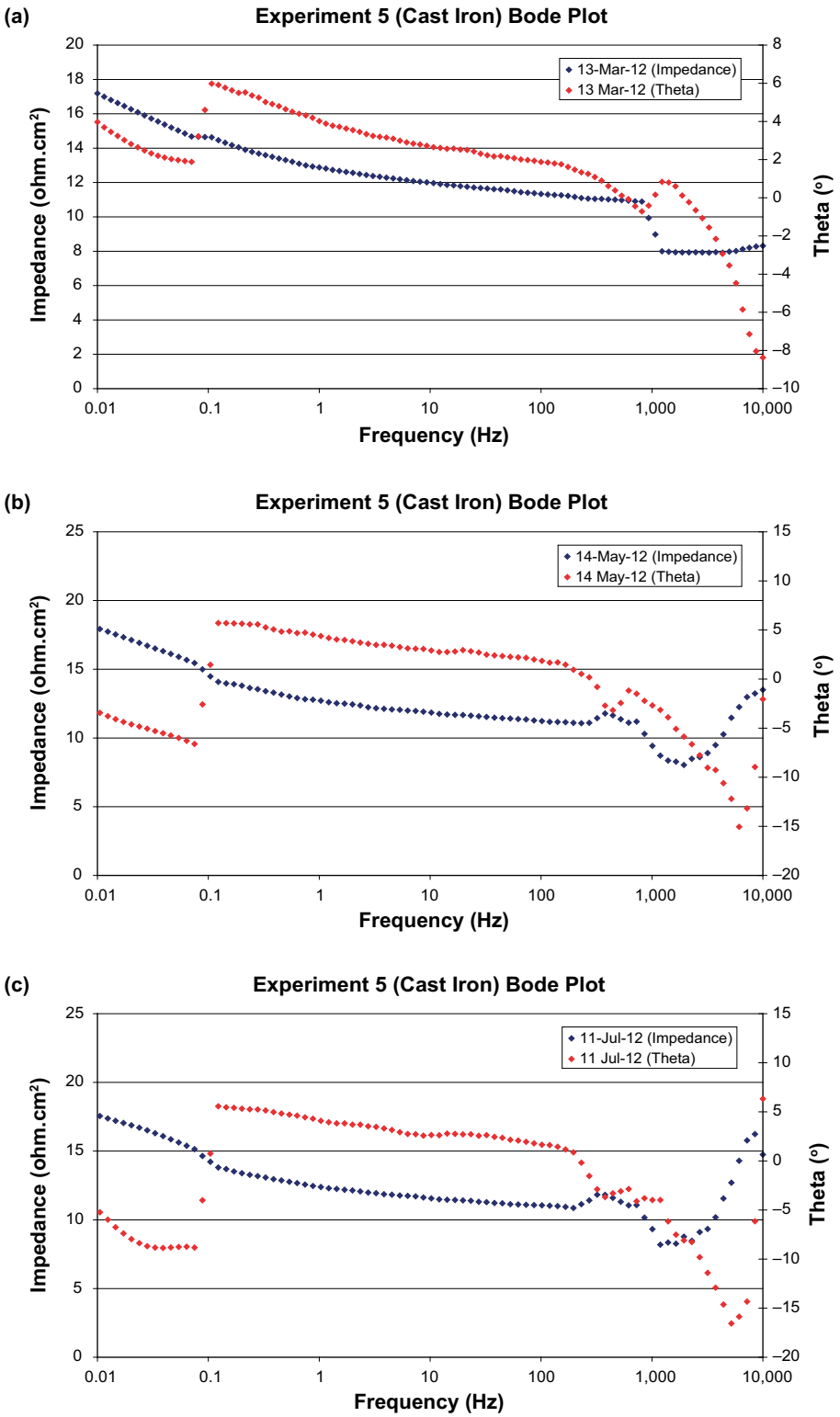

Figure A1-20. *Bode plots of cast iron in Experiment 5 (low density bentonite) in (a) March 2012, (b) May 2012 and (c) July 2012.*

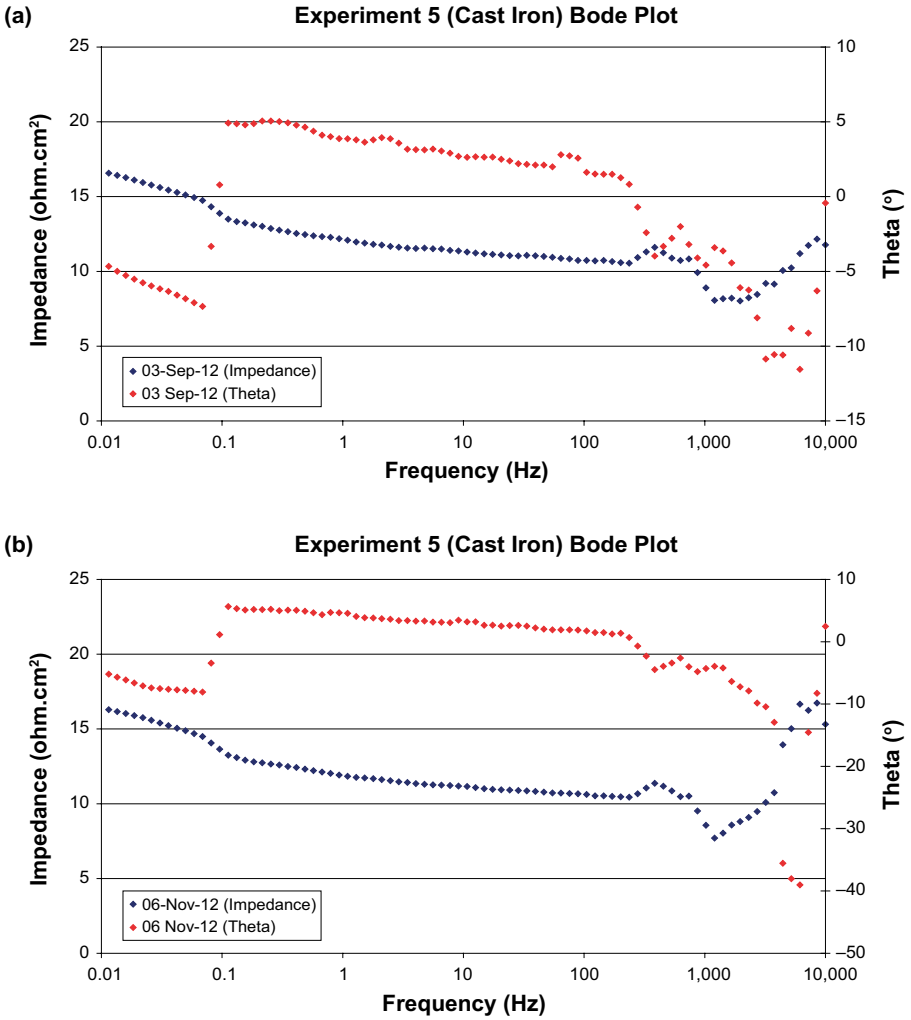

Figure A1-21. *Bode plots of cast iron in Experiment 5 (low density bentonite) in (a) September 2012 and (b) November 2012.*

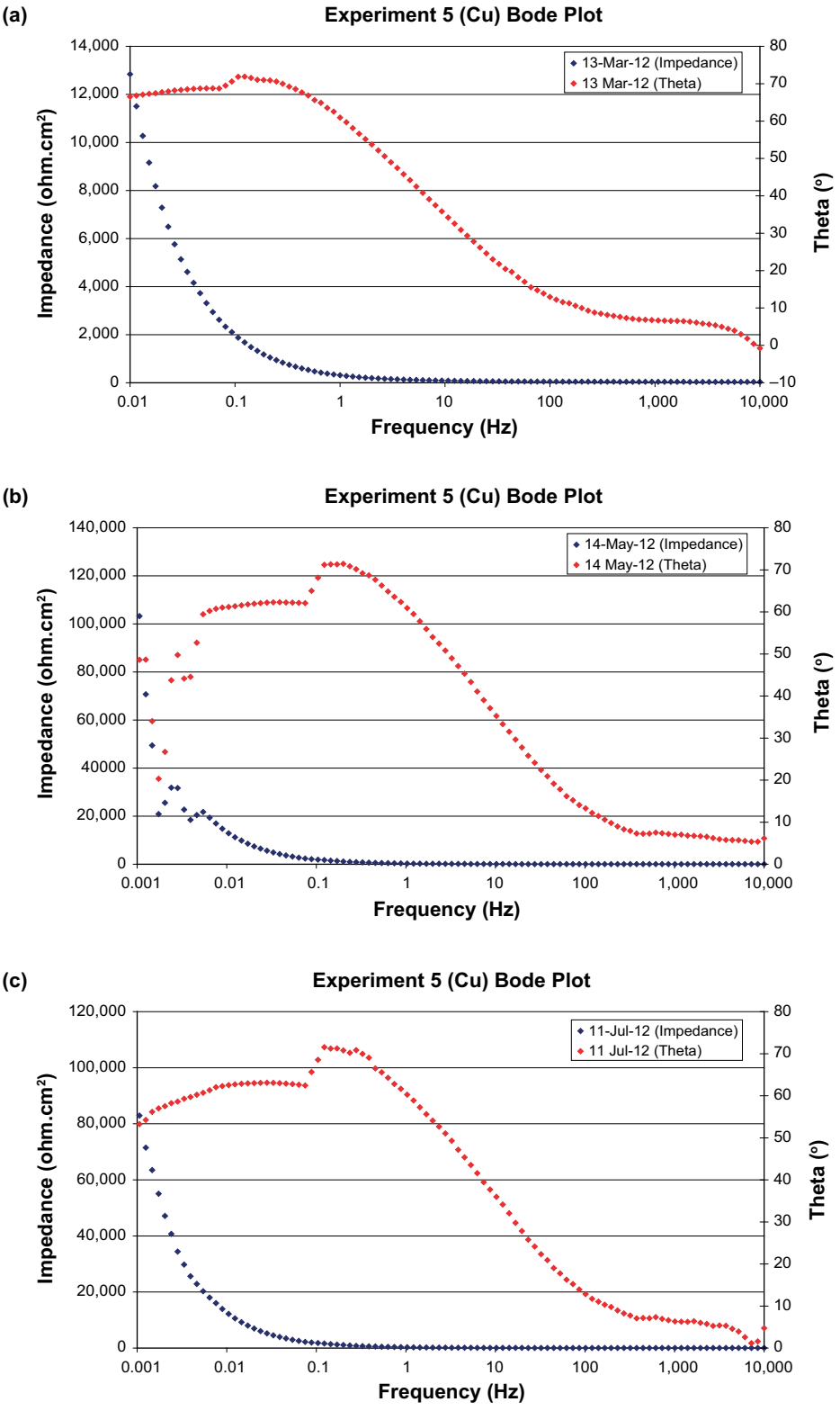

Figure A1-22. *Bode plots of copper in Experiment 5 (low density bentonite) in (a) March 2012, (b) May 2012 and (c) July 2012.*

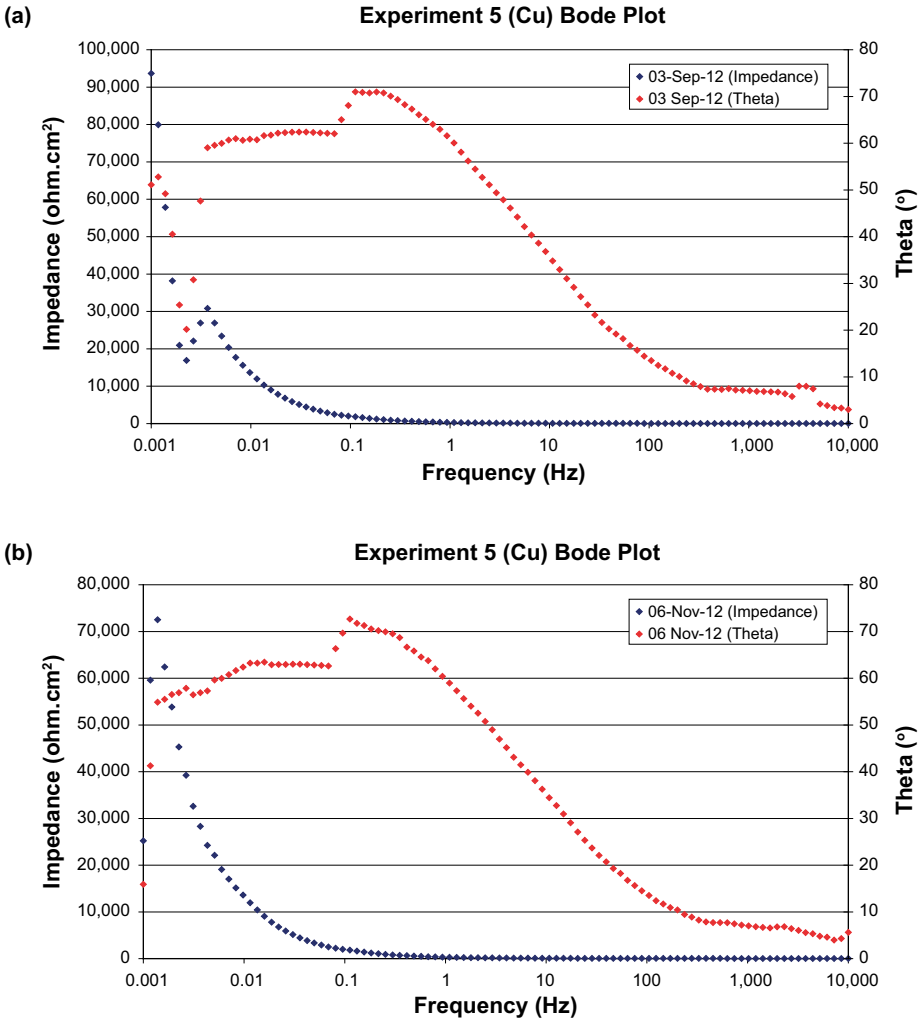

Figure A1-23. *Bode plots of copper in Experiment 5 (low density bentonite) in (a) September 2012 and (b) November 2012.*

Appendix 2

Electrochemical corrosion rate measurements for Experiment 4 during 2011 and 2012

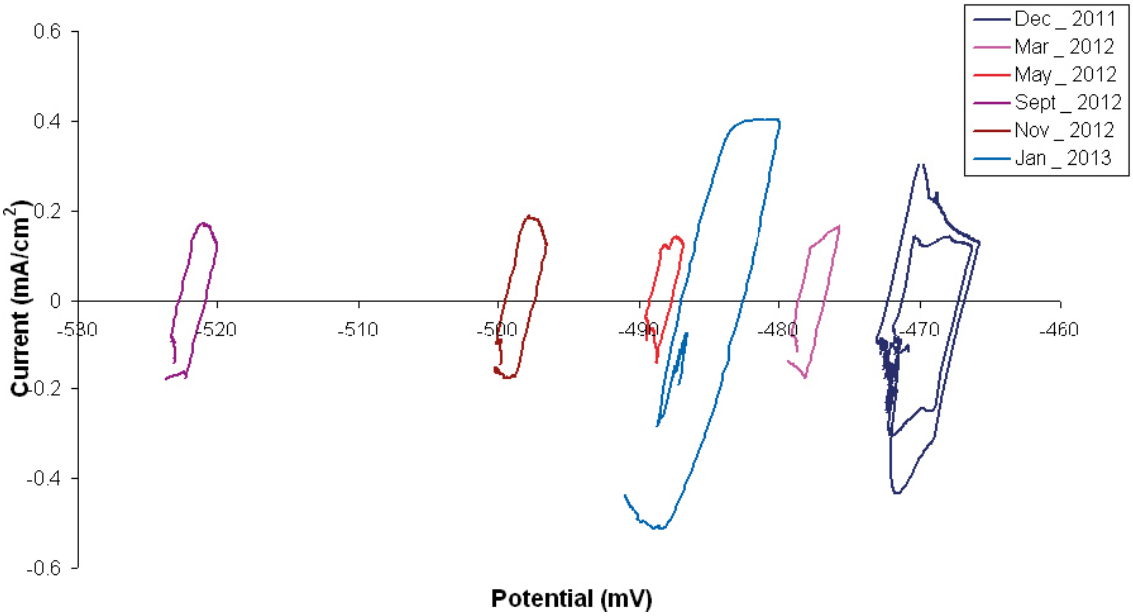

Figure A2-1. *LPR plots of cast iron in Experiment 4 (compacted bentonite).*

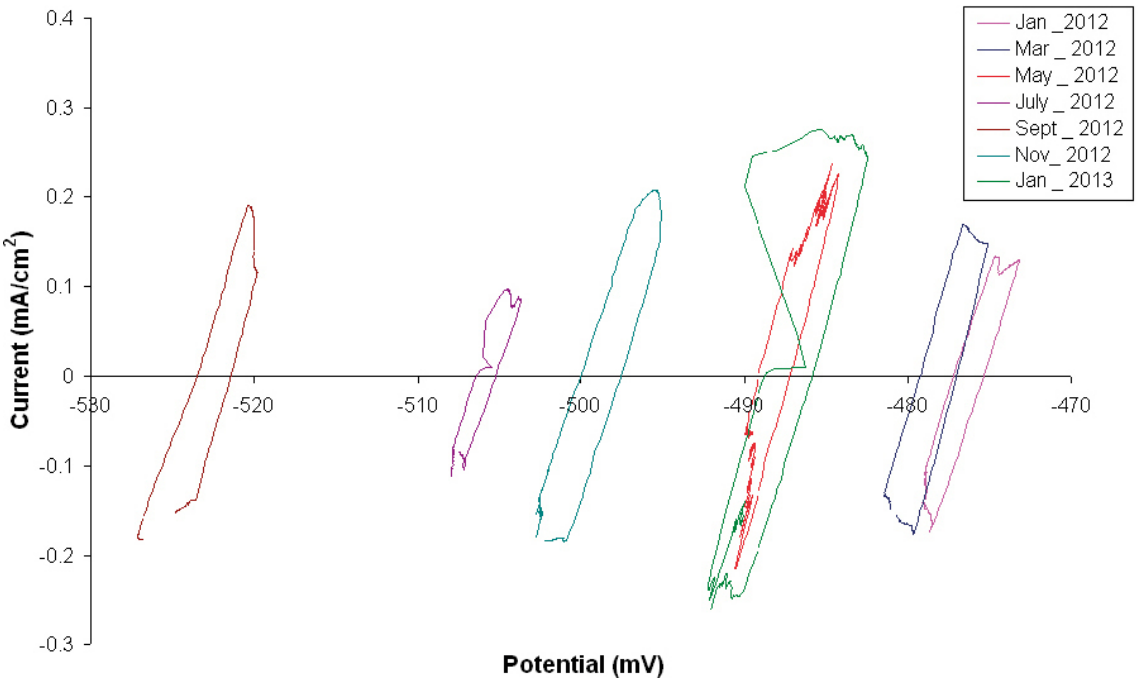

Figure A2-2. *LPR plots of copper in Experiment 4 (compacted bentonite).*

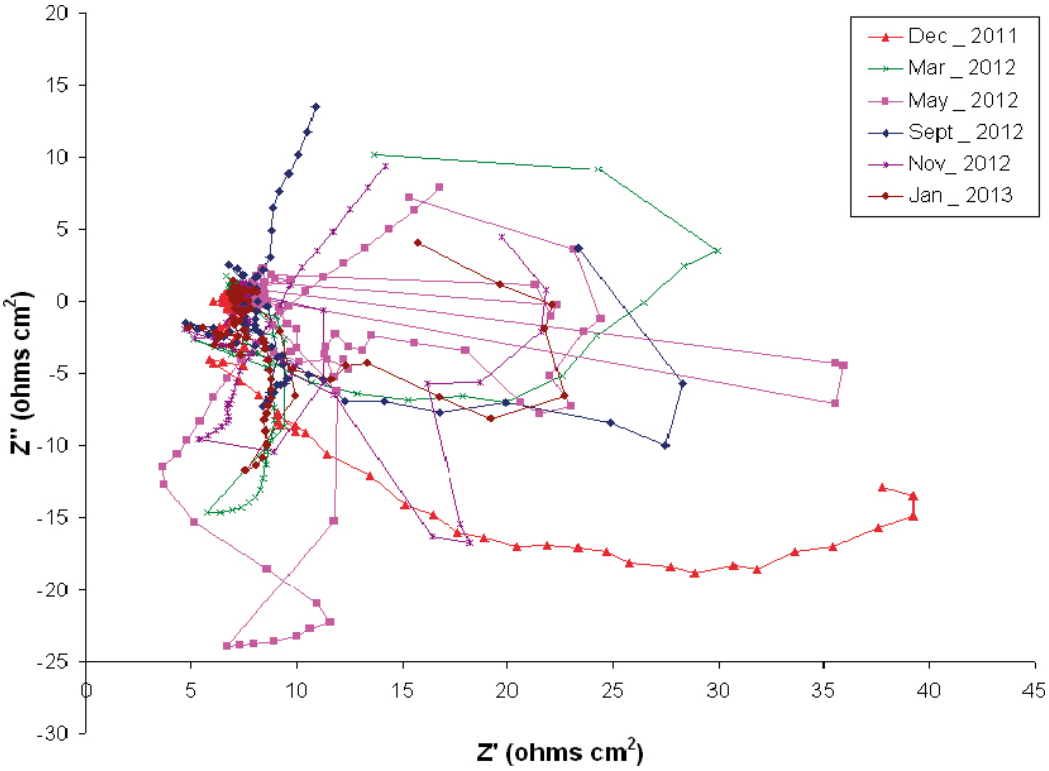

Figure A2-3. *ACI plots of cast iron in Experiment 4 (compacted bentonite).*

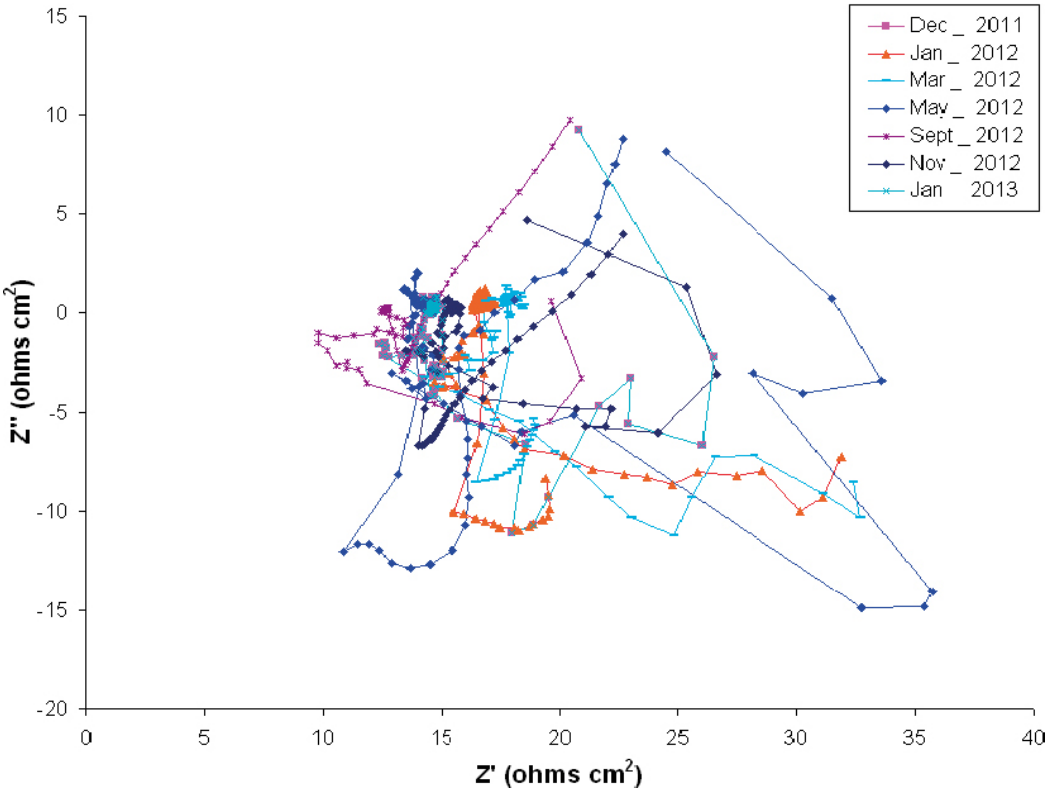

Figure A2-4. *ACI plots of Copper in Experiment 4 (compacted bentonite).*

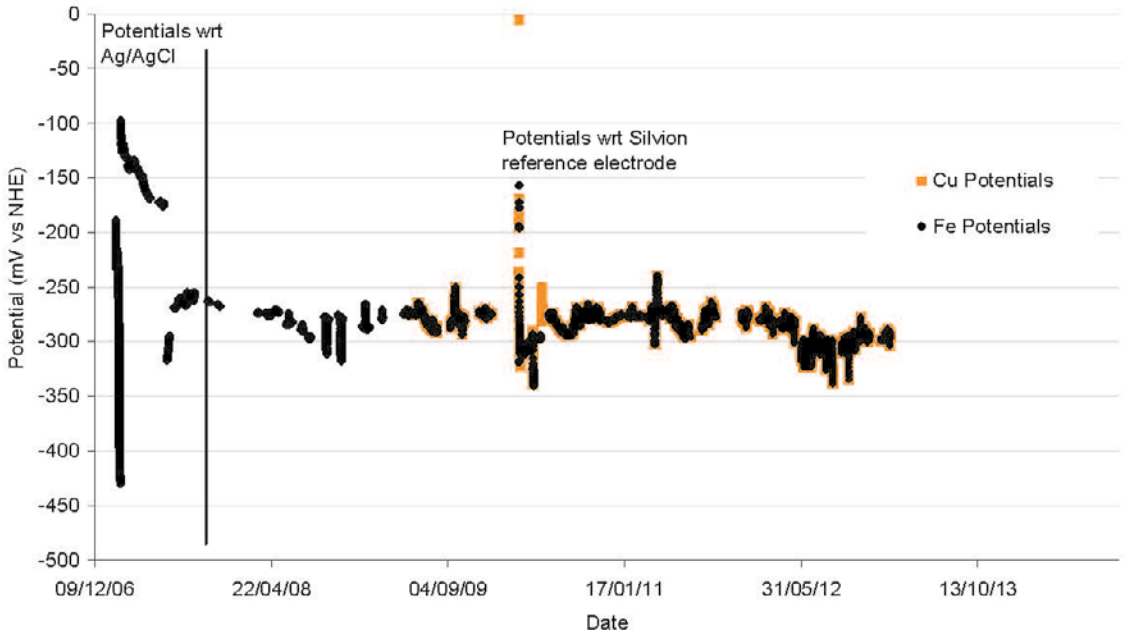

Figure A2-5. *Results of corrosion potential cast iron and copper electrodes in Experiment 4 (compacted bentonite).*